Toughening polymer surfaces

Haider K. Ali
University of Wollongong

Toughening Polymer Surfaces

A thesis submitted in fulfilment of the requirements
for the award of the degree

DOCTOR OF PHILOSOPHY

from

UNIVERSITY OF WOLLONGONG

by

Haider K. Ali

MEngSt. (Auckland University)

School of Mechanical, Materials and Mechatronics Engineering

July 2006

DECLARATION

I, Haider K. Ali, declare that this thesis, submitted in fulfilment of the requirements for the award of Doctor of Philosophy, in the School of Mechanical, Materials and Mechatronic Engineering, University of Wollongong, is wholly my own work unless otherwise referenced or acknowledged. The document has not been submitted for qualification at any other academic institution.

Haider K. Ali

July 2006

ACKNOWLEDGMENTS

I would like to express my sincere thanks to my supervisor, Professor Hugh Brown for providing help and support during the course of my study. A grateful acknowledgment is also extended to SOLA Optics for sponsoring this project, and in particular to Dr. David Lewis for his technical input. In addition, I would like to thank the following people for their assistance and support over this work:

Prof. Michael West and his PhD students Bradley Glass and Bane Lake for their support with the FEMCAD software,

Dr. Peter Innis and Mr Avirs Dipers from the School of Science for their instruction regarding the use of Raman spectroscopy and the polariscope located in their department,

Ms Lorelle Pollard for her kindly administration support,

Dr. Chris Lukey, Dr. Wang Huillang, and Ms. Siu Wah Wai from the Polymer Group for their scientific involvement and advice,

Mr. Chandana Herath from the Electrical engineering for his PC support,

Mr. Ron Marshall with his staff at the UOW engineering workshop,

Mr. Greg Tilman and Mr. Bob Dejong for their technical contribution and support.

Also I would like to thank the librarian staff at the UOW general library for their genuine help and assistance.

ABSTRACT

The thermoset resin poly diglycol carbonate, commercially called CR-39 has excellent optical properties, is cheaper than other ophthalmic materials and is considered one of the best plastic materials for the industry. CR 39 is known to be a brittle, highly cross-linked polymer. Applying coating layers significantly affects the toughness of ophthalmic lenses; a crack will first start on the surface of the coating and propagate through to the lens. One procedure to stop cracking, although not favoured by the industry because of its cost and detrimental effect on the optical properties, is to place a thin, rubbery layer between the coating and CR-39 ophthalmic lens.

An alternative method to stop the cracking is to toughen the lens material itself by placing the upper and lower surfaces under compressive stress. Swelling the lens surface can generate compressive stress and generating a multi-composite stressed layer lens can significantly improve fracture toughness.

An axisymmetric model of the spherical lens was built and a static load was applied on the central region in order to analyse stress distribution on the surfaces of the lens. It was found that tensile stress dominates the lower surface when the load was applied on the top surface. A volumetric swelling was introduced into the axisymmetric model to generate compressive stress onto the swollen surface while the tensile stress region on the lower surface was moved towards the central region

of the spherical lens. The volumetric swelling transferred the stress in the horizontal axis from the tension to the compression region.

More than one system has been designed to evaluate the best swelling agent; chloroform was the best solvent and a mixture of chloroform with acrylic acid (monomer) was found to be the best swelling agent for the CR-39 ophthalmic lens. Ultra Violet (UV) light initiated polymerisation was used to polymerise the monomer within the surface of CR-39 ophthalmic lens. The temperature during this process remained below the glass transition temperature (Tg) of CR-39 polymer.

Raman spectroscopy was used to examine the residual vinyl group in CR-39 polymer and monitor the diffusion process of the monomer in the CR-39 lens surface and the polymerisation process of the diffused monomer. The depth of this treatment was measured by using the mapping technique in Raman spectroscopy. The stress generated from swelling the lens surface was measured by photoelasticity. A 3-point bending device was developed and attached to a circular polariscope to measure the optical stress coefficient of CR-39 because it is a transparent material.

Fracture energy was evaluated using the static impact and dynamic tests and significant improvements from treating both upper and lower surfaces and applying a hard coating to the treated lenses were observed. Surface characterisation techniques were used to determine the effect of the treatment applied to the CR-39 ophthalmic lenses. Ultra-Micro Indentation System (UMIS) analysis measurements using Berkovich and spherical indenters showed a decrease in the elastic modulus. Dynamic Mechanical Analysis (DMA) measurements using the penetration and

single cantilever modes showed an increase in loss modulus and a decrease in storage modulus accompanied by a lower compression modulus for the treated surfaces. Atomic force microscopy (AFM) studies revealed that the treated surface of a CR-39 ophthalmic lens was smoother than an untreated surface.

TABLE OF CONTENTS

LIST OF FIGURES

LIST OF TABLES

LIST OF PRINCIPAL SYMBOLS

AA	acrylic acid
BEE	benzoin ethyl ether
BP	benzophenone
ADC, CR-39	diethylene glycol bis allyl carbonate
DVB	divinyl benzene
IPP	diisopropyl peroxydicarbonate
MAA	methacrylic acid
ST	styrene
TBPB	tert-butyl peroxybenzoate
TBP	tetra-butyl peroxide
VA	vinyl acetate
SR, HR	scratch resistance coatings
AR	anti reflective coatings
OPS	oxide polishing solution

UMIS	ultra-microindentation system
UV	ultra-violet
AFM	atomic force microscope
DMA	dynamic mechanical analysis
FTIR	fourier transform infrared spectroscopy
CSIRO	Commonwealth Scientific and Industrial Research Organization
SOLA	Scientific Optical Laboratories of Australia
USA	United States of America

σ_x	stress in x-direction
σ_{xt}	tensile stress in x-direction
σ_{xc}	compressive stress in x-direction
P	pressure load
p'	distributed pressure
a	distance of the applied pressure to the centre of the spherical deformable body
r	radius of the deformable body
$\frac{\rho_g}{\rho_g^o}$	grain density ratio
k_g	bulk modulus
θ	expansion temperature

su_w	saturation and the pressure stress in the wetting fluid
ε_g^{th}	volumetric thermal strain
$\alpha_g(\theta)$	thermal expansion coefficient for the solid matter
I_L	laser intensity
ν_o	wave number of monochromatic beam radiation (from the laser light)
ν_i	wave number of *i*th vibrational mode
$d\alpha$	change in polarizability
dQ	change in the normal coordinate length of the vibration
Tg	glass transition temperature
wt_s	swollen weight
$wt_{\text{int.}}$	initial weight
C_g	stress-optical coefficient
Δn	change in birefringence
R	relative retardation
$(P-Q)$	principle stresses
Stdve	standard deviation
Br	Brewster
E	elastic modulus
t	thickness
E^*	composite modulus
D_i	diameter of the indenter
D_m	diameter of the residual impression
F	applied force
A	contact area
K_{Ic}	critical stress intensity factor or fracture toughness
G_c	critical strain energy release rate or fracture energy
C	crack length
E/H	modulus to hardness ratio
δ_e	elastic displacement
ν_m	Poisson's ratio for the indented material
ν_i	Poisson's ratio for the indenter
E_m	elastic modulus for the indented material
E_i	elastic modulus for the indenter
$h_{p\max}$	plastic penetration at maximum load

$\left[\frac{dP}{dh}\right]_{F\max}$	unloading slop at maximum load
$F_{\max}$	maximum indentation load
H_b	hardness using Berkovich indenter
H_{sph}	hardness using the spherical indenter
E', $E_{storage}$	storage modulus
E'', E_{Loss}	loss modulus
E_{comp}	compression elastic modulus
E_{Sph}	elastic modulus measured by UMIS spherical indenter
RMS	roughness mean squared

CHAPTER 1

INTRODUCTION

1.1 BACKGROUND

Optical transparent polymers can be made from thermoset resin or thermoplastic polymer and research into improving their fracture toughness has become an important field in polymer engineering. For example, adding an interlayer such as fibre or silica particles to the polymeric materials to increase the modulus and toughness has been used in some applications. More emphasis needs to be placed on toughening the transparent polymer because transparency and the optical properties associated with surface hardness and toughness are essential. Very little research into improving the fracture resistance of optical polymers has been carried out.

Polymers cast from diallyl monomers, particularly poly(diethylene glycol-bis-allyl carbonate), known commercially as CR-39 (Columbia Resin 39 or Allymer 39), are being used in a variety of applications ranging from optical devices to nuclear track detectors. The properties of the final product depend on the polymerisation conditions where the polymers form densely cross-linked networks with better thermal and dimensional stability than comparable thermoplastics. CR-39 ophthalmic polymers are glassy and cross-linked and are recognised as brittle, fragile materials.

Diethylene glycol bis allyl carbonate resins are a very successful commercial product used where high optical transparency together with low density and acceptable surface hardness are important. They have become more popular than other materials for ophthalmic lenses (having 50% of the world market) because of their lower cost and better optical properties. Although CR-39 resin has a satisfactory impact strength for many practical applications it is flaw sensitive which means some applications would be enhanced if the impact strength could be improved.

Coatings may decrease fracture resistance by reducing the tensile strength of the surface of the lens. As a lens flexes under pressure it is thought that a coating which is harder than the lens itself will crack more easily than the uncoated substrate. Indeed it has been found that the Anti Reflective (AR) and Scratch Resistance (SR) coatings dramatically reduced the required energy to fracture, presumably because the harder coating cracks with flexure before the softer substrate and injects a crack into the CR-39 substrate.

The main purpose of this research is to develop a technique that will improve the fracture energy of ophthalmic lenses without introducing an interface between the lens substrate and the hard coatings. Placing a soft layer as an interface between the hard coating and lens substrate helps to prevent or slow down the crack injection to the lens material.

Generating a compressive stress in the polymeric surface may improve the fracture resistance of the ophthalmic lenses. In glass science the ion exchange or “stuffing” method has been used to generate compressive stress onto the surface of the glass but with ceramics, the slip-casting technique has been employed to generate compressive surface stresses. In this current study the volumetric swelling technique was used to generate compressive surface stresses and thus a technique similar to that for

toughening glass and ceramic surfaces, has been developed for polymer surfaces. The CR-39 ophthalmic polymer was chosen because of its highly cross linked network and brittleness and for this project stuffing or swelling the surface is the appropriate technique required to achieve the objective.

This thesis investigates the possibility of stuffing the monomer into a highly cross-linked surface polymer, the addition of which will swell the surface volumetrically and generate compressive stress into the surface. The most important task of this project is to investigate the possibility of swelling a high cross-linked polymer surface by comparing the appropriate swelling agent to the CR-39 cured polymer while considering its transparent properties.

Plano power* ophthalmic lens made from CR-39 Allyl resin were treated with a swelling agent and tested. A convex-lens with an outer surface parallel to the inner surface and a homogeneous thickness and zero power is known as a plano power lens.

Cured CR-39 polymer does not dissolve in any solvent. Different types of individual monomers have been used to diffuse into the polymeric surface but identifying a suitable monomer that can diffuse into the CR-39 polymer within an appropriate environment is the primary task of the experimental part of this thesis.

Figure 1.1 shows the CR-39 ophthalmic lens with a scratch resistant (SR) coating as a primary layer and an anti reflective (AR) coating as a secondary layer. The AR coating is more brittle (E = 60 GPa) than the SR layers or the CR-39 polymer. A crack from the brittle surface can begin easily and propagate all the way through the bulk material causing a catastrophic fracture. The industrial solution to this problem is to use a soft, rubbery, primer layer between the lens surface and the SR layer. This primer layer prevents a crack from being injected into the bulk material of the lens

from the layers of the hard AR and SR coatings. This primer has not been favourably received or used within the industry because of the cost and its side effects on the optical properties of each lens.

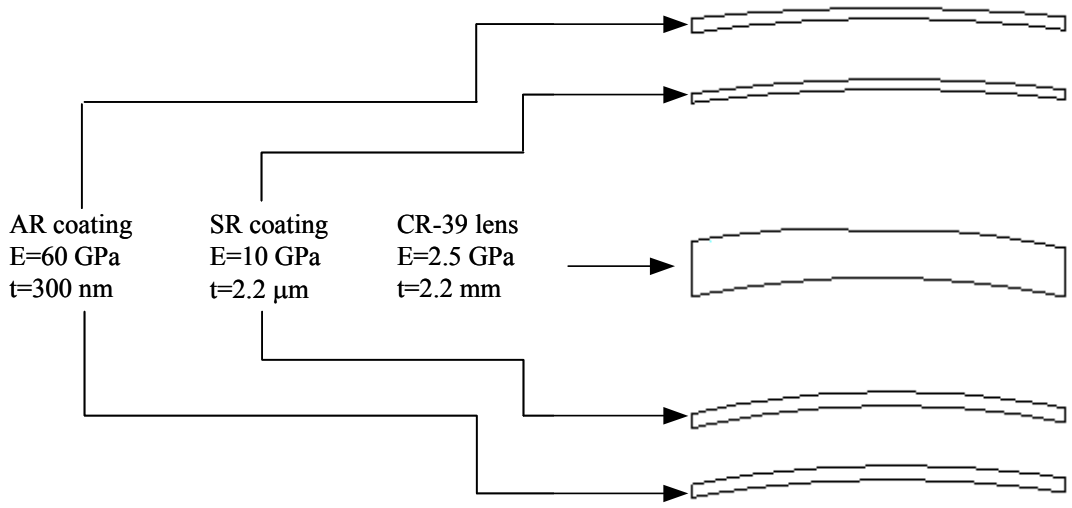

Figure 1.1. CR-39 lens and coating layers associated with their elastic modulus and thickness.

** Plano power lenses is an industry term meaning that the lens thickness is constant, this gives a lens no any refracting power, such as those used for sunglasses and safety goggles.*

1.2 THESIS STRUCTURE

In this section a broad overview of each chapter and its contents will be presented.

The introduction in Chapter One describes the aims of this project, which are to improve the fracture energy of ophthalmic lenses. It also gives a background into the process in this project used to toughen the ophthalmic lenses and the coating system of the finished lens.

Chapter Two is a literature review that broadly covers some theoretical background on the fracture and toughness relevant to these lenses. It also reviews the effect of applying coating layers to enhance fracture energy and then discusses techniques that are currently used to improve toughness. The previous work and other methods of toughening ophthalmic lenses are also described. This chapter also presents some techniques used to strengthen materials such as glass and ceramics by introducing compressive stress to their surfaces. The last part of this chapter investigates the physical and mechanical properties of the polymer employed to produce the ophthalmic lenses used in this project. This information is important for understanding how introducing compressive stresses onto the surfaces of ophthalmic lenses improves their fracture energy.

Chapter Three describes how concave spherical lens are modelled, presents the distribution of stress while a static load is applied to the modelled lens and then presents the effect of volumetric swelling onto these stresses. This chapter shows how a crack is likely to begin from the lower surface while a load is applied to the upper surface and how the stress that caused this crack can be reduced by introducing compressive stress to the surface generated by volumetric swelling.

The modelling aspect of this project is essential for understanding how generating

compressive stress to the surface of a lens slows down crack initiation.

Chapter Four focuses on finding the appropriate chemical (monomer) that causes a compressive stress in the surface to actually be generated. It describes the technique used to diffuse the monomer into a highly cross-linked polymer such as the substrate from which the ophthalmic lens is made. It also describes the Ultra Violet initiation technique used to graft polymerise the monomer into the lens material and its analysis by Raman. Measurement of the depth of the monomer penetrates into the surface is presented using the Raman mapping technique, including the reason for using micro Raman rather than other techniques of polymer spectroscopy such as FTIR.

Chapter Five contains two sections. The first explains the methodology and processes used to measure the stresses generated in the ophthalmic lens surface, including the use of a circular polariscope to evaluate these stresses. A 3-point bending device was designed, manufactured, and attached to the circular polariscope to measure the stress optical coefficient of the ophthalmic lens used in this project. The second section discusses how the treatment affected the ophthalmic lens mechanical properties with emphasis on measurement of the fracture energy of the treated and untreated lenses using both static and dynamic impact tests. This section further presents the effect of applying coating layers on fracture energy. Chapter Six describes how the mechanical properties and topology of a treated surface compared with an untreated surface using UMIS, AFM, and DMA instruments. Correlations of the indentation results using the spherical and Berkovich indenters with the DMA penetration mode results are presented and the surface roughness analysis using AFM contact mode is described.

Finally, in Chapter Seven, this general discussion and conclusions are brought together with suggestions and recommendation for future work.

CHAPTER 2

Literature Review

The literature review in this chapter is in four sections. In the first section the fracture mechanics of polymers is reviewed in general, and the fracture of thermoset polymers is described in particular. The second section deals with the fracture of ophthalmic lenses and investigates the fracture toughness of ophthalmic lenses. The third section describes techniques of improving the fracture energy by applying a compressive stress to the surface of solid materials such as glass and ceramics. The final part reviews mechanical, physical and structural properties of diethylene glycol bis allyl carbonate (CR-39).

2.1 FRACTURE

Fracture can be defined simply as the creation of new surfaces within a body through the application of external forces. It is possible to classify materials as being either 'brittle' like glass which shatters readily or 'ductile' like pure metals such as aluminium which can be deformed to high strains before they fail. Polymers are found to exhibit both of these two types of behaviour depending upon their structure and the conditions of testing.

In general polymers have a lower fracture strength than other materials such as metals or ceramics [1]. In practice fracture originates from local concentrations of stress at flaws, scratches or notches. Considering an elliptical hole in a thin sheet under applied stress, σ_o as shown in figure 2.1, the axial stress near the crack tip, σ_t can be written by the following equation:

$$\sigma_t = \sigma_o\left(1 + 2\sqrt{a/\rho}\right)$$

where ρ is the radius of curvature of the tip and $2a$ is the major axis.

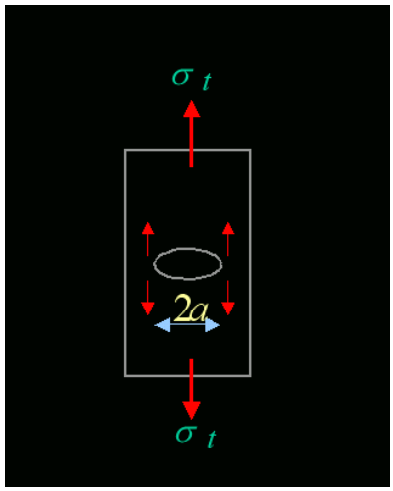

Figure 2.1. An elliptical crack subjected to a uniform stress.

2.1.1 Griffith theory

Griffth's theory involves an energy balance relating strain energy release to the increase in surface free energy [2]. Griffith calculated the energy released by putting a sharp crack into a plate as shown in figure 2.2, and related this to the energy required to create a new surface and obtained the following equation:

$$\sigma_f = \left(\frac{2E\gamma}{\pi a} \right)^{\frac{1}{2}}$$

where σ_f, is the fracture stress, E is the Young's modulus, a is the crack length, and γ is the surface energy of the materials.

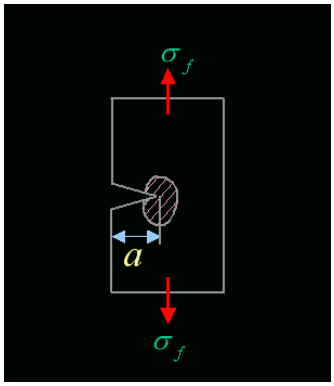

Figure 2.2. Sharp crack in a thin plate.

Griffith's equation can be modified to include the plastic deformation around the crack tip which occurs in less brittle materials by replacing 2γ with the critical strain energy release rate $G_c{}^*$. Therefore the above equation can be written for plane stress as:

$$\sigma_f = \left(\frac{EG_c}{\pi a} \right)^{\frac{1}{2}}$$

The expression can be written in plane strain terms such that:

$$\sigma_f = \left(\frac{EG_c}{\pi(1-\nu^2)a} \right)^{\frac{1}{2}}$$

where ν is Poisson's ratio. Fracture energy is the total amount of energy per unit crack area dissipated during crack growth. The assumption of Griffith's approach was that for any particular material the fracture stress was controlled by the size of the flaws present in the structure. The strength of any particular sample can be increased by reducing the size of these flaws. It has been found that the strength of brittle polymer can be increased by reducing the size of the induced flaws at the polymer surface [3].

$G_c{}^*$ is the critical strain energy release rate, and represents the elastic energy per unit crack surface area that is available for infinitesimal crack extension, in some literature is defined as fracture energy.

2.1.2 Linear elastic fracture

It has been shown that the stress field around a sharp crack in a linear elastic material could be uniquely defined by a parameter named the stress intensity factor, K, and stated that fracture occurs when the value of K exceeds some critical value, K_c [4]. The advantage of the stress-intensity factor approach is that K_c may always be expressed in the form:

$$K_c = Y\sigma_c a^{1/2}$$

where Y is the geometry calibration parameter, a is the initial crack or notch length, and σ_c is the applied stress at the onset of crack growth.

The quantity Y is a non-dimensional function of crack length and geometry of specimen, for the infinite plate the value of Y is equal to $\pi^{1/2}$. K_c is defined as the fracture toughness since it characterizes the resistance of a material to crack propagation.

G_c is the parameter that accounts for energy consumed by plastic and viscoelastic dissipation in the region surrounding the crack tip, in addition to the increase in the surface energy due to new crack area.

G and K are related by a simple relationship. For plane stress conditions the relationship is given by:

$$G_c = \frac{K_c^2}{E}$$

and for plane strain:

$$G_c = \frac{K_c^2(1-\nu^2)}{E}$$

where E is Young's modulus and ν is Poisson's ratio. Thus, a critical G_c criterion is analogous to a critical K_c criterion, with K_c combining both material properties, i.e. G_c and E.

2.1.3 Fracture in thermoset glassy polymers.

Glassy thermoset polymers are cross-linked polymers that are generally used below their glass transition temperatures. These glassy polymers are generally recognised as brittle, inflexible materials. The most common class of glassy polymers are epoxy resins. Generally thermoset glassy polymers are insoluble in all solvents as they have a complex three-dimensional molecular structure. Such cross linked polymers can be difficult to characterise chemically, and their structure can be varied by employing different types and amounts of curing agents to control the degree of cross-linking. The degree of cross-linking for a thermoset polymer can be estimated by measuring the modulus of the polymer in the rubbery state above the glass transition temperature.

2.1.3.1 Crack propagation in glassy thermosets

Glassy thermoset polymers tend to be rather brittle, failing at relatively low strains with very little plastic deformation. Therefore, they readily meet the requirements for linear elastic fracture mechanics. The fracture surfaces of glassy thermoset polymers are relatively featureless when compared with the surfaces of brittle glassy thermoplastic polymers such as polystyrene. The fracture surface of a cross-linked glassy polymer depends upon both the structure of the polymer and the specimen

geometry. One of the most characteristic features in thermoset crack propagation is that often cracks propagate in unstable manner, in contrast to glassy thermoplastics where propagation is normally stable or relatively smooth and continuous. However, continuous crack propagation can also be obtained in glassy thermosets. For continuous propagation the crack grows at a fixed load or a fixed value of the stress intensity factor suggesting there is very little plastic deformation at the crack tip during crack propagation.

For unstable crack propagation after crack initiation, rapid propagation takes place, leading to the stress intensity dropping until the crack is arrested. Then the specimen is loaded again to another initiation value when further crack propagation occurs by repetition of the same process. The unstable crack propagation in glassy thermoset polymers is believed to arise from crack tip blunting. It is suggested that low yield stress promotes crack tip blunting and hence unstable propagation. The crack jump behaviour can be explained as follows: With a highly blunted crack tip, when the crack eventually propagates, the energy release rate is much higher than required for continuous propagation, and hence the crack rapidly accelerates. When the specimen is depleted of the energy required for the further crack propagation, crack arrest occurs.

2.1.4 Effect of network structure on fracture toughness

2.1.4.1 Effect of cross-link density

Experiments on thermoplastics and cross-linked polystyrene have revealed that the entanglement network, and the cross-linked network, play an important role in

determining the deformation mode of the polymer glass. Glassy polymers with a low density of network strands will craze, whilst those with a higher network density will deform by shear[5]. Those with extremely high network densities will predominantly deform elastically i.e. CR-39 polymer.

The microdeformation and network structure had been studied in films of epoxies with different cross-link densities [5].

The cross-link density of the epoxies films has been adjusted by changing the initial resin molecular weight and the stoichiometric fraction of curing agent. It had been concluded that (i) high cross-link density in epoxies leads to shear deformation predominating over crazing and it is unlikely that epoxies craze; (ii) a transition from shear deformation to crazing with a decrease in the network cross-link density does not occur.

The molecular weight, M_c, between cross-links was varied by using epoxy resins of different epoxy equivalent weights: the higher equivalent weight, the higher is the value of the M_c [6]. It was found that an increases in M_c enhances the fracture energy, G_c, for the unmodified resin and causes a dramatic increase in G_c for the rubber toughened resin. These findings were attributed to an increased in the inherent ductility of the matrix as M_c increased. A greater effect was observed for the rubber-modified resin because the rubbery particles initiated a large number of energy-dissipating shear zones.

Some research has been done on the epoxy matrix of an epoxy system cured with piperidine. Different molecular weight between cross-links of the epoxy network were obtained by changing the curing time and temperature. It has been found that the maximum plastic strain capability of the matrix (area under stress-strain curve)

was dramatically increased as the value of M_c increased. The increased ductility of the matrix as the cross-link density was decreased was reflected in higher values of G_c.

2.1.4.2 Glass transition temperature of the matrix

It has been observed that the Tg of the matrix decreased as the degree of cross-linking was reduced as shown in table 2.1. The value of the Tg may also be influenced by other parameters, such as the degree of interchain attraction[7]. Low interchain attractive forces, which may give an increase in matrix ductility, often lead to low Tg values. Thus, thermosetting polymers that are extremely tightly crosslinked and possess high interchain attractive forces (and hence have high Tg) are difficult to toughen to a high level as this is frequently achieved at the expense of a decrease in Tg. The need to develop very tough thermosets without sacrificing high glass transition temperature presents an exiting and rewarding challenge.

Table 2.1. Effect of crosslink density on fracture energy.[7]

Please see print copy for Table 2.1

2.2 FRACTURE OF OPHTHALMIC LENSES.

Much research has investigated fracture of inorganic glass lenses. Less has been published for CR-39 lenses. Dain[8] tested both glass and CR-39 safety lenses with a static load device, with fracture load rather than energy, as the criterion. Using a ball-on-ring mount, he varied ball and ring size and found that for glass, fracture load decreased slightly with decreasing ball size but did not change with ring size. In contrast, for CR-39 lenses, fracture load did not change with ball size, but increased dramatically with decreasing ring size. In addition, the variation in fracture load was greater for glass than for CR-39. He attributed these findings to different fracture mechanisms (Hertzian for glass, flexure with rear-surface failure for plastic), where the flexure mechanism is highly dependent on annulus size and relatively independent of surface flaws. It is quite plausible, however, that the mechanism for glass and plastic may still be fundamental the same: flexure leading to rear surface failure. The larger variation in fracture pressure for glass could be attributed to greater variation in flaw severity or density. The amount and area of flexure may be quite different for the two materials, leading to different susceptibilities to a change in ring size. Dain used a pneumatic device which measured fracture pressure, or load, only. Finally Dain has concluded that static testing should not be used to compare different materials, but that comparisons of lenses of a given material would be valid. He [8] also conclude that a flexure mechanism is involved (either back surface or edge failure) and hinted that edge failure may be the more likely of the two, but industry testing supports the rear surface failure hypothesis.

Some research within the industry has shown a general correlation between static and drop ball testing, whereas other practitioners have suggested that the behaviour of

plastic lenses is rate-dependent, being more brittle in impact testing and more flexible under static conditions [9].

2.2.1 Impact testing of ophthalmic lenses

Several testing procedures have been used or proposed to evaluate the resistance of ophthalmic lenses to breakage. The most common is the drop ball test, which measures the height from which a ball must be dropped to break a lens. In the alternative procedure, commonly termed "static-load testing", a machine is used to measure the load required to break a lens. In actual use, eye glass lenses break under a variety of conditions: however, when eye injuries occur as a result of lens breakage, the failure has been found to be most commonly caused by an impact from a relatively massive and slowly moving object [9].

The Australian and American standards have agreed to use drop-ball acceptance tests, consisting of a 7/8 in (22 mm) ball from 72 in (1.8 m) and a 1 in (25 mm) from 50 in (1.3 m) [10]. For selecting personal protective equipment, most safety officers, engineers and optometrists demand compliance with the requirements of the relevant standard. It had been reported that the safety spectacles with lenses of either allyl resin or thermally toughened glass will meet the drop-ball requirement of the Australian and American standards if their center thickness is 3.0 mm or more. The use of 2 mm or thinner lenses is not recommended and the use of 2.0 mm or thinner thermally toughened glass lenses is strongly deprecated [10].

The U.S. Food and Drug Administration (FDA) has mandated a version of drop-ball test that can be used for ophthalmic lens testing. The standard FDA test specifies that

a 2 mm thickness ophthalmic lenses passes the test, if it does not fail when impacted by a ball of 5/8 inch (15 mm) diameter made from steel dropped from a height of 50 inches (1270 mm). This standard FDA test yields 2 Kg-cm impact energy [11]. Figure 2.3 shows the average impact energies that resulted in fracture of 2 mm lenses as a function of test ball size for three different lens materials i.e. CR-39, chemically treated glass and heat treated glass. For a given energy level, increases in ball size mean decreases in velocity and drop height. The red horizontal dotted line in figure 2.3 indicates the American National Standards Institute's acceptable level and DFA standards for impact resistance of prescription ophthalmic lenses.

In practice, lenses barely pass, and occasionally fail, the tests of the American National Standard Institute (ANSI) and the FDA standard [11]. When the impact test results were considered in terms of the size of the ball with which the lenses were struck, the performance of the different lens material can be evaluated. It can be seen that CR-39 provides superior impact resistance to small missiles. Using a ball size of approximately 13 mm in diameter (which was close to the size of the standard 5/8 inch, ball) chemically treated glass lenses were tougher than the CR-39 lenses. Heat treated glass lenses were very weak for small ball size but improve continuously as the ball size increases.

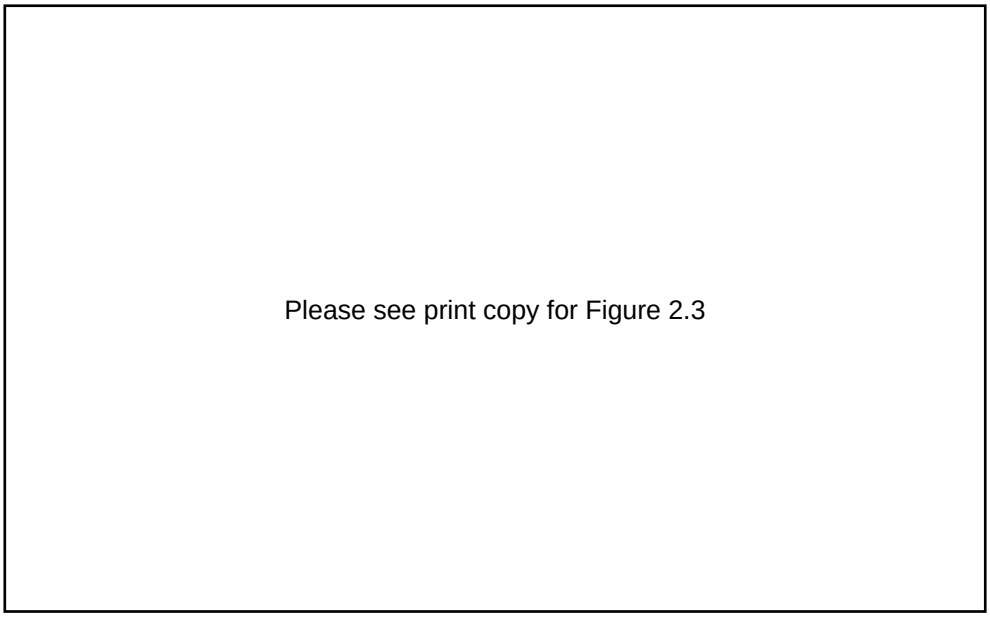

Figure 2.3. The FDA standard test for spectacle lenses.[11]
CR-39 (solid line), chemically treated glass (dashed line), and heat treated glass (dotted line) with different ball size, the FDA standard level is represented by red (dashed-dotted line).

McAuliffe et al. [12] used the standard FDA test to develop a mathematical model of the impact for ophthalmic lenses. The model consisted of calculating the load-deflection relationship of a spherical lens loaded at central point, combined with calculating the deflection at which fracture occurred. From this model the impact energy required to deform a lens to fracture was obtained [12]. It was assumed that the lens is deformed elastically under impact loading. However the stored elastic energy in the lens is equal to the kinetic energy of the drop weight for the maximum deflection of the lens at the point of load application. This stored energy was represented as the area under the load-deflection curve of the lens. The model was initially developed for plano lenses, as the constant thickness lens simplified the

calculation of the impact energy, but the model was extended to prescription lenses, as the majority of production involves prescription lenses.

Table 2.2 shows the impact results for plano lenses from the modelling calculation and the experimental results for different types of thermosetting resins, where R1 is designated to a poly-diallyl diethylene glycol carbonate (CR-39) [12].

Please see print copy for Table 2.2

Table 2.2 Experimental and predicted impact results for plano lenses made from the different resins [12].

2.2.2 Crack initiation of ophthalmic lenses

The fracture of ophthalmic lenses has been understood using the flaw theory which states that fracture occurred when the tensile stress acting on any flaw in the material reaches a critical value, which depends on the size and shape of the flaw. When this criterion is met, a crack propagates rapidly through the materials. The fracture-initiating flaws can be either intrinsic material inhomogeneities or surface flaws. For ophthalmic lenses in practice, however, surface flaws resulting from grinding and

polishing or from abuse in handling normally initiate fracture.

For a lens like, shallow spherical shell carrying a static load over a small circular area at the apex, Roark and Young [13] have summarized the equations that relate the maximum surface tensile stress, σ, and the maximum deflection, Δ, to the applied load at failure, P, these equations are:

$$\sigma = K\frac{P}{t^2}$$

$$\Delta = A\frac{PR}{Et^2}$$

where *R* and t are the radius of curvature and thickness of the lens, respectively, and *K* and *A* are coefficients which depend on a friction coefficient, μ, between the ball-and-lens combination.

It was predicted from the above equations that the ratio P/t^2 should be constant for any given lens material. This result was experimentally tasted by Sciaf [14] using a ball-on-3-ball test configuration (mounting the tested lens on three balls instead of a ring), which was sufficiently close to ball-on-ring mounting test. It was shown that the failure load was proportional to lens thickness squared [15] as shown in figure 2.4.

Please see print copy for Table 2.4

Figure 2.4. Static-load data for chem-tempered glass lenses versus lens thickness squared.

2.2.3 The Effect of coating layers to the fracture toughness of ophthalmic lenses.

John et al. [16] used static load testing to investigate the effects of scratch-resistant (SR) and anti-reflective (AR) coatings on the fracture resistance of CR-39 lenses. The fracture resistance of CR-39 lenses is greatly affected by surface characteristics, and thus coatings may have a weakening effect on ophthalmic lenses. The 140 cast finished CR-39 ophthalmic lenses used by John et al. [16] were supplied from American Optical factory. All lenses were plano power with a base curve of +6.50 D. In optometry science, a convex lens with its outer and inner surfaces parallel and thus with a uniform thickness and zero power is known as a plano power lens. The lenses

were all edged on a single edger to be circular with a 51 mm diameter. The center thickness was measured for each lens with a lens calliper to 0.1 mm.

The 140 lenses were divided into 4 test groups of 35 lenses. One group consisted of two-sided factory-coated SR lenses. Another group consisted of two-sided factory-coated AR lenses. The remaining uncoated lenses were randomly assigned to two other groups. The control group remain uncoated; the second group was prepared for the AR coating but not actually coated (AR-prep). The preparation process involved ultrasonic cleaning of the lenses in a solution of mixed hydroxides for 12 min at 52 ^{o}C, and a curing time of 2 hr at 78 ^{o}C, which was followed by 1 to 1½ hr in a vacuum oven at 39 ^{o}C. The second test group went through the above process and was vacuum-coated with a five layer AR coating on both surfaces.

An Instron static load tester was used to evaluate the fracture toughness. A steel ring and steel ball were attached to the Instron, and a high cross head speed was employed to use the instrument as static load impact tester. The results of the static impact test are shown in Figure 2.5. AR coating caused a greater reduction in fracture energy than did SR coating. There was no significant difference in fracture energy between the uncoated and AR-prep groups.

John et al. [16] showed that AR coating reduced the required fracture energy by 63% and SR coating reduced the fracture energy by 57%. John et al conclude that the results from the static load test are qualitatively consistent with drop ball test, coatings, either SR or AR, dramatically decrease the fracture resistance of CR-39 lenses, presumably because the harder coating cracks in flexure before the softer substrate would.

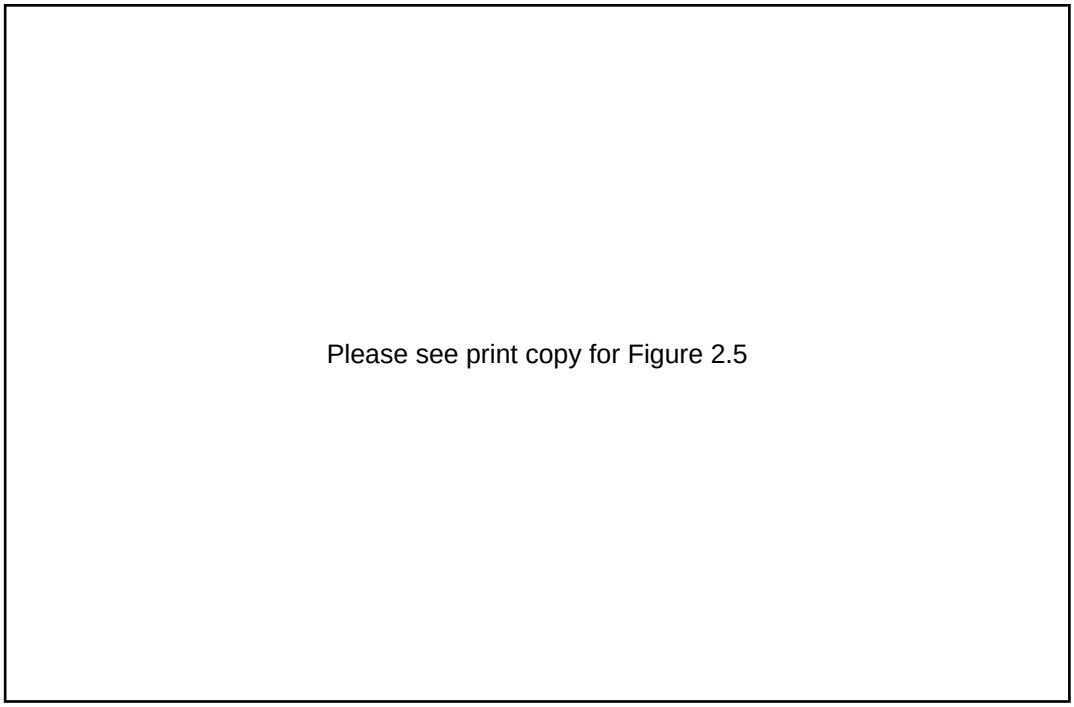

Figure 2.5. Fracture energy for treated and untreated samples.[16]

2.2.4 Toughening CR-39 resin

Pittolo et al. [17] polymerised the CR-39 monomer and Urethane Acrylates (UA) to form an interpenetrating polymer network (IPN). The fracture toughness was evaluated by using the double torsion method to test flat specimens of the polymer and standard drop ball test was used to test Plano lens. They showed that CR-39 resin can be toughened by the incorporation of a second flexible network, and no loss of mechanical or optical properties occurred. This second network must consist of a flexible backbone chain with a high cross link density.

IPNs are defined as a combination of two or more polymer networks that are synthesised in such a way as to cause the two networks to interpenetrate. The most common method to improve the toughness of crosslinked polymers is the addition of elastomeric modifiers that phase separate upon curing and form discrete domain phases of an average size of several micrometers in the thermoset matrix. However, thermoset systems that can be effectively toughened by the dispersed rubbery phase generally have a relatively low crosslink density. As the resin matrix is crosslinked more tightly, its capacity to deform by shear yielding is reduced and the addition of the rubbery phase does little to improve toughness. Pittolo et al and Frounchi et al [17], [18] studied the fracture behaviour of IPNs prepared from CR-39 and UA oligomers. The IPNs were prepared by forming the PUA network first by ultra-violet light initiation of the UA oligomer after which the CR-39 network was formed by convention thermal polymerisation. Two PUA networks were investigated. Series I formed a loosely crosslinked PUA network. Series II formed a tight highly crosslinked PUA network. For the series I the tensile strength decreased, also the Young's modulus decreased slightly. The fracture toughness as measured by K_{1c} was slightly decreased as well. For series II IPNs, however, the fracture toughness increased as shown in figure 2.6 [17]. The Young's modulus remained essentially constant, whilst the tensile strength increased to a maximum under certain condition of UA composition. The difference in properties between these two IPN series relates to their differing molecular structure. The series I IPN forms a relatively loose network which contributes considerable ductility to the overall network and causes significant deterioration in the overall strength and stiffness of the IPN. On the other hand the series II IPN forms a highly crosslinked tight network. This imparts some ductility due to the inherent flexibility of the urethane backbone, but at the same time

imparts a significant increase in the fracture toughness. It is the combination of the high crosslink density of the second network, coupled with the inherent flexibility of the chains that give rise to this fracture toughness increase.

Finally, it was concluded that the mechanism of the crack propagation in CR-39 resin can be controlled by the plastic deformation at the crack tip. CR-39 resins can be toughened by incorporation of a second flexible network, and that seemingly no loss of mechanical or optical properties occurs.

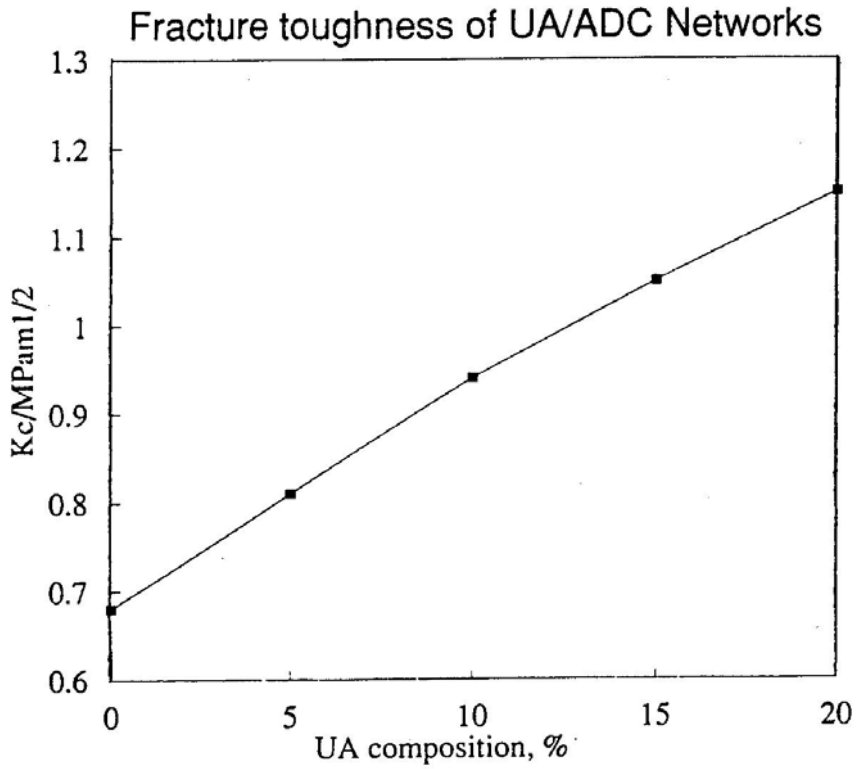

Figure 2.6. Fracture toughness versus UA composition.

2.2.4.1 Morphology and mechanical properties of interpenetrating polymer networks of CR-39 and poly(urethane).

Interpenetrating polymer networks (IPNs) are one of the fastest growing fields in multicomponent polymer materials [19]. IPNs were defined in the previous section as a combination of two or more polymers in a network form, in which at least one of them was synthesized and/or crosslinked in the immediate presence of the other. When both polymers are polymerised and crosslinked simultaneously with non-interfering modes, such as step-wise and chain polymerisation, the IPN is known as a simultaneous interpenetrating network (SIN) [20]. Most IPNs involve heterogeneous systems, with one phase elastomeric and the other phase glassy. This combination of elastomeric and glassy networks allows IPNs to range in properties from filler-reinforced elastomers to rubber-reinforced (high-impact) plastics, depending on which component becomes the continuous phase. Some attempts have been made to improve the fracture toughness of CR-39 polymer by introducing simultaneous interpenetrating networks (SIN) based on CR-39 resin and polyurethane (PU) [20]. Trimethylolpropane (TMP) was used to form the SIN based on CR-39 and PU to improve the interfacial bonding of the two networks. It has been found that the fracture toughness increased as the PU composition of the SIN was increased. It was also found that the enhancement of fracture toughness of the SIN with the increase in strength of the PU phase as the TMP content increases as shown in figure 2.7. It can be seen that the fracture toughness slightly decreases at very high TMP content, possibly due to a decrease in the toughness of the PU phase. Alternatively it may be attributed to the very large size of the domains, which have a relatively small interfacial area and so less interlocking between the two phases.

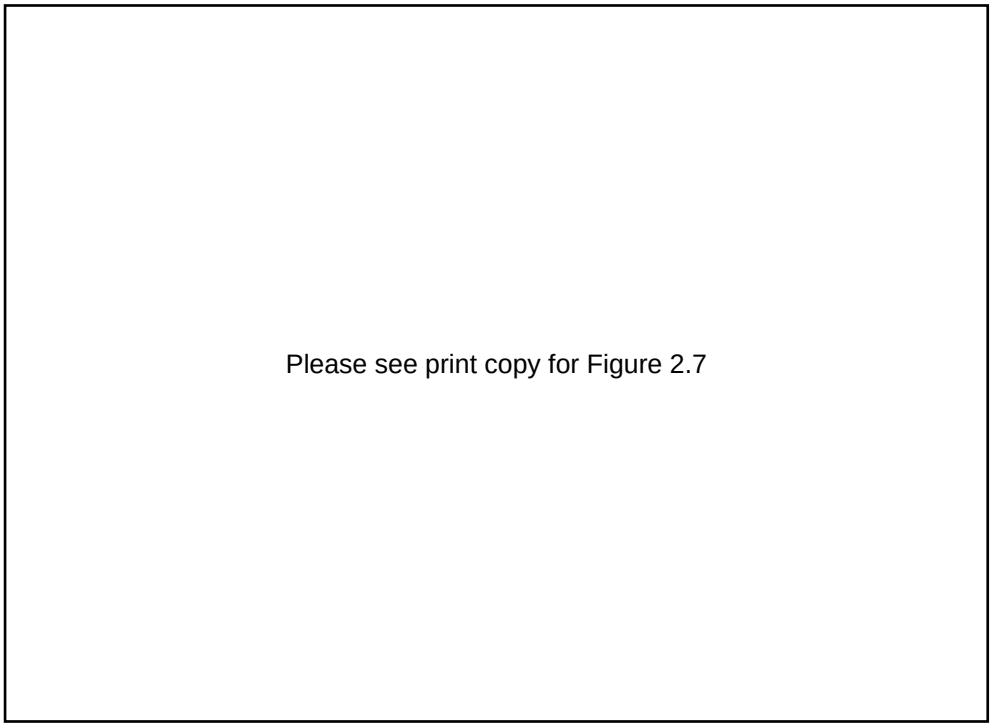

Figure 2.7. Variation of stress intensity factor K_c of PU/CR-39 SIN as a function of TMP.[20]

It was found that the final morphology of simultaneous interpenetrating polymer networks of polyurethane and CR-39 was a function of synthesis conditions. The extent of phase separation was dependent on the relative rate of formation of both networks. In samples where the formation of the PU network occurs well ahead of the CR-39 gelation, extensive phase separation resulted. It was found that the spongy morphology of discrete PU domains was not effective in toughening the CR-39 matrix. These samples showed poor mechanical properties, whilst in samples where the formation of both networks is nearly simultaneous or the CR-39 gelation is faster than PU networks, a fine co-continuous or very fine dispersed morphology was obtained. The toughness of these samples was moderately higher than neat thermoset glassy CR-39 resin due to increased ductility of the matrix [21].

2.2.5 Mechanical properties of CR-39 composites

In many classes of glassy polymers, much of the macroscopic response of the material is controlled by crazing [22]. When crazing occurs under well-controlled conditions, as in high impact polystyrene blends, it provides a mechanism of inelastic deformation improving the material toughness. The incorporation of a rubbery phase into a brittle polymer matrix has long been recognised as a means to significantly toughen the material. The area of application of filled plastics could be widened considerably if their fracture toughness can be improved [23]. The highly cross-linked micro-structure of network polymers often leads to low resistance to crack initiation and propagation. It is important to increase the toughness of these materials without causing any major loss in their other desirable properties such as high modulus, high strength, and high glass transition temperature. This section describes the fracture toughness of CR-39 composites by the addition of a rigid interface such as thermoplastic polymer or nano-sized silica particles.

2.2.5.1 Rigid thermoplastic toughening CR-39 polymer

The most common method to improve on the toughness of thermoset polymers involves the addition of elastomers. However the rubbery inclusions often lower both the modulus and the glass transition temperature. The use of rigid thermoplastics as tough, ductile polymers as an alternative method of toughening thermoset resins has had varying success in recent years. It is envisaged that network polymers based on this method may be toughened without negatively affecting their other useful properties. The prevalent method in producing a thermoplastic second phase is to

first dissolve the thermoplastic polymer into the thermoset monomer and later allow it to phase separate during the network formation process of the thermoset resin.

Blends of the thermoset poly (allyl diglycol carbonate) (CR-39) with thermoplastic polymethacrylates have been prepared by dissolving polymethacrylates in CR-39 monomer [24]. The aim was to investigate the effect of use of rigid thermoplastic on the fracture properties of CR-39 polymer in order to find a way to enhance fracture resistance of this thermoset material.

Two grades of poly (methyl methacrylate) (PMMA) Elvacite 2009 and Elvacite 2021, and one grade of poly (ethyl methacrylate) (PEMA) Elvacite 2042, were dissolved in acetone and then mixed with the CR-39 monomer. Acetone was evaporated at room temperature and a viscous transparent solution of polymethacrylates in CR-39 monomer was obtained and cast into a glass mould by the injection of the solution and the temperature was slowly increased from 50 ^{o}C to 85 ^{o}C over a period of 21 hrs. The flexure modulus, E, and fracture toughness, K_c, were determined using an Instron tensiometer, at room temperature. The flexure modulus was measured in the three point bending device while the fracture toughness was evaluated from the critical stress intensity factor K_c using single edge notched tensile test specimens. Table 2.3 shows the mechanical properties of the CR-39 blends with 5% and 10% (w/w) thermoplastic polymers of PMMA and PEMA. It has been found that the flexure modulus was slightly increased from 2.4 GPa in the CR-39 polymer to 2.6 GPa in the blends containing thermoplastic polymer. It can be seen that the fracture toughness was significantly increased resulting from PEMA blends. The fracture toughness improvement can be attributed to the contribution of the PEMA, which is more ductile than the rigid PMMA thermoplastic polymer. In rubber-toughened resins, the toughening is due to the yielding of the cross-linked

matrix resin. The rubber-toughening mechanism becomes progressively less effective as cross-linked density is increased. CR-39 is a highly cross-linked polymer which will not permit adequate yielding, thus, the toughening mechanism in the blends appears to depend upon the ductile drawing of the thermoplastic component polymer. PEMA, which is a rigid ductile thermoplastic, was shown to play an effective toughening role in the blends.

Table 2.3. Mechanical properties of the CR-39 polymer blends. [24]

Please see print copy for Table 2.3

2.2.5.2 Nano-sized silica particles toughening CR-39 polymer

Rigid particulate fillers such as silica, alumina or glass spheres have been used in thermoset resins such as epoxies and unsaturated polyesters to obtain a higher stiffness and fracture toughness. In particulate-filled resins, hard particles can improve the fracture toughness by crack pining, deflection of the crack front, including plastic deformation in the matrix surrounding the particle, or fracture of the particle.

The composites of CR-39 resins (an excellent optically transparent glassy thermoset plastic) with a submicron-particle size silica, Aerosil, have been examined to investigate the properties of the resulting nano-composites[25]. Two types of Aerosil silica were mixed with CR-39 monomer. Aerosil 200 and Aerosil 300 with average particle size of 12 and 7 nm and particle surface area of 200 and 300 m^2/g

respectively were mixed and stirred at 1000 rpm with CR-39 monomer to obtain a uniformly dispersed suspension [25]. The maximum concentration of Aerosil that could be dispersed in CR-39 was about 4% by weight. Above this concentration the viscosity of the mixture was found to be extremely high, forming a water-clear gel. The suspension was then transferred to glass mould and polymerised in a heating cycle to obtain transparent samples with a low degree of haze. Fracture toughness was evaluated by measuring the critical stress intensity factor K_c obtained using single-edge notched bend (SENB) and single-edge notched tensile (SENT) tests. Although both SENT and SENB test specimens were used, the trends for both were identical and only the results for the SENB specimens were reported as listed in table 2.4. The results show that all three measured mechanical properties increase in the composites as compared to the CR-39 resin. Whilst the tensile strength and flexure modulus increased only marginally the fracture toughness of the 2% Aerosil 200/CR-39 composite showed an increase of 20% as shown in table 2.4. It was also found that the glass transition temperature and modulus of composites were relatively increased. Finally it was revealed that extremely fine particles (nano-sized) were not as effective in toughening thermoset glassy polymers as were large micro-sized particles.

Table 2.4 Mechanical and fracture properties of CR-39/silica nanocomposite. [25]

Please see print copy for Table 2.4

2.2.6 High impact resistance for a new ophthalmic lens material

Various characteristics are required of transparent synthetic resins as ophthalmic lenses. Of these, the refractive index is quite important. Lenses made from materials having high refractive index can be thinner than those from materials having a low refractive index to give same focal distance and can advantageously make lightweight lenses. Impact resistance is also important and advantageous for plastic lenses compared with brittle glass materials.

Diethylene glycol bis (allyl carbonate), poly (methyl methacrylate), and polycarbonate are the materials most commonly used in plastic lenses. However, the diethylene glycol bis (allyl carbonate) and poly (methyl methacrylate) resins have low refractive indices of 1.49-1.50 [26]. When these resins are shaped into plastic lenses, a center thickness, an edge thickness, and curvatures of the lens become great compared with those of inorganic optical glass lenses. The polycarbonate resin has a relatively high refractive index of 1.58-1.59 [27], but it is prone to birefringence in shaping and, thus, is defective in optical homogeneity. Moreover, because the poly(methyl methacrylate) and polycarbonate resins are thermoplastic resins materials and not crosslinked, they tend to fuse in processing such as in cutting or grinding. They have not been satisfactory as a material in the field in which such processing are required.

Research to produce a new ophthalmic lens material having excellent ophthalmic lens performance [28] has been described. This ophthalmic lens material was produced by radical polymerisation of a mixture of a bifunctional methacrylate, such as tetraethylene glycol dimethacrylate or triethylene glycol dimethacrylate, a styrenic

monomer such as styrene, and acrylonitrile. The bifunctional methacrylate ethylene glycol dimethacrylate was also examined as a crosslinker but it showed poor impact resistance because of its short crosslinking distance between two double bonds. Tri(ethylene glycol) dimethacrylate (3EG), and tetra(ethylene glycol) dimethacrylate (4EG), which have a longer chain between two double bonds, are expected to have higher impact resistance because of the increase of the flexibility. Table 2.5 summarizes the results of the physical properties and impact strength of the ophthalmic lenses produced by monomer composition using 4EG and 3EG compared with diethylene glycol bis(allyl carbonate) (CR-39) [28]. It was found that a composition containing more than 40% EG could give a quite large impact resistance. In bulk polymerisation of the dimethacrylate, unpolymerized vinyl groups were left as pendant double bonds. These residual pendant double bonds may play a role in giving the high impact resistance when a large amount of 4EG was copolymerised. Finally, it was found that the best monomer composition for ophthalmic lenses contains of 4EG to produce a polymer with excellent impact resistance, a high refractive index and other optical properties.

Table 2.5 Ophthalmic lens materials produced by 3EG and 4EG monomers [28].

Please see print copy for Table 2.5

2.3 APPLYING A COMPRESSIVE STRESS INTO THE SURFACE AND FRACTURE TOUGHNESS

2.3.1 Applying compressive stress into glass surface

Glass is one of the oldest materials manufactured by man as documented by samples many thousands of years old. However, because of its brittle nature, the use of glass has been limited to non-structural applications. It is well known that glass is strong under compression and weaker in tension. The presence of sub microscopic flaws, (Griffith, 1920), has been shown to account for premature fracture.

Since glass always fails in tension due to the surface microflaws, there are two obvious courses of remedial action; (i) Prevent/remove the microflaws and protect the surface, (ii) Create a compressive stress on the surface which must be overcome before the glass can break in tension [29].

The removal of surface microflaws on large glass articles by careful etching is not practical in that flaws would probably be reintroduced during the application of the protective coating. Even if this did not occur a single penetration of the coating could lead to catastrophic failure of the article [30]. Most attempts to improve the strength of the glass have revolved around the production of a layer of material at the glass surface that is under compression. It has been found that the compressive layer must be extended beyond the depth of the microflaws before effective strengthening can be obtained.

In glass science ion exchange has been used to strengthening the glass surface. The principle ion exchange or “stuffing” technique was first described in (1962) [31].

Soda-lime-silica glass was treated in melts of KNO_3 at a temperature below the glass transition temperature of the glass and a considerable compressive stress was found to be generated at the surface. Since that time the greater part of the literature relating to strengthening of glass has been devoted to the ion exchange method [31].

Some research has been done on strengthening the glass lenses in the ophthalmic industry. It has been found that glass lenses can be strengthening by either of two processes, heat-tempering and chem-tempering. A number of investigators found that chem.-tempered lenses had much more resistant to breakage than heat-tempered lenses under similar test conditions. Hence thinner and lighter lenses can be made by designing a chem-tempered process to give lenses with a better fracture resistance than can be obtained by toughened by a heat-tempering process.

It was found that the stress profile in thermally tempered glass was roughly parabolic in shape as shown in Figure 2.8. It can be seen that the maximum compressive stress, which occurred at the glass surface, is approximately twice the tensile stress in the center. The compressive stress layer produced by chemical strengthening glass is relatively thin as shown in figure 2.8 [30], and thus the balancing tensile stresses are small compared to those in thermally toughened glass. Chemically strengthened glass therefore does not break up into small fragment upon fracture unlike thermally toughened glass which produces small, relatively blunt fragments on fracture. Though chemical strengthening is more versatile and produces higher stresses than thermal strengthening it is also considerably more expensive and is only used where its cost can be justified, for example in the production of windows for spacecraft or in the strengthening of intricate ware.

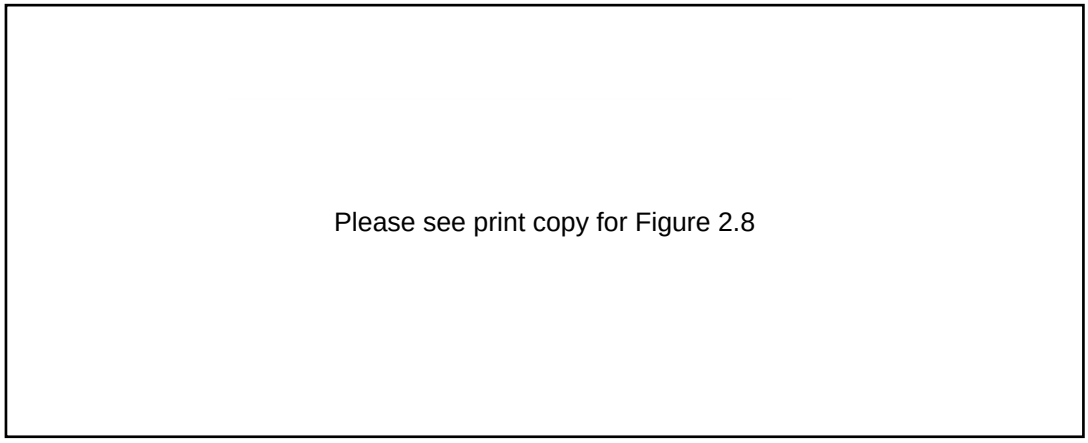

Figure 2.8. Stress profiles in thermally and chemically tempered glass.[30]

2.3.1.1 Effect of the ion exchange to the crack formation resistance

Mechanical characteristics of solids are frequently determined by the state of residual stresses in the near surface region, and this state may be changed by the chemical and thermal treatment to which the material was subjected. In general, the state of stresses in a near-surface layer of a material can be determined by using the Vickers diamond indenter [32], [33]. The Vickers hardness number and the crack-formation resistance were determined for soda-lime silicate glass subjected to chemical treatment in an $AgNO_3$ bath. The ionic exchange was performed in a thermostatic bath of fused salts for 2 hours at a temperature of 673 K stabilized within 1 K; on average, 2% $AgNO_3$ was diluted in 98% $NaNO_3$. The effectiveness of the induced $Na+ \rightleftharpoons Ag+$ ionic exchange process was modified by thermal annealing of the exchanged specimens in air and gaseous hydrogen.

It has been observed that that the hardness number VH, was slightly increased for the treated specimens. The cracks were initiated at relatively low indentation loads from

the glass surface and continued to develop during unloading. The crack formation resistance Pc increased from 1.5 N to about 2.1 N for the exchanged specimens, and the largest value of Pc was found to be 2.7 N for freshly exchanged specimens additionally annealed for 10 minutes at 400 ^{o}C in a gaseous hydrogen atmosphere. The crack formation resistance Pc decreased to 1 N for prolonged annealing for 15 hours at 550 ^{o}C. It was concluded that in the ionic exchanged glass, the stresses in a near-surface layer were generated mainly due to differences in the ionic radii of the ions taking part in the exchange process. These stresses were found to be tensile for smaller ions and compressive for larger ones.

The chemical treatment of soda-lime silica glass was studied for the $K^+ \rightleftharpoons Na^+$ ionic exchange. It was found that this exchange induces large compression stresses in the near-surface layer, and these stresses were relaxed at temperature well below the glass-softening point but well above the room temperature. Although the ionic radius of silver ($R_{Ag} \approx 1.26$ Å) was almost equal to that of potassium ($R_K \approx 1.33$ Å), the strengthening effect induced by silver was unexpectedly small. This was thought to be related either to some extraordinary properties of the silver-exchanged system or to some limitations of the models proposed by the fracture mechanics. Nonuniform distribution of silver particles (evidenced optically), related to the high electronic polarizability and high diffusivity of silver, resulted in smaller distortion of the matrix and thus in a smaller increase in Pc. It was found that silver fits the glass structure without producing large internal stresses. It was also found that the diffusion coefficient of silver was changing continuously within the glass volume.

2.3.1.2 Ionic migration effects on the mechanical properties of glass surfaces

It is well known that the mechanical properties of glasses are dependent on their surface state [34]. It has been found that the ionic migration process can be induced by external electric field. Such migration produces ionic modification at glass surfaces [34]. Alkali ions, as Na+ in soda-lime glasses, can drift under the influence of the electric field leaving a layer depleted of sodium ions in the glass close to the anode. Samples of soda-lime silicate glass with 1.2 mm thickness were prepared for the ionic migration process. Two kinds of electrode were used: (a) thermal evaporated vacuum deposited silver metal films on the glass; (b) aluminium plates pressed against the glass samples. Using aluminium plates as electrodes, hydrogen ions penetrate into samples substituting for alkaline ions. With deposited silver films as the electrode, Ag+ ions penetrate into the glass substituting for Na+ ions in the depleted region. The hardness of the ionic modified surface was measured using the nanoindentation technique. Surface residual stress induced by the ionic migration was calculated by the measurements of the radial crack lengths generated by the Vickers indentation, using the lengths obtained for the modified and the pristine surfaces [34]. The results were summarized in table 2.6.

Table 2.6 Residual stress for the samples submitted to ionic migration[34].

Please see print copy for Table 2.6

These results show that the presence of an internal hydrogen layer produced a tensile residual stress at the sample surface. A compressive stress was observed as a result of Ag+ ions layer near the anode region. It was also observed that the residual stresses for glasses with ionic migration performed using silver film electrodes increases with the thickness of the layers modified by Ag+ ions. For the samples with hydrogen ions replacing Na+, the residual stress decreased with the depth of the modified layer.

It is well established that the surface hardness increases if the surface is under compression and decreases if the surface is submitted to tensile stress. Analysing the hardness and residual stresses for the samples on which the electric field was applied using aluminium plates, a residual tensile stress and a decrease in the hardness of the affected region were observed. For the samples with penetration of silver ions, no alteration in hardness was observed when comparing the region modified by ionic migration with a virgin sample. It was expected the hardness would be larger in this region since a compressive stress was dominating the modified surface.

Figure 2.9 shows the hardness as a function of tip penetration depth for the samples in which the electric field was applied using silver deposited electrodes. The results for the samples with modified layers with depth of 1 and 3 μm were presented in figure 2.9. It can be observed that the hardness of the modified samples was relatively lower than the virgin sample. In theory the residual stress was calculated assuming the substitution of a Na^+ ion, with radius of 0.098 nm, by an Ag^+ ion with radius of 0.12 nm gave 320 MPa. Some stress relaxation occurred after the penetration of the Ag^+ ions as the measured value of the residual stress was found to be 142 MPa. The measured residual stresses could be attributed to the relaxation of the stresses caused by the growth of existing flaws in the glass.

It seems that the potassium-exchanged system can improve the fracture toughness of the glass more efficiently than silver as cited in reference [34]. The article on potassium ion exchange was not obtainable. For this reason, the silver system was described in this section as an example of improving the fracture toughness of the glass by the ion-exchange technique.

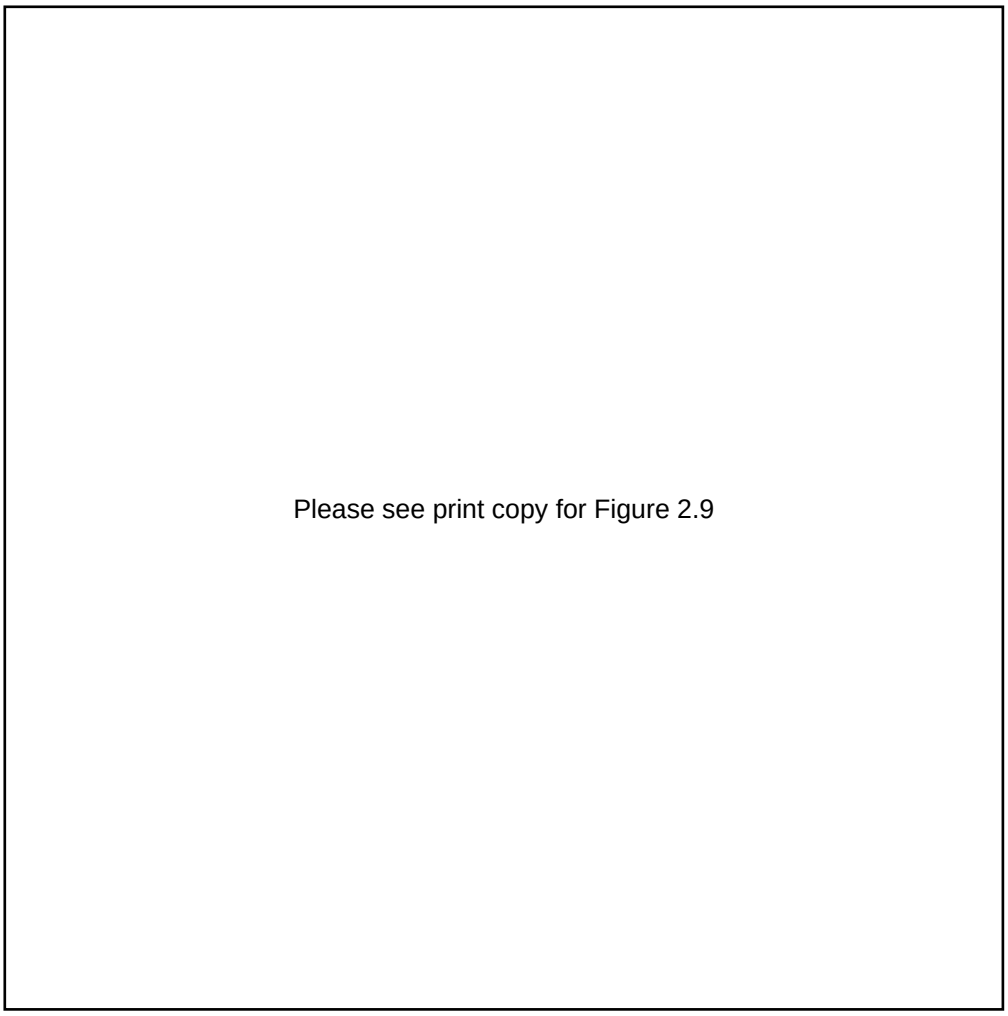

Figure 2.9. Hardness as a function of tip penetration, obtained by nanoindentation, for glass samples submitted to ionic migration using silver films as electrodes[34].

2.3.2 Applying compressive stress into ceramic surface

Chih-Hung [35] made a layered composite by using two different materials as the outer layer and inner core. This layered composite was fabricated by slip casting and pressureless sintering. A compressive stress was generated on the outer surface because of the difference in coefficients of thermal expansion between the constrained inner core and outer layer.

Chih-Hung [35] showed that the layered composites exhibited greater strength, apparent fracture toughness and damage resistance due to the presence of compressive surface stresses in the layer. It was found that the compressive stress is proportional to the normalized inner core thickness (the ratio of inner core thickness divided by the overall thickness). The higher normalized inner core thickness ratio obtained a larger apparent fracture toughness and damage resistance due to the formation of higher compressive surface stresses. It has been found that the influence of residual stresses is apparent on the crack size. Figure 2.10 shows indents on outer surfaces of layered composite and a monolithic sample respectively. It has been shown for an indent load of 500 N, crack size in the layered composite sample and monolithic sample were respectively 0.22 and 0.34 mm. It was assumed that the crack pattern is mainly influenced by the stress state not by the flaws on the surface because of the outer layer thickness is much bigger than the depth of the flaws. The size of the compressive residual stress in surface layer was measured by the Vickers indentation method. The measured compressive stress was found to be 311 MPa for a Si_3N_4-TiC layered composite with a 250 μm thickness of the Si_3N_4 outer layer.

Figure 2.10 shows SEM micrographs of the Vickers indentation using a load of 500

N on the surface for the un stressed monolithic sample and composite stress layered sample.

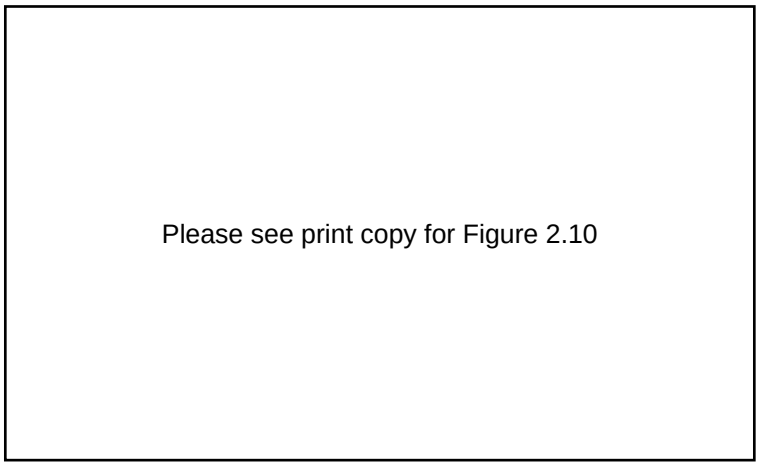

Figure 2.10. SEM micrographs of Vickers indentation of a load of (a) un stressed monolithic sample and (b) composite stress layered sample[35].

2.3.3 The Generation of compressive stresses into the ceramic by the surface oxidization.

Over the past few years, the thermal-shock strength behaviour of non-oxide ceramics such as silicon nitride (Si_3Ni_4) and silicon carbide (SiC) has been extensively investigated using the water-quenching technique [36], [37], [38]. In general, the water-quenching thermal-shock tests were performed in an air atmosphere by quenching the heated specimens into a water bath. To establish thermal equilibrium before quenching, the specimens were held at the desired high temperature for a certain period of time. Some oxidation on the surfaces of non-oxide ceramics may occur. It has been shown that such an oxidation can increase the mechanical strength by blunting or healing surface flaws [39], [40], [41]. Thermal-shock tests were conducted on Si_3N_4 specimens of 36 mm (length) × 4 mm (width) × 3 mm

(thickness) dimensions using a technique developed by Vandeperre and co-workers [42]. As shown schematically in figure 2.11 [43], the specimen was covered with mullite blocks on all sides except one (36 mm × 4 mm). After heating in air at a rate of 5 ^{o}C/min to a preset temperature and holding at this temperature for 30 min, the specimen was quenched into a water bath at 20 ^{o}C.

The first set of thermal-shock experiments, the tensile surface was exposed to air, the quenched specimens were denoted as AE. In the second set of thermal-shock experiments, the tensile surface was protected from air by covering the top side of the specimen with an additional mullite plate, which separated automatically from the specimen in the quenching process.

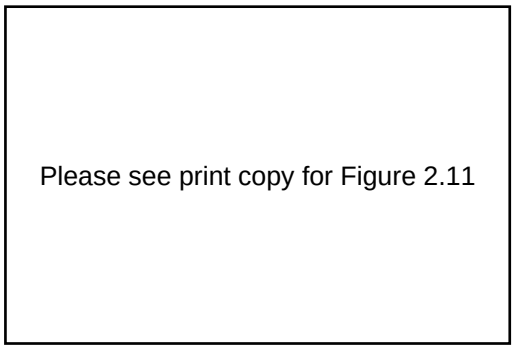

Figure 2.11. Schematic diagram of test arrangement used for thermal-shock experiments[43].

The quenched specimens with the "air unexposed" tensile face were designated as AU. The residual strength of the quenched specimens was evaluated at room temperature using a three-point bending test with a support distance of 30 mm a crosshead speed of 0.5 mm/min. Figure 2.12 [43] shows the residual strengths of the AE and AU specimens after quenching from different temperatures, with respect to the oxidized specimens AE2. It can be seen that the strength of the AU specimens remained almost constant up to 600 ^{o}C, and then decreased gradually with the

increasing severity of thermal shock.

On the other hand, it was interesting to notice that the AE specimens showed a 16% and 29% increase in strength after quenching from 800 ^{o}C and 1000 ^{o}C, respectively. This was considered to be a consequence of surface oxidation before quenching, as evidenced of a similar increase in strength for the oxidized AE2 specimens. The increase in strength of the oxidized specimens could be attributed to (i) the healing of surface cracks, and (ii) the generation of surface compressive stresses, which can compensate for the tensile thermal stresses on the surface of the specimens during quenching process. Hence, a significant increase in the mechanical strength was observed.

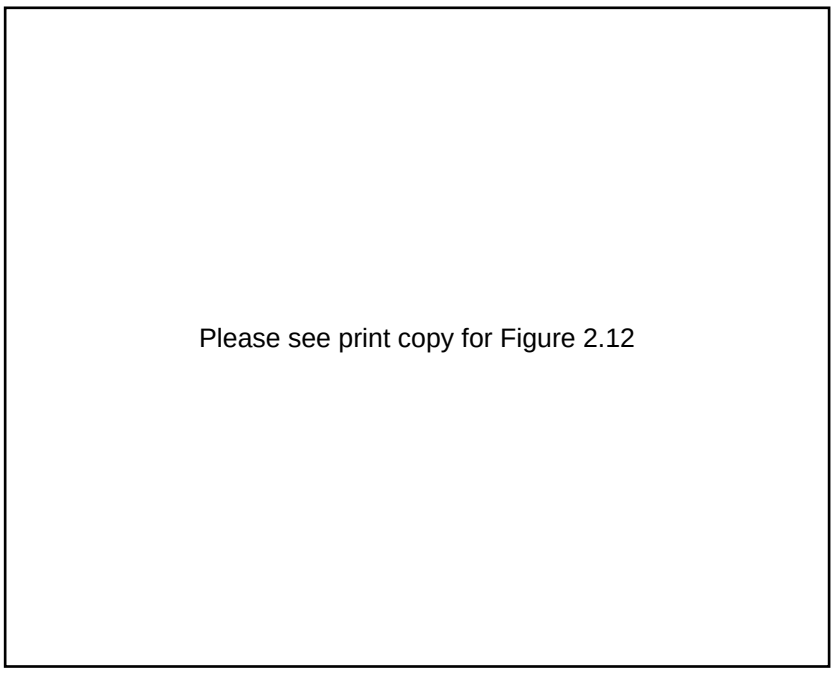

Figure 2.12. Effect of thermal shock on the fracture strength of Si3N4 ceramics. Solid diamonds represent the AE2 specimens oxidized at the stated temperature, whereas the open and closed circles represent the AU and AE specimens quenched from the states temperature, respectively[43].

2.3.4 The Generation of compressive stresses into the bioactive material

Apatite-containing glass-ceramics are bioactive and thus potentially important for the development of materials suitable for surgical implantation, such as artificial dental roots, artificial bone and joint replacements [44]. In addition to bioactivity, high mechanical strength is required for the above applications.

Glass-ceramics in the system MgO-CaO-SiO_2-P_2O_5 have been found to meet these requirements. It has been found that the above glass-ceramic system can be strengthened by two-step heat treatment [44]. Glass-ceramics samples which were nucleated at 710 to 790 ^oC and crystallized at 850 ^oC for 5 hours showed a fairly high bending strength of 250-410 MPa.

It had been noticed that the strength level (250-410 MPa) of this glass-ceramic material was relatively higher than other not toughened apatite-containing glass-ceramics materials (50-88 MPa). The high mechanical strength of these glass-ceramic materials was attributed to the generation of the surface compressive-stress which was closely related to the growth of surface layer with lower average thermal expansion than that of the materials in the bulk regions.

Changes in the glass-matrix composition, resulting from the growth of surface-nucleated apatite crystals, induced the formation of a secondary crystalline phase, as a layer from the sample surface.

A compressive stress can be generated by introducing a phase with lower coefficient of thermal expansion into the surface region. Therefore, upon cooling, the core of the glass-ceramic contracted more than the outer shell, creating a compressive stress in the plane of the surface. [44].

It can be concluded from the above literature review that the compressive stresses can be generated into the surfaces of glass, ceramics, and bioactive materials. These compressive stresses could enhance the fracture toughness of materials and improve the crack resistance.

2.4 CR-39

CR-39 was first developed by Pittsburgh Plate Glass Company in May 1940 [45]. Columbia Southern Company in Barberton, Ohio was a subsidiary company to Pittsburgh Plate Glass Co. where the CR-39 resin was investigated. The team which worked to developed CR-39 resin gave a name of "Columbia Resins" for this project [45]. The team isolated compounds and identified them by code numbers. The 39th compound was the most promising because it offered unique characteristics. Other name of CR-39 resin was an allyl diglycol carbonate (ADC) monomer [45].

The first commercial use for CR-39 monomer during the second war world involved combining the resin with fibreglass to form a molded fuel tank for air craft. Another innovative use for CR-39 resin during the war was production of transparent tubes for use in aircraft. These tubes made of CR-39 resin replaced glass tubes which often shattered during the combat, spraying the fuel throughout the cockpit. When the war ended in 1945, the intention was to use CR-39 resin in non military applications [46]. The ophthalmic industry indicated some initial interest, particularly because of the material's resistance to impact. Until 1960, PPG's primary CR-39 resin sales were for flat sheet applications. As the optical industry gradually learned how to cast

lenses from CR-39 resin, and how to edge and surface these new lens, sales to the optical industry grew slowly but steadily until 1975 when more than 90 percent of Pittsburgh Plate Glass's CR-39 resin sales were to the optical trade [45].

The thermoset polymer, allyl diglycol carbonate (CR-39), is known as an excellent material for a number of industrial, medical and optical uses. This polymer has good optical clarity, structural stability and a high degree of resistance to heat, abrasion, impact and inertness to most chemicals [47].

Diethylene glycol bis (allyl carbonate), or 4, 6, 9, 12, 14-pentaoxa-1, 16-heptadecadiene-5, 13-dione, is a divinyl monomer known commercially as CR-39 resin (Columbia Resin 39 or Allymer 39).

2.4.1 Preparation of CR-39 monomer

Various methods are available for preparing diallyl diglycol carbonate monomer [48]. Commercially it is manufactured by reacting phosgene and diethylene glycol with allyl alcohol in the presence of an alkali such as sodium hydroxide to produce the diglycol carbonate monomer as shown in the following scheme, prepared by Solomon and Qureshi [48]. This monomer is polymerised by heating in the presence of a catalyst, such as benzoyl peroxide, to form the polymer.

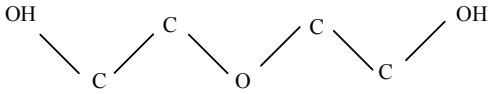

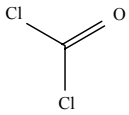

Diethylene glycol

Carbonyl chloride (phosgene)

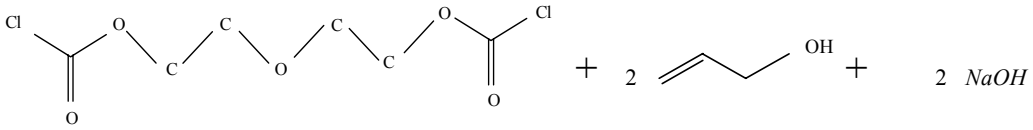

Diethylene glycol bis (chloroformate)

allyl alcohol

alkali
sodium
hydroxide

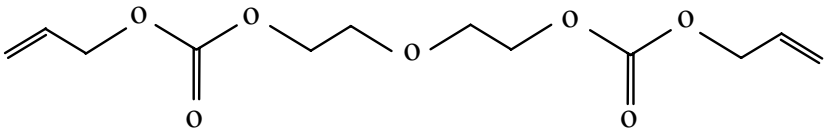

or

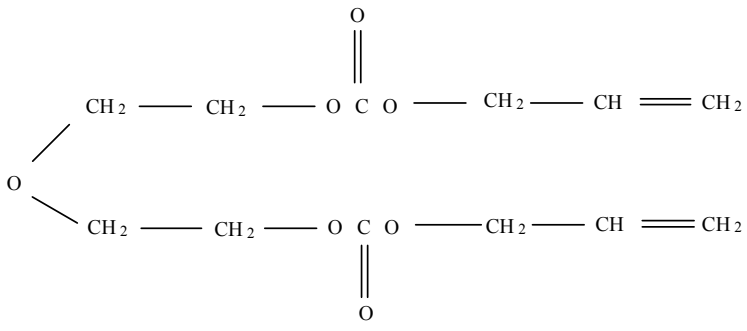

Diethylene glycol bis allyl carbonate (CR-39)

2.4.1.1 Curing CR-39 resin

CR-39 allyl diglycol carbonate has been widely used as a material for corrective eyeglass lenses due to its lightness, safety, and optical quality. Casting of the monomer must generally be carried out at relatively low temperatures (40-90 ^{o}C) and over a long period of curing time, nearly 1 day, because of the highly exothermic nature of the polymerisation reaction [48]. If the removal of the heat of polymerisation is not sufficient in the curing system, the polymerisation is accelerated vigorously. Eventually, the rapid curing fractures the lenses owing to the high shear stress. Glass moulds are often used to cast the CR-39 resin. However because of a shrinkage of about 14% in volume during polymerisation glass moulds often separate from the lens during polymerisation, if not it is sometimes difficult to detach the product from the mould after curing.

In the past, benzol peroxide was used to initiate polymerisation of CR-39 in a casting process [48]. The polymerisation using benzol peroxide was highly exothermic, and heating occurred leading to more rapid polymerisation and additional liberation of heat. Eventually, the rapidly curing mass fractures from the high shear forces developed and the polymerisation initiator was not used efficiently. The popular choice in industry today is a peroxydicarbonate because of its low colour and decomposition temperature. The progress of the polymerisation of CR-39 monomer has been investigated using diisopropyl peroxydicarbonate (IPP) as a thermal initiator to examine a relationship between the residual amount of allyl groups and the undecomposed amount of the polymerisation catalyst in a rising temperature process [49]. The CR-39 monomer and IPP (3.4% to the monomer) were used without purification. They were introduced together and polymerised at 40-90 ^{o}C for

24 hours. A practical advantage of using IPP over other catalysts was that it gave cast lens better colour tone and better colour stability. It was reported that the polymerisation of CR-39 monomer using IPP was usually carried out between 40 and 90 ^{o}C and the decomposition products of IPP were 2-propyl alcohol, acetone, and carbon dioxide (CO2). A residual amount of IPP was calculated as follows:

$$C_t = C_o e^{-kt}$$

where C_o *i*s initial concentration of IPP, C_t a concentration of IPP at t hours, and

$$\log_{10} k = 18.0 - (6.15 \times 10^3) / T$$

where T is the absolute temperature. The residual amount of allyl groups in the polymers was evaluated by Raman spectroscopy using a band intensity ratio of the allyl C=C and the carbonate C=O stretching mode. The amount of CO_2 decomposed from IPP catalyst was measured using a Raman band intensity ratio of the CO_2 vs. the carbonate C=O stretching mode. Figure 2.13 shows the calculated residual amount of IPP along a typical curing temperature curve, the residual amount of allyl groups, and the observed amount of CO_2. It can be seen that the decreased amount of allyl groups corresponded well to the decreased amount of IPP in the first half region of the curing process. In the latter half, the polymerisation did not proceed in proportion to the initiator decomposition because the migration of reactive monomer was difficult after gelation and the initiator decomposed much more at a higher temperature. Moreover, carbon dioxide was produced from further decomposition of the initiator radical and was stored in the polymer. At 90 ^{o}C, the residual amount of allyl groups remaining in the polymer was about 7%, and IPP disappeared completely. The inner temperature of the lens was slightly higher than the oven the oven temperature until 21 hours [49].

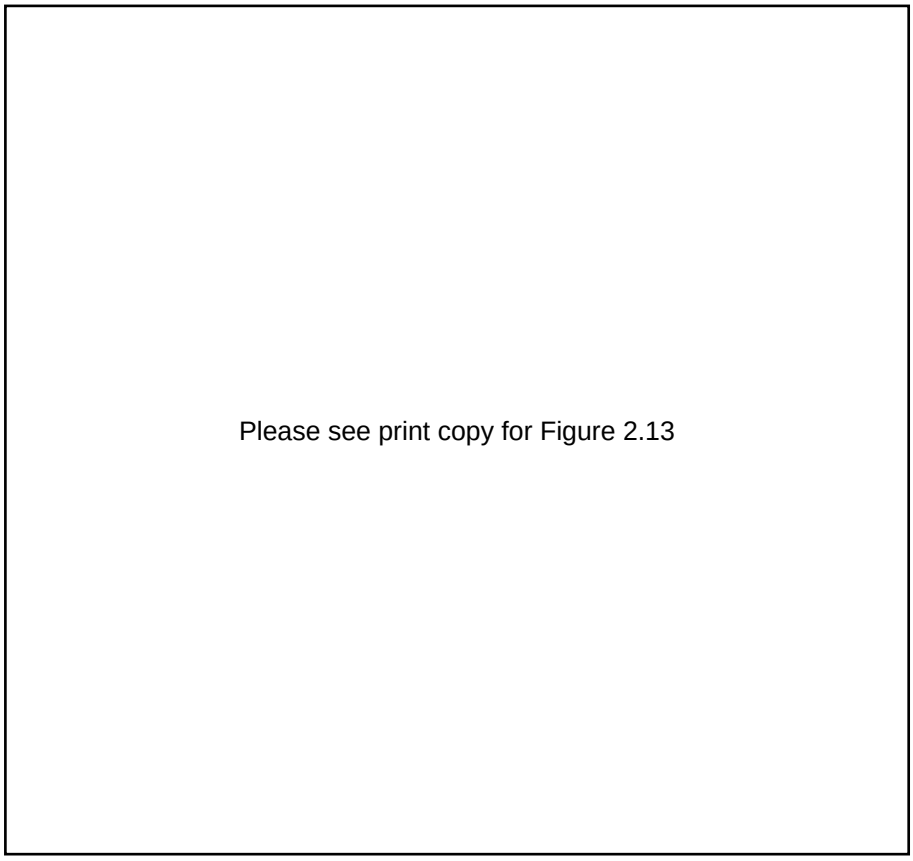

Figure 2.13. Curing time vs. residual amount of allyl groups, calculated residual amount of IPP, evolved amount of CO_2, and inner temperature of lens during polymerization along a rising temperature curve. [49]

2.4.1.2 Conversion of C=C bond in CR-39

The conversion of C=C bond in CR-39 has been studied by Sullivan and Donnell [50], and it was found that the use of CR-39 as an industrial monomer requires a very high conversion in polymerisation to obtain satisfactory mechanical properties and stabilise the product. It has been found that the polymerisation of CR-39 resin cannot be carried out isothermally because this would cause high temperatures throughout the reaction, an excessive rise in temperature due to the exotherm, and then void formation, cracking, and discolouration [50]. For these reasons a suitable profile of

temperature changes is used in commercial practice. The suitability of laser Raman spectroscopy for quantitative analysis over the entire conversion range was demonstrated during an investigation of the polymerisation of diethylene glycol bis allyl carbonate (CR-39) in bulk, with benzol peroxide as a thermal initiator. Figure 2.14 shows the polymerisation process for CR-39 performed to approximately 40% C=C consumption at 75 ^{o}C, after which the temperature was increased to 85 ^{o}C and the polymerisation continued to a 90% conversion [50]. It was concluded that the consumption of C=C reached at least 95% and the affect of the polymerisation temperature was ascertained. It was also found that the isothermal results can be combined to predict the behaviour of polymerisation when the temperature is increased in steps, during polymerisation.

It has been found [51, 52], that the residual un-polymerised allyl group (C=C) bond was affected by the type and amount of thermal initiator used to cure the CR-39. It was also found that different peroxide initiators yield networks with up to 100% conversion of allyl groups for curing CR-39 monomer. Four different peroxides with different decomposition temperatures were used: diisopropyl peroxydicarbonate (IPP), benzol peroxide (BP), tert-butyl peroxybenzoate (TBPB) and tetra-butyl peroxide (TBP). In a polymerisation process initiated by radicals such as curing CR-39, polymerisation was controlled by the rate at which the initiator decomposed. The temperature-time curing regime already established for a given initiator can be used to derive an equivalent curing regime appropriate for another initiator, provided that the temperature dependencies of their decomposition rate constants were known. Table 2.7 shows the curing temperature steps for CR-39 resin using these four thermal initiators. The density of cross-links and the associated glass transition temperature of a polymerising system steadily increases during curing to a point

where the glass transition temperature reaches the curing temperature. When this condition occurs the polymerisation rate slows dramatically and curing practically stops due to the restricted mobility of the polymerising groups.

Raman spectroscopy was used to examine the reaction of the allyl groups during the curing of CR-39 resin [51]. The reaction of CR-39 cured with (BP) and (TBPB) initiators was not determined because the Raman spectra exhibited a strong fluorescence. Figure 2.15 shows Raman spectra for CR-39 resin cured with two different thermal initiators (TBP) and (IPP). The absence of residual un-polymerised allyl groups in the sample cured with (TBP) initiator shows that curing under these conditions is complete. The glass transition temperature and the corresponding cross-linking density can be increased by curing at higher temperatures using optimal amounts of initiators active in a higher temperature range, and if the concentration of initiator exceeds that required for a full conversion of the allyl groups, the density of cross-links is reduced due to a decrease in the length of polyallyl chains.

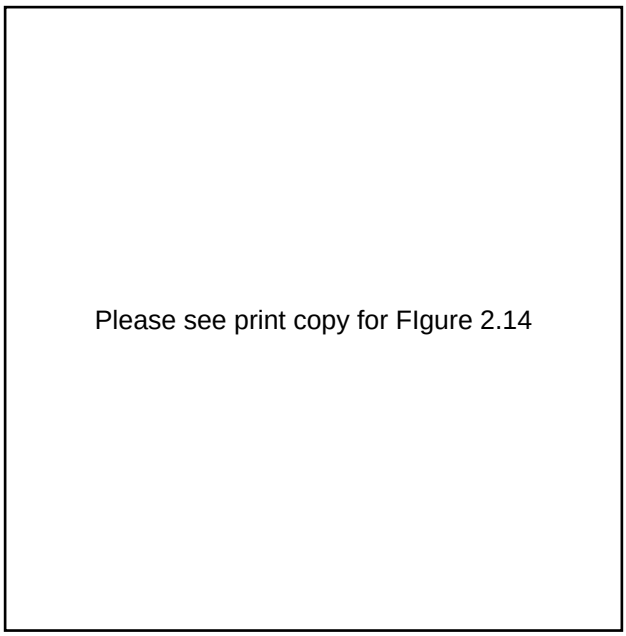

Figure 2.14. Conversion of C=C bond in CR-39 monomer at 75 ^{o}C (o) and 85 ^{o}C (•). [50]

Table 2.7. Curing regimes and glass transition temperatures (Tg) in the multi-step polymerisation of CR-39 for different initiators.[51]

Please see print copy for Table 2.7

Please see print copy for Figure 2.15

Figure2.15. Raman spectra of CR-39 monomer (1), cured CR-39 resin with IPP initiator (2), cured CR-39 resin with TBP initiator.[51]

2.4.2 Physical and mechanical properties of CR-39

The CR-39 monomer is moderately toxic and is know to cause skin irritations in some people [48]. The monomer is miscible with higher alcohols, for example, pentanols, and also ketones, esters, hydrocarbons, and many other organic compounds, but is insoluble in water, ethylene glycol, and glycerol. Unlike styrene and most acrylic monomers, diallyl esters such as CR-39 do not readily undergo thermal polymerisation when heated without radical catalysts. The CR-39 monomer has relatively good stability when stored, but some increase in viscosity of uninhibited monomer may be observed after several months. Typical properties of the CR-39 polymer castings are listed in table 2.8 [48]. The CR-39 polymer is resistant to common solvents and reagents but attacked by oxidizing acids.

Table 2.8. Physical and mechanical properties of clear full cured CR-39 polymer[48].

Please see print copy for Table 2.8

2.4.2.1 Mechanical properties of CR-39

The mechanical properties of CR-39 were investigated by [53] by forming a tensile specimen from a sheet of CR-39. The commercially obtainable sheets of CR-39 were cast-polymerized between glass plates, producing a highly transparent, hard, strong sheets. CR-39 sheet possesses an optical clarity equal to that of plate glass. It was found that a shrinkage of 14% in volume occurred when CR-39 polymerized. It has been found that the stress-strain curve of CR-39 is linear to about 3000 psi [20 MPa], with a definite decreasing of the modulus of elasticity above this value. Below 3000 psi, the modulus of elasticity is approximately 250,000 psi [1723 MPa]. Figure 2.16 shows the stress-strain curve for CR-39 where four specimens were tested. It was observed that the stress-strain curve was straight to about 3000 psi [20 MPa] with a definite decreasing of the modulus of elasticity above this value.

"Stress-to-Rupture" tests were carried out for tensile specimens at both room and elevated temperature to determine the relationship between stress and time-to-rupture. The highest strength values found in CR-39 were mainly in the range of 7000 to 7350 psi [48 to 50 MPa] and were obtained in short time (1 to 5 sec) fracture tests at room temperature.

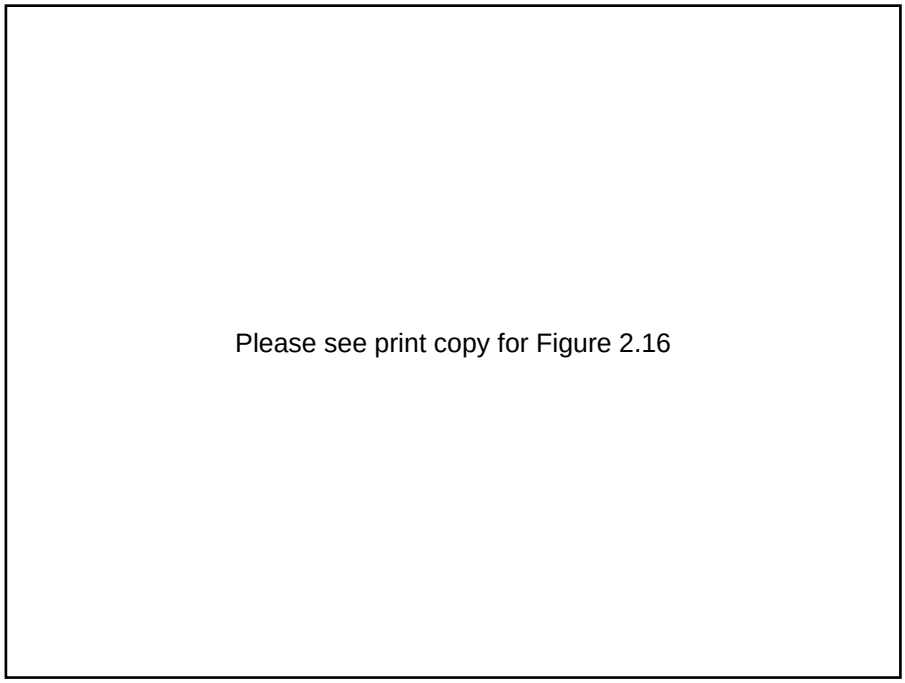

Figure 2.16. stress-strain curve for CR-39 [53].

2.4.2.2 Effect of annealing on CR-39

An attempt was made to increase the strength of CR-39 by a heat treatment process, the idea was to cause some further polymerisation and cross-linking in the three dimensional macro-molecular structure of the resin [53].

Two specimens were annealed for 1 hour at 120 ^{o}C and then cooled to room temperature to be prepared for tensile test. Both were broken in short time tests; one failed at 5730 psi, while the other failed properly at 6550 psi, which would indicate that the heat-treating had little if any effect on tensile strength. It was observed that too long an annealing process or too high an annealing temperature will produce disastrous results in sheet CR-39 in term of colour change and crack formation on the surfaces.

2.4.2.3 Stress-freezing in CR-39

Freezing method of stress analysis is where the fringes are locked or frozen into the model as a result of heat treatment. This method is not used in this project, however, stress-freezing in CR-39 is described briefly to evaluate the suitability of CR-39 for photoelasticity analysis, where this phenomenon is employed in chapter five.

The phenomena of stress-freezing was investigated in CR-39 by loading small beams with central concentrated loads and annealing them for 1 hour at 110 ^{o}C. After slow cooling to room temperature, these beams showed frozen stress patterns indicating a fairly high optical sensitivity at elevated temperature but without a large deformation that occurred in Bakelite BT-61-893.

A factor for use in comparing various plastics as to their suitability for three-dimensional photoelastic work was proposed by Hetenyi [53]. This factor considers the optical sensitivity of the resin at high temperature as related to its limit of proportionality and rigidity: "Suitability Factor" = $C = E\sigma / \eta^2$

where E is modulus of elasticity at elevated temperature, σ is the ultimate stress, and η is the stress-optical constant at elevated temperature.

It may at first be assumed that CR-39 would be a better material for three-dimensional photoelastic work than other polymers because of its high value of the suitability factor of 99.4. However, other difficulties were presented which would seem to rule out CR-39 for this purpose. The applied constant load must be kept low because of the large drop in strength at elevated temperature. The relatively high rigidity of CR-39 at elevated temperature, allows only small deformation, the measurement of which might be difficult and inaccurate. It was found that the "frozen stresses" in CR-39 changed appreciably in time, which would necessitate measurements in any specimen very soon after the annealing process.

2.4.2.4 Stress optical properties of Columbia resin, CR-39

The stress optical properties of CR-39 polymer were investigated by Coolidge [53] by forming a tensile specimen with a cross section of 1/2" × 0.215" (12.5×5.4 mm) in the region of pure tension was loaded in the field of the polariscope. The load was applied slowly and the increments measured between alternate maximum darkening and lightening in the shank of the specimen. It was found that the relationship between the fringe order and the stress-fringe is linear up to somewhere between 2500 and 3000 psi* ≈ (17 - 20 MPa), with a fringe value of about 8 as shown in figure 2.17. Optical creep was particularly noticeable after the seventh fringe, with the fringe order changing slowly at constant load. However, the stress-fringe relationship in CR-39 can be considered linear up to a stress slightly below 3000 psi (20 MPa), keeping the time factor constant in the loading cycle of a simple tension test. It was observed that the stress-optical coefficient can not be considered constant in CR-39 because of the relatively high optical creep as described by Cloud [54]. The stress-optical coefficient (Cg) value for CR-39 was found to be 37×10^{-12} Pa^{-1}** in pure tension test at 7th fringe order and stress value of 2500 psi (17 MPa) respectively [53].

In the stress range of 1000 to 3000 psi (7 to 20 MPa), in pure bending tests, optical creep amounted to about 11% after 15 minutes at constant load, 14% after 30 minutes, and 26% after 3 hours. The load was applied through holes along the neutral axis to produce pure bending in the central sections of the CR-39 beams of $\frac{1}{4}$"×1"×9" (6.3×25.4×228.5 mm) dimensions. It has been found that an increase in the fringe order at all values of fibre stress was the same at any time, which could be expected a proportionality between strain and fringe order and the cross sections of the beams remaining plane in bending.

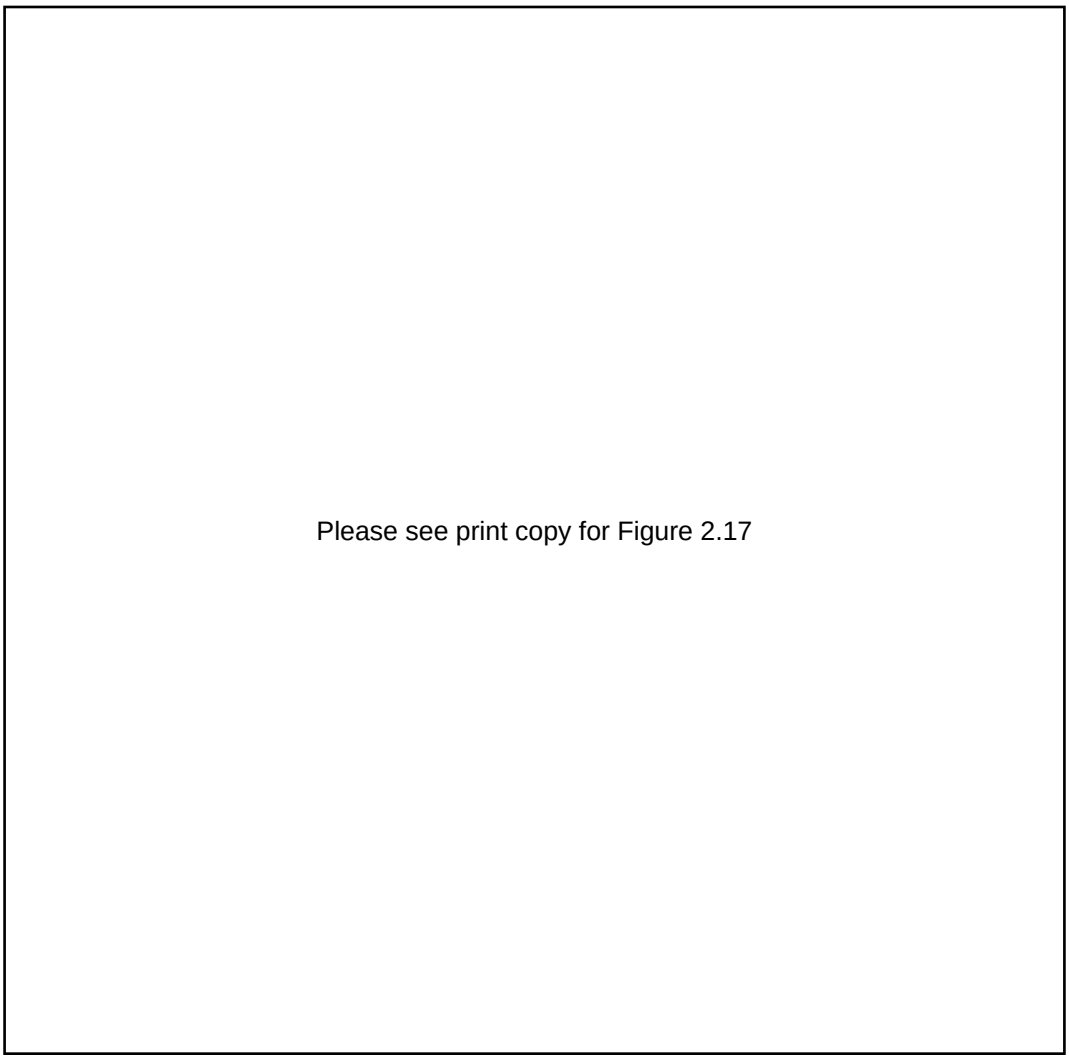

Figure 2.17. stress-retardation curve for CR-39.[53]

Stress-optical coefficient in the glassy state (Cg) of various polycarbonates were measured Shirouzu et al. [55] by attaching the tensile machine into a crossed transmitted light polariscope. The applied stresses and transmitted light intensities were measured as function of applied strain. It was found that the transmitted light intensity was zero when the specimen is optically isotropic i.e., no stress was applied,

because of the principal axes of the polarizer and the analyser were set perpendicular to each other. Birefringence was produced by the application of stress.

The amount of produced birefringence (Δn) is proportional to the applied stress (σ) provided that the stress is not too large, and the stress-optical coefficient in the glassy state (Cg) is defined as: $Cg = \Delta n / \sigma$

Different values of Cg were obtained for a various chemical structure of polycarbonates. The measured stress-optical coefficient values were in a range from 20 – 70 Brewster** [55]. Three possible mechanisms were considered of birefringence production by stress; orientations of constructive units i.e. CO bonds in each of the carbonate units of BisAPC polycarbonate, alignments of atomic groups and distortion of bond angles and bond lengths. Two mechanisms were observed in the polycarbonates, the first, in which the motion of constructive units produced birefringence. The second mechanism, in which constructive units cannot move at room temperature, causes distortion of the chemical bond length and angles, and may produce birefringence (during stressing) when the specimens are stressed.

*1 PSI = 0.0067 MPa

**Brewster is named for Sir David Brewster (1781 – 1868). It is a unit of stress optical coefficient, used by physicists studying how light passing through a substance is affected when the substance is put under stress. Symbol, Br. (1 Brewster = $10^{-12}Pa^{-1}$) [56].

2.4.3 Softening the CR-39 surface.

Thermoset polymer of allyl diglycol carbonate (CR-39) is known as an excellent material for a number of industrial, medical and optical uses [57]. This polymer has good optical clarity, structural stability, high resistance to heat, abrasion, impact, and inertness to most of the chemicals. Its hardness (Rockwell, M 95-100) is an advantage in many of its applications but restricts its use in certain other areas such as in making contact lenses because it causes mechanical irritation with the eye tissues, etc. Recently, it has been observed that the surface of CR-39 can be softened permanently by laser treatment without affecting its bulk properties [57]. This is an important phenomenon for two reasons. Firstly, it offers a unique method of softening of a thermoset polymer which by definition cannot be softened on heating. Secondly, irreversible surface softening of CR-39 increases the usefulness of this polymer in areas such as eye implant like contact lenses and artificial cornea, etc. It has been shown that a controlled irreversible surface softening can be obtained in the thermoset polymer of allyl diglycol carbonate (CR-39) without degrading [57] its bulk properties on treating it with a cw-CO_2 laser. A 125 W cw-CO_2 laser was used for treating the CR-39 sheets (1.6 mm thick, manufactured by SGL Homolite of U.S.A) [57]. The power density and beam residence time of the laser beam were designed to be adjustable during the treatment process of CR-39 sheets. Hardness of the CR-39 sheets was measured by using Vickers hardness tester. The pyramidal diamond tip of the hardness tester was allowed to penetrate vertically into the polymer under an optimum weight of 100 g for 35 second. The diagonals of the indentations on the laser treated and untreated surfaces were measured using a microscope. The surface hardness was measured, based on the fact that the hardness

is inversely proportional to the area of the indentation which is proportional to the square of its diagonal. The thickness of the laser softened surface was estimated based on the observation that the bulk etch rate of the treated polymer surface (about 50-200 μm/h depending on the treatment) was much higher than the untreated surface (1.2 μm/h). The depth of the treated region was thus estimated to be in the range of 8-30 μm when the fluence of the laser beam was varied from 10-40 J/cm^2.

It was noticed that the CR-39 samples treated at low fluences (up to 20 J/cm^2) appeared to be like the untreated samples with same optical clarity. Very shallow non-uniformities corresponded to the laser beam intensity distribution appeared at the surface of the samples treated at higher laser fluences. The transparency of the treated region was reduced gradually and the formation of a thin yellowish translucent layer took place, when the fluence was beyond that for volatile decomposition of CR-39. Laser treatment resulted in the formation of a heterogenous microstructure with interlinked polymer cluster and pores. It makes the treated surface coarse compared to the untreated one. The average size of a unit (polymer cluster or pore) in the heterogenous structure was found to depend on the power density and the residence time of the laser beam. In general, on increasing the laser fluence during the treatment, the size of the resulting microstructures increased. It was observed that the density of the clusters and pores was increased in the region of higher absorption and reduced where the absorption was relatively weak. These non-uniformities in the absorption were due to compositional irregularities in the polymer itself. Such non-uniformities were expected to change the local hardness at the treated surface correspondingly. The hardness of the laser treated surface was evaluated with respect to the laser power density at a constant beam residence time and vice versa. Variation of the hardness of the laser treated surface (HL) relative to

that of the untreated one (HN) with respect to the laser power density at a constant beam residence time is shown in figure 2.18 [57]. For fluence below the threshold for the volatile decomposition (25 J / cm^2), the hardness decreased rapidly on increasing the power density and beyond this threshold, the hardness tends to saturate. It was apparent that the surface hardness of CR-39 can be reduced to about 60% of its original value before the surface starts degrading due to the laser induced chemical decomposition beyond 25 J / cm^2.

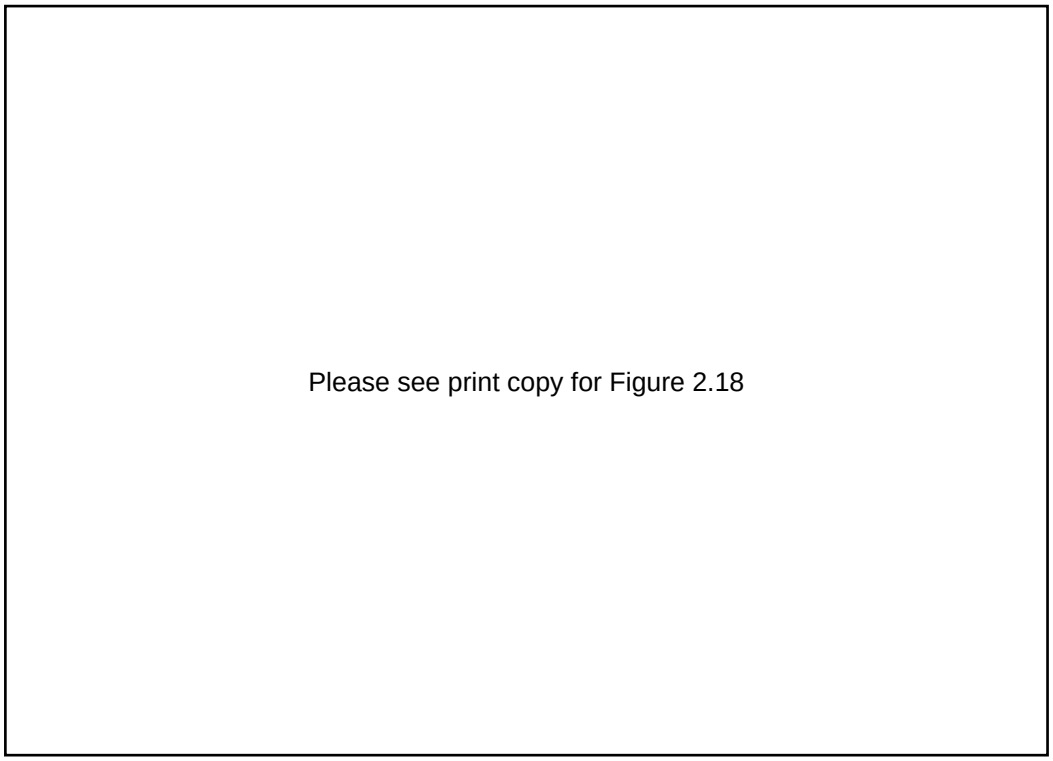

Figure 2.18. Hardness of the laser treated CR-39 surface (HL) relative to that of the untreated one (HN) at different power densities and a constant beam residence time of the CO^2 laser beam[57].

A similar effect of surface softening was found on the beam residence time dependence for a constant power density of the laser beam. Experimental values for the hardness of the treated surface at and below the threshold fluence for the softening could not be obtained because of practical limitations. The main limitation

was that at these fluences the thickness of the softened layer was found to be comparable or less than the depth of the indentation which the pyramidal tip of the hardness tester formed in the polymer.

Finally, it was concluded that the controlled laser treatment of CR-39 surface in the fluence range of 9-25 J/cm^2 resulted an irreversible softening at the surface without chemical decomposition in the polymer. The oligomers formed due to the laser induced depolymerization cool rapidly resulting in a heterogenous porous microstructure. The softening can be explained by dismantling the microstructure of CR-39 surface, in fact that the strong covalent bonds between the monomers were broken during the laser induced the depolymerization [57]. Once the volatile decomposition was initiated at (25 J/cm^2) the softening tended to be saturated and also the optical clarity began to be degraded. Therefore in the range of 9-25 J/cm^2 a useful surface modification of CR-39 can be done with a CO_2 laser.

In this current project, the surface of CR-39 lens was softened after exposing the lens to the UV light. It was first thought that the depolymerization effect occurred within the surface, but finally it was concluded that the softening occurred because of the plasticisation effect as discussed further in chapter 6.

2.4.4 Dynamic mechanical properties of homopolymers on CR-39

Polymers cast from diallyl monomers, particularly diethylene glycol-bis-allyl carbonate (CR-39), have found applications in many areas [58]. The properties of the final product were found to depend closely on the polymerization conditions, and the polymers form densely crosslinked networks that have better thermal and

dimensional stability than comparable thermoplastics. Benzoyl peroxide (BPO) was used as a thermal initiator to polymerise CR-39. The glass transition temperature (Tg) is the one of the most important properties exhibited by a polymer, determining its physical state and influencing other properties such as rheological characteristics, mechanical stiffness and toughness [58].

Dynamic mechanical analysis was used to investigate the changes in the dynamic mechanical properties in the glass transition region during homopolymerisation of diallyl monomers. A Perkin-Elmer DMA7 instrument employed in three point bending mode using a sample of approximately 3 mm diameter and 15 mm long. The CR-39 monomers were provided from two different original suppliers. Temperature/time scan was carried out at a frequency of 1 Hz. A heating rate of 5 K min^{-1} was used for a temperature/time scans. The maximum point of the tan δ peak was taken as a measure of Tg. Figure 2.19 shows the DMA curves of CR-39 samples polymerized to 95 % conversion. These samples were polymerized at 90 ^{o}C with 3 % BPO thermal initiator using CR-39 from two different suppliers. The peak at 95 ^{o}C in the DMA curves was assigned to glass transition temperature in the polymer. Figure 2.19 shows that there were no differences in the dynamic thermal properties of the resultants products of testing two samples prepared from CR-39 monomers provided from two different suppliers.

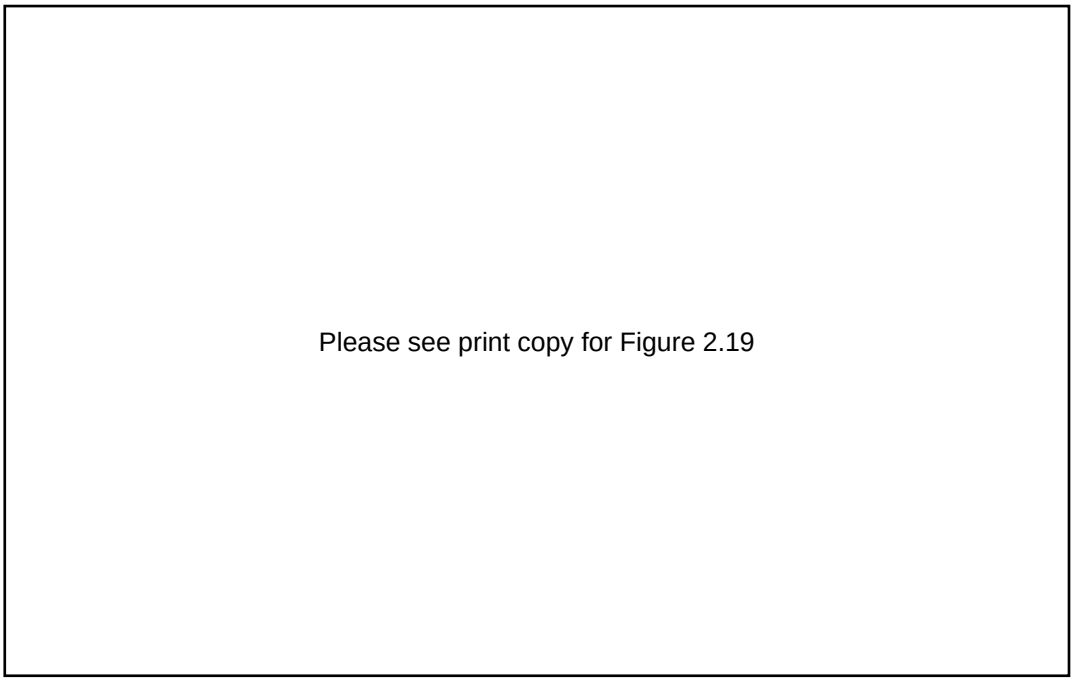

Figure 2.19. Tan δ versus temperature curves for two 95% polymerised CR-39 samples.[58]

Figure 2.20 shows the loss modulus curves for CR-39 samples cured under two different conditions. One sample was cured at 70 ^{o}C with 1.5 % BPO (slow cure) and the other was cured at 90 ^{o}C with 5 % BPO (fast cure). In both cases the conversion was 95 %.

After the first cure, the samples were heated to 110 ^{o}C to effect complete conversion. As was observed at low conversion, the sample cured at the slower rate showed a broad loss modulus, Tg relaxation curve, compared to the sample cured at the higher rate. This increase in the width of the loss modulus peak for the lower reaction rate may be due to an increased breadth of the network chain length distribution. A lower rubbery modulus was also observed at the faster cure rate. This was related to the formation of microgels in the early stages of polymerisation followed by formation of a macrogel via linking of these microgel regions. In fast cure systems, microgel

may have a higher crosslink density, thus a higher modulus was expected. However, the modulus of the composite was determined primarily by the modulus of the matrix phase, i.e. the macrophase. The macrophase of the fast cure system had a lower crosslink density, and thus a lower modulus.

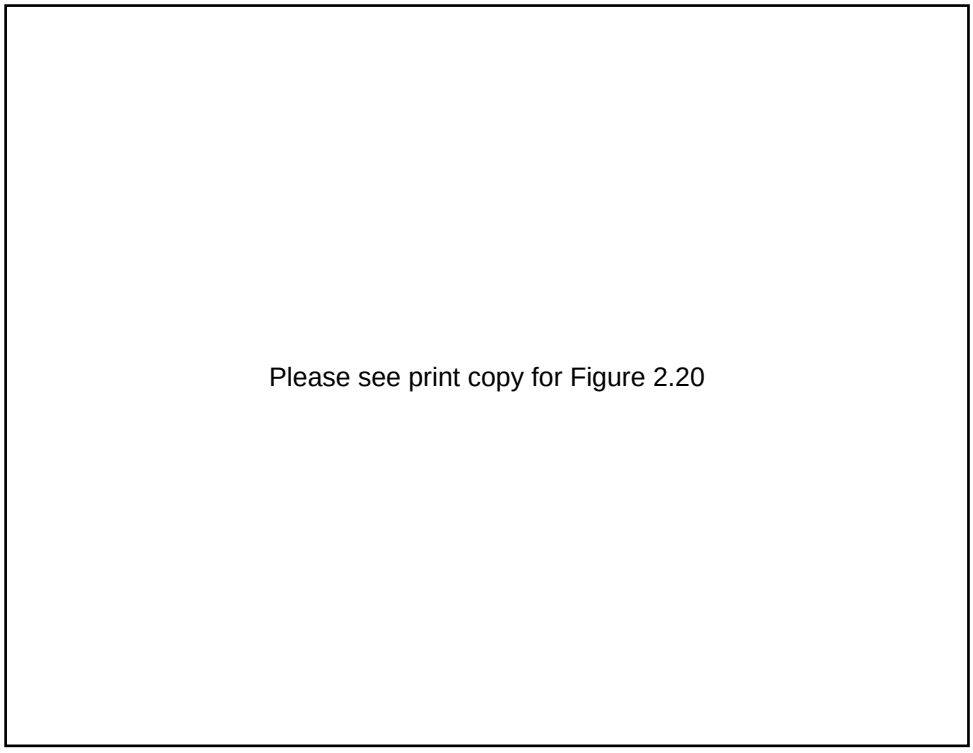

Figure 2.20. Loss modulus curves of the poly CR-39 cured at (a) 70 ^{o}C with 1.5% BPO and (b) 90 ^{o}C with 5% BPO.[58]

The plots of tan δ versus temperature for the reaction mixture of 1% BPO/CR-39 cured at 80 ^{o}C to different conversions are shown in figure 2.21. It can be observed that the samples exhibited a gradual increase in the width of tan δ curve with conversion, particularly after about 66% conversion. The broadening of tan δ had been explained as being due to the increased width of the network chain distribution. Therefore, the broadening of the tan δ curve should be due to heterogeneity introduced in the system. Beyond 66% conversion, the crosslinking was found to be heterogeneous.

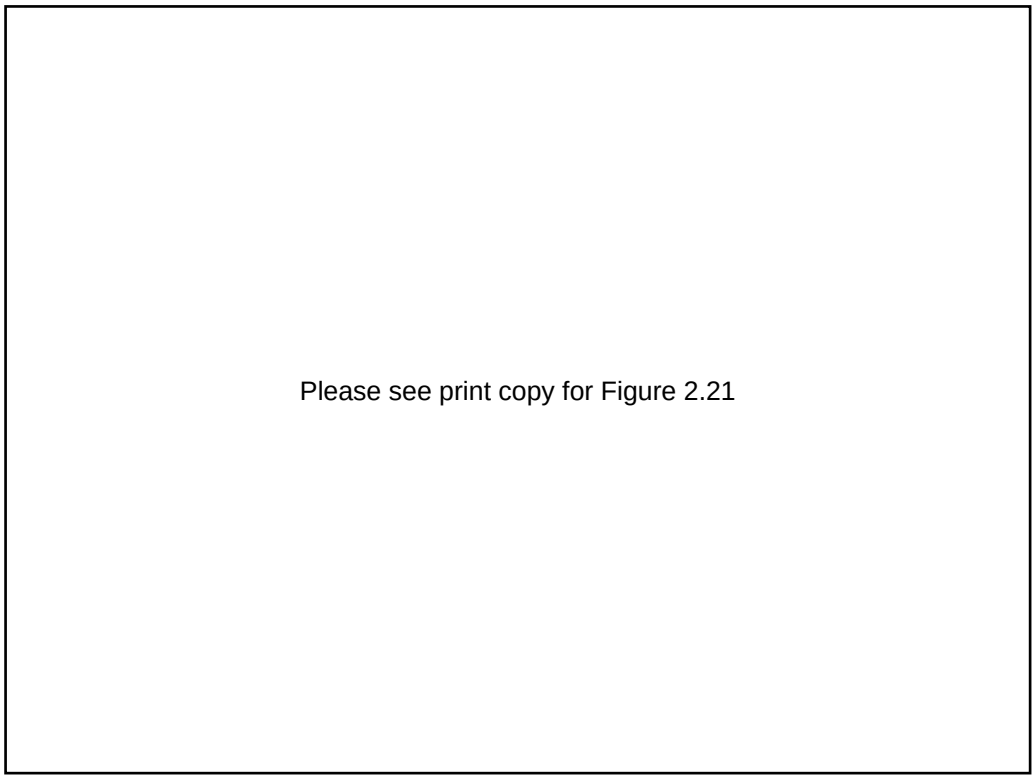

Figure 2.21. Plot of tan δ versus temperature of the samples of CR-39 cured to (a) 43%, (b) 50%, (c) 66%, (d) 87% conversion.[58]

It was found that the uncrosslinked CR-39 contains long side chains segments. These side chains contribute to the segmental mobility in poly CR-39. Even though in CR-39 the first crosslinked network (gel) begins to form at about 22-23% C double bond conversion, most of the long side chains remain free up to about 50% conversion, contributing to high segmental mobility in the polymer. It was found that the intensity of the tan δ peak at the glass transition temperature reflected the extent of mobility of the macromolecular chain segments at that temperature. Since crosslinks restricted main chain mobility in the polymer, one would expect that the area under the loss modulus curves versus temperature to increase with decrease in crosslink density. This trend will be reflected in the intensity of the tan δ peak.

Figure 2.22 shows the tan δ versus 1/Mc for homopolymerised CR-39. An increase

in the crosslink density reduces the tanδ. Two linear regions can be observed, an initial region characterised by a small slope and a second region where the slope was much greater, with the intersection between these two regions. Similar effects had been observed in other crosslinking systems, for example, in polypropylene glycol networks a decrease in tanδ max was observed at high crosslink densities.

It has been found that different network transition regions for fully polymerised homopolymer CR-39 can be identified by DMA analysis. Controlled, slow curing of CR-39 was shown to give networks which were homogeneous with higher crosslink densities in the macrophase than observed for rapid cure. During the homo-polymerisation of CR-39, the segmental mobility of the polymer remained unchanged until 60% of the double bonds were converted, but beyond this conversion the segmental mobility commenced to drop again significantly.

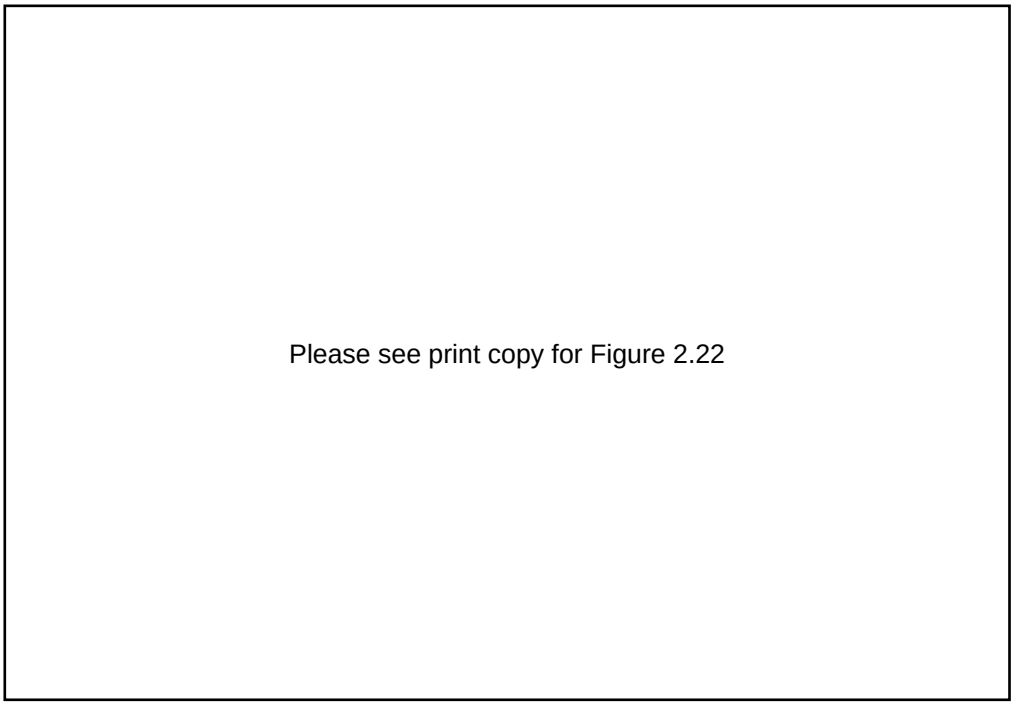

Figure 2.22. Tan δ max versus 1/Mc for CR-39 polymerisation.[58]

2.4.5 Indentation size effect of CR-39 polymer

Microhardness testing is a well established technique for assessing the resistance of materials to deformation. The deformation involved in the indentation process is related to abrasive scratching, wear and cutting. The hardness of the CR-39 was measured using a knoop indenter on a microhardness tester [59]. The diamond indenter was allowed to penetrate vertically downwards into the CR-39 circular disk sample under a range of applied loads for 5 seconds to form a plastic deformation on the sample surface.

The hardness, Hk, was calculated by the following formula [59]:

$$Hk = 14.229P / d^2$$

where P was the applied load on the indenter, and d was the length of the long diagonal of the indentation. It has been observed that the indentation zone does not follow the indenter shape due to elastic recovery underneath the indenter during the unloading process. Figure 2.23 shows Knoop microhardness as a function of the applied load.

An inverse indentation size effect has been described where the apparent microhardness decreases with decreasing applied load, for the materials such as, Al and germanium crystals (Ge) [60], [61]. An observation was reported of an inverse type of indentation size effect in CR-39. The inverse indentation size effect was explained by assuming a soft layer exists at the surface of CR-39. The hardness reaches a constant value of 150 MPa for indentation loads larger than 5 g [59].

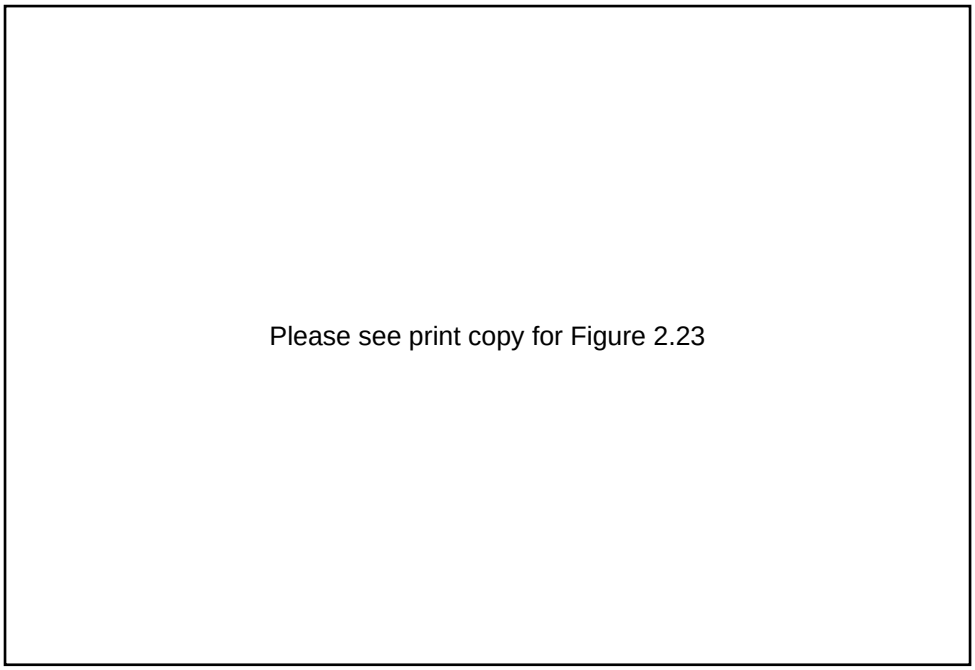

Figure 2.23. Knoop microhardness as a function of the applied load[59].

2.4.6 Relaxation and recovery measurements of CR-39

The Vickers hardness is defined as the ratio of the load to the true contact area. For metals (elastic/plastic material) the hardness gives an indication of strength (hardness equivalent to three times of the yield stress) of the metals [62]. For ceramics and glasses (elastic/fracture materials) developments in the understanding of indentation mechanisms and associated localized cracking for brittle materials has led to renewed interest in microindentation techniques for measuring the fracture toughness of these materials [63, 64]. For polymers (viscoelastic materials), the time-dependent viscoelastic properties are considered. It has been found that the indentation test for viscoelastic materials gives different results, depending upon whether the indentation

measurements were made after the load was removed or while the load was still applied [65]. However, it is useful to distinguish the significance of the two parameters: the ratio of the applied load to the deformed area is the measurement of hardness (H). Nevertheless, the ratio of the applied load to the deformed area after load removal is a measurement of surface resistance to damage (SRD), rather than hardness.

It was realized that, for transparent materials, the indentation process could be continuously observed from the other side of tested specimen. The time-dependent deformation properties of diallyl diglycol carbonate (CR-39) have been investigated and compared with another transparent polymeric material, poly(methyl methacrylate) (Perspex) [66]. For an indentation load of 150 g, figure 2.24 shows how the L/A ratio (load to area ratio) changes with time during the load-on and the load-off periods for both Perspex (P) and CR-39 (C). Each point represents measurements made from a separate photographs; the scatter indicates the experimental error in measuring the indentation areas. From the different shape of the curves, it can be seen that the relaxation characteristics of the two materials were quite different. The off-load region shows that the Perspex had greater surface resistance to damage (SRD) than the CR-39 and that whereas the recovery was apparently elastic for CR-39, the Perspex had both elastic and time-dependent viscoelastic recovery. The recovery upon removal of the indenter, was always qualitatively observed by the resultant “pin-cushion” shape, however, the indentation under load showed up another difference between the two materials tested. The indentation in Perspex always had a square outline under load, indicating that the surface around the indenter had remained flat, but for the CR-39 the indent outline under load was “pin-cushion” shaped, indicating that the material around the flat

faces of the pyramid had been pulled down during indentation. For metals this "shrinking-in" is associated with a capacity to work hardening [62]. It was observed that the indentation diagonals increased with time under load and decreased when the load was removed. Thus the conventional commercial Vickers hardness test must be considered inappropriate for such materials. Finally, It was concluded that the poly(methyl methacrylate) (Perspex) is more resistant to indentation and relaxes to a stable indentation state more quickly than CR-39. The recovery of CR-39 was almost entirely elastic, but for Perspex the recovery had a significant time-dependent component.

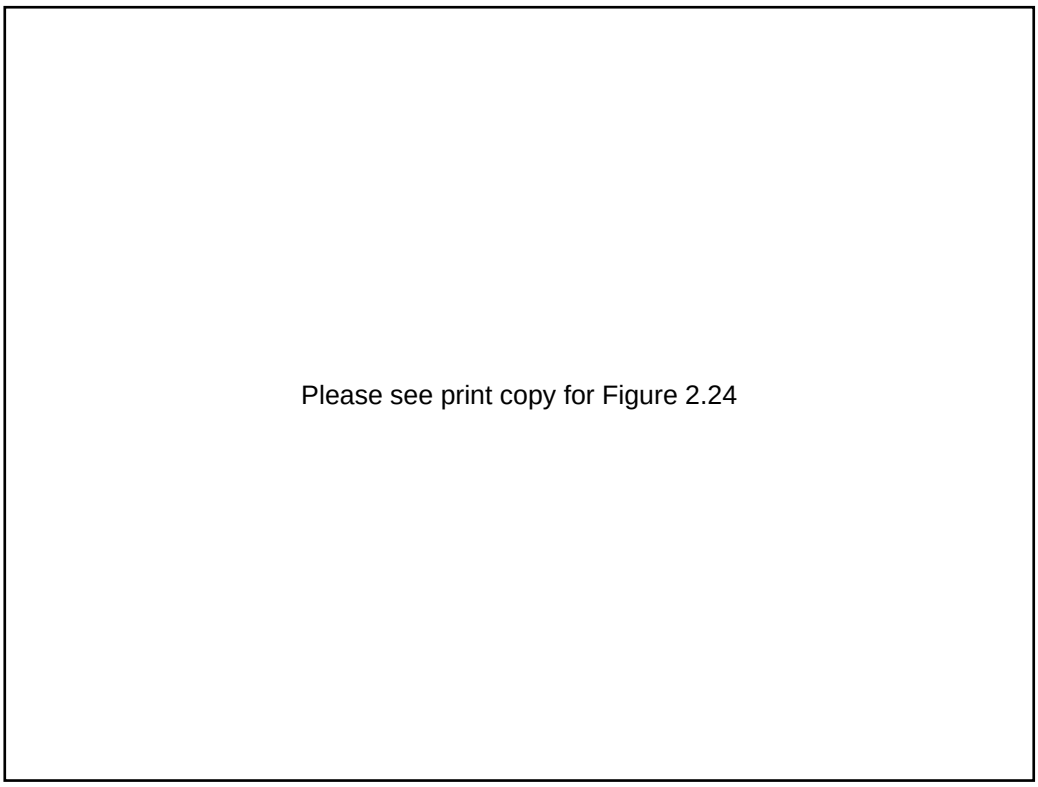

Figure 2.24. Variation of L/A with time for indentations in Perspex (P) and CR-39 (C), while the load of 150 g was applied and after it had been removed. [66]

2.5 CONCLUSIONS

It was found that diethylene glycol bis allyl carbonate (CR-39) is one of the common plastic materials for the ophthalmic lenses industry. It is considered to be brittle compared with polycarbonate. Its fracture resistance is greatly affected by its surface characteristics and applying coatings may reduce fracture resistance.

In epoxy resins rubber particles or glass fibers with an appropriate interface coupling agent can be used to increase toughness but such techniques cannot be used in CR-39 as they reduce the optical clarity of the material. In glass science the ion exchange or "stuffing" method is used to generate compressive stress on the glass surface. With ceramics materials, the slip-casting and thermal-shock techniques are employed to generate compressive surface stresses. However, no research or study was found which employed the positive effect of generating compressive stresses into a polymer surface. In this current project, the volumetric swelling technique has been investigated to generate compressive surface stresses into the CR-39 Plano ophthalmic lens.

The dynamic mechanical analysis showed that the values of $\tan\delta$ and loss modulus are dependent on the cure conditions of CR-39, which itself is correlated to the consumption of C=C bonds. An increase in Tg with conversion for homopolymerisation of CR-39 was observed. This increase in Tg contributed to the consumption of monomer and an increase in cross link density, which reduces the mobility of the polymer chains.

The micro hardness testing technique showed that CR-39 has a relatively soft surface with time-dependent deformation characteristics. The relaxation hardness of CR-39 and its resistance to surface damage was found to be rather lower than other transparent materials such as poly (methyl methacrylate). It was also found that the recovery of CR-39 was almost entirely elastic.

CHAPTER 3

Finite element modelling

3.1 INTRODUCTION

Finite element modelling originated as a method for analysing stress. In this chapter a quarter section of a lens will be modelled and a static load applied to the centre and distributed according to Hertzian formula. The load generates stress within the lens and it is this distribution of stress on the surfaces of the model that is presented in this chapter. Stress distribution in the x, y, and z directions will be analysed, and presented as a von Mises and hydrostatic distribution of stress. FEMCAD software [67] was chosen as an interface for mesh generation with the analytical modelling software (ABAQUS). The model generated from the FEMCAD software has been modified by changing the mechanical properties, constraints, and load application.

3.2 OBJECTIVES

The main objective of this chapter is to present theoretical modelling of the stress distribution analysis for a spherical lens with the same dimensions as the lens used in the impact test. Static loads were applied to the centre of the lens and distributed vertically up and down to analyse the dispersal of stress on the upper and lower surfaces. The load range was chosen so that when it was distributed onto the lens it would never reach values high enough for unstable deformation or fracture.

The model includes the volumetric swelling to the surfaces of the lens, to investigate the effect of swelling on the stress distribution on both the lower and upper surfaces in the presence of an applied load. The amount of the volumetric swelling should be relatively low, otherwise permanent deformation occurs.

The major aim of this chapter is to evaluate the stress distribution qualitatively within the convex lens when subjected to a central loaded zone and show how these stresses are affected by the volumetric swelling. There was no literature found that describe the qualitative stress analysis for the spherical lens subjected to a central load in the presence of the volumetric swelling.

In this chapter, the horizontal stress or the stress in the in-plane direction will be considered in detail in the stress analysis sections and, as the von Mises stress and hydrostatic stress will be used to model deformation, they are described in the next section.

3.3 THEORETICAL CONSIDERATION FOR A VON MISES AND HYDROSTATIC STRESSES

By convention all tensile stress components are considered positive [68], and therefore the three dimensional element shown in figure 3.1 is shown in a state of positive stress.

Two identical subscripts (e.g., σ_{xx}, σ_{yy}, σ_{zz}) indicate normal stress while a different pair (e.g., σ_{xy}) indicate shear stress. The nine stress components shown in figure 3.1 are reduced to six independent components because there are no rotational effects around any axis, so $\sigma_{xy} = \sigma_{yx}$, etc.

With elastic deformation, a stressed body returns to its original configuration if all the loads are removed. A particular level of stress, defined as the yield strength, must be reached to cause plastic deformation. Any yield criterion is a hypothesized mathematical expression of the states of stress that will induce yielding. The most general form of yield criteria is:

$$f\left(\sigma_x, \sigma_y, \sigma_z, \tau_{xy}, \tau_{yz}, \tau_{zx}\right) = \text{ constant C}$$

or, in term of principal stresses,

$$f\left(\sigma_1, \sigma_2, \sigma_3\right) = \text{C}$$

Von Mises [Hosford] criterion assumes that yielding will occur when some value of the root-mean shear stress reaches a constant. In a more general form, von Mises criterion can be written as:

$$\sigma_o = \frac{1}{\sqrt{2}} \sqrt{(\sigma_x - \sigma_y)^2 + (\sigma_y - \sigma_z)^2 + (\sigma_z - \sigma_x)^2 + 6(\tau_{xy}^2 + \tau_{yz}^2 + \tau_{zx}^2)}$$

While the hydrostatic stress is the mean of three principle stresses [69], it can be written as:

$$\sigma_h = \frac{1}{3}(\sigma_1 + \sigma_2 + \sigma_3)$$

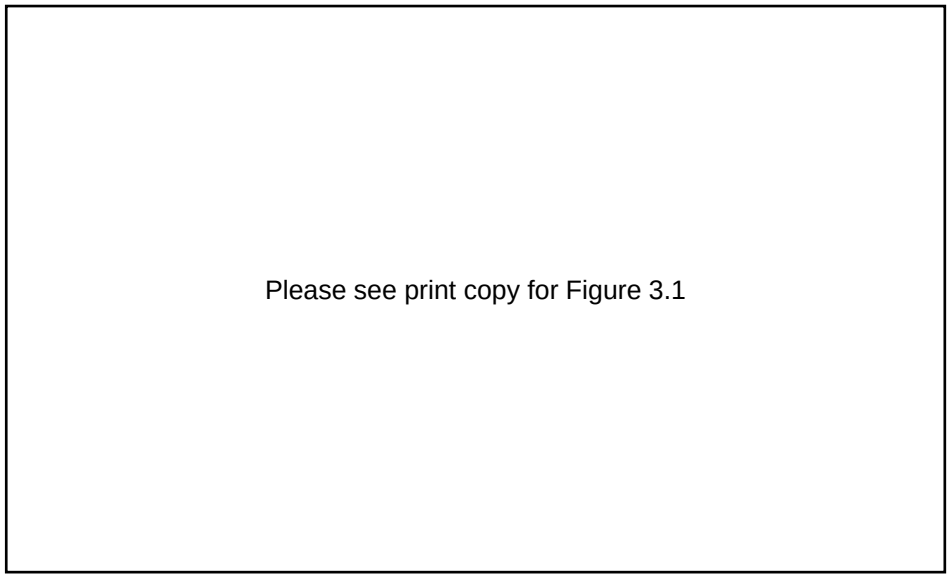

Figure 3.1. Stressed element for a homogeneous state of stress.[68]

3.4 MESH GENERATION

The first step in this finite modelling work was to build the lens geometry and apply a static load onto the top surface to identify the distribution of stress generated on the surfaces. FEMCAD software was used to generate the mesh that the finite elements model was built from, and the quarter section of the spherical lens was built using the 2D element type QUAD8, as shown in figure 3.2.

Each QUAD8 type element is a two dimensional, linear rectangular shell type with eight nodes defining each element topology.

Refering to figure 1.1 and for this lens, the 2.2mm thick concave surface and 87.2mm diameter was defined as the quarter section surface of lens geometry. It was assembled axisymmetrically in order to construct the volume geometry that defines the spherical optical lens, as shown in figure 3.3.

QUAD8 is one element for modelling an axisymmetric geometry, which has the

same property and specification as the CAX8 type element in ABAQUS software [70], but with the added advantages of producing a smooth mesh and deforming when a load is applied. The mesh was modelled uniformly throughout with 7 elements dispersed through the thickness of the lens.

120 elements were used along the radius bringing the total number of elements from which the lens was built to 840, as shown in figure 3.3.

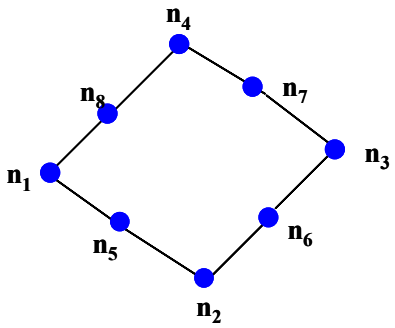

Figure 3.2. QUAD8 element for mesh generation.

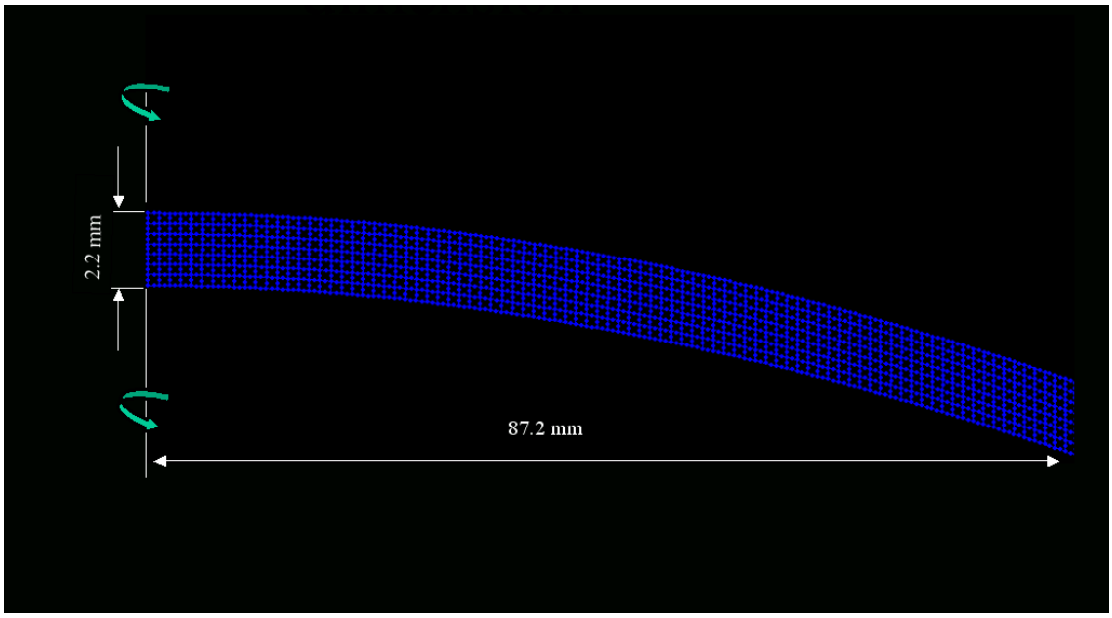

Figure 3.3. Standard mesh model in x and y directions and the horizantal depth (z-axis) in the rotation direction

3.5 CONSTRAINTS AND LOADS APPLICATION ON THE TOP SURFACE OF THE LENS

The spherical lens was mounted on the 25.4 mm diameter mount as specified by the FDA standard (the US food and drug administration) [11] during the actual impact test. In a real impact test the original lens deformed elastically until fracture occurred. To confirm that the model reflects the behaviour of the lens material, uniaxial tensile tests were conducted on a 2mm thick sheet of CR-39 polymer. Figure 3.4 shows the stress-strain curve for the film of CR-39 polymer. This strip of CR-39 polymer deformed almost elastically until it fractured without any apparent plastic deformation occurring.

The designed model was mounted with one degree of freedom constraint. Two constraints were used to support the lens in the y-direction. The first one is represented by the mount radius (C1) and the second one (C2) was placed at the end of the lens to hold it steady, as shown in figure 3.5. The centre of the lens is supported by constraint (C3) to permit free movement in y-direction only, which is representing the axisymmetric model.

The elastic parameters chosen for the generated model were a uniform Young's modulus of 2.5GPa and Poisson's ratio of 0.3 respectively [71, 72]. The static load was distributed in the centre of the lens according to the Hertzian theory of elastic contact [73], as shown in figure 3.5. The static load was 1.35 KN which corresponded to the maximum fracture load for the dynamic impact test provided from SOLA Optics. This load was applied to the modelled lens as a pressure load. The pressure load was applied vertically to the middle of the 8-nodal element on the top face of the elements and then distributed onto 7 elements according to the

following Hertz elastic contact equation:

$$P = p'\{1-(r/a)^2\}^{-1/2}$$

where p' is the distributed pressure of the distance a from the centre of the spherical deformable body with a curvature radius of r.

The load P applied onto the upper surface of the lens as a static pressure distributed in the central region of the lens.

The highest pressure of 218 (MPa) was applied to the first top element which corresponds to the centre of the lens. Static pressure was reduced to 210, 192, 163, 108, and 36 MPa on the next five elements away from the centre, reaching zero on the seventh element, as shown below in figure 3.5.

In a qualitative basis for a circularly supported plate loaded in a central region, the lower surface will be subjected to a tensile stress while the upper surface is under a compressive stress.

Theoretically the maximum tensile stress that resulted in the lower surface can be evaluated approximately using a number of different assumptions. Blake [74] has defined the stress in the centre of a circular plate subjected to a large deflection generated by a central uniform load as:

$$S = F(\delta,t)E\frac{t^2}{R^2}$$

where F is a function of the deflection δ and thickness t for a circular plate having the radius R and the modulus E. Using Blake's assumption and the measured maximum displacement of 6 mm [12], the stress in the central point of the lens was calculated and found to be 450 MPa.

The maximum tensile stress that occurs at the centre of the lower surface of the lens can also be determined using the equation derived from elementary theory of bending by Timoshinko and Woinowsky [75]:

$$\sigma_{\max} = \frac{P}{h^2}\left[(1+\nu)\left(0.485\log\frac{a}{h}+0.52\right)+0.48\right]$$

where P is the applied load on a simply supported circular plate having thickness, h and Poison's ratio ν, in which a is the outer radius where the plate is supported. Using the above equation, the maximum tensile stress was found to be 456 MPa on the lower surface.

The third approach to evaluate the maximum stress generated on the lower surface is by determining the maximum bending stress from the maximum bending moment as derived by Young [76]:

$$M_{\max} = \frac{W}{4\pi}\left[(1+\nu)\ln\frac{a}{r_o'}+1\right]$$

where W is a uniform load over a small central circular area of radius r_o' of a circular thin plate simply supported on a circular mount of radius a . The maximum bending stress can then be calculated by using the maximum moment as:

$$\sigma_{\max} = 6M/t^2$$

where t is the thickness (2.2 mm), and the radius of the loading zone (r_o' = 4.3 mm) that is equivalent to the distance between each element (0.725 mm) multiplied by the actual number of loaded elements (6 elements). The stress at the central region thus was calculated and found to be 319 MPa.

The above calculations of the stress using different formulae and assumptions, have been made so that comparison can be drawn with the result obtained from the numerical modelling work that is presented in the following section (3.7.1).

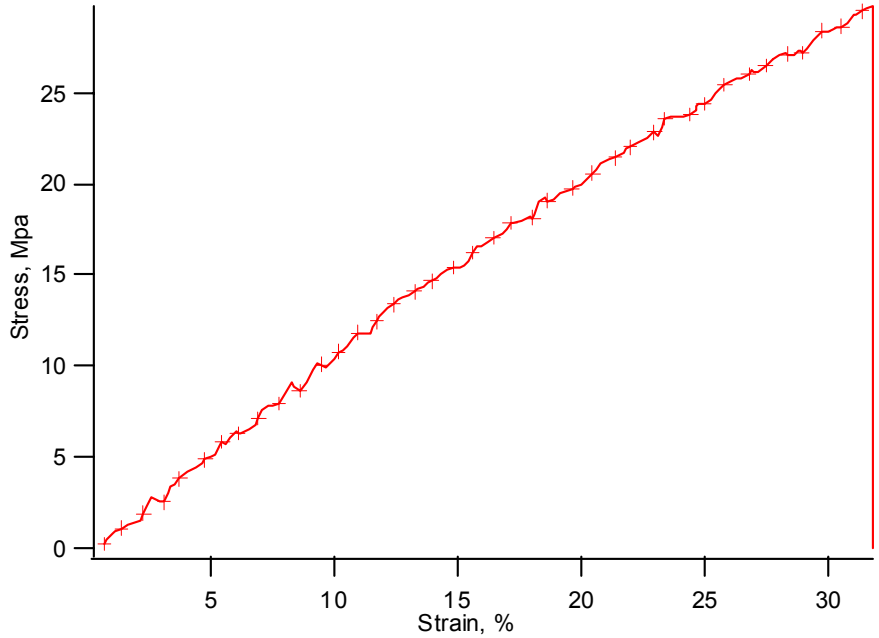

Figure 3.4. Uniaxial tensile test for the CR39.

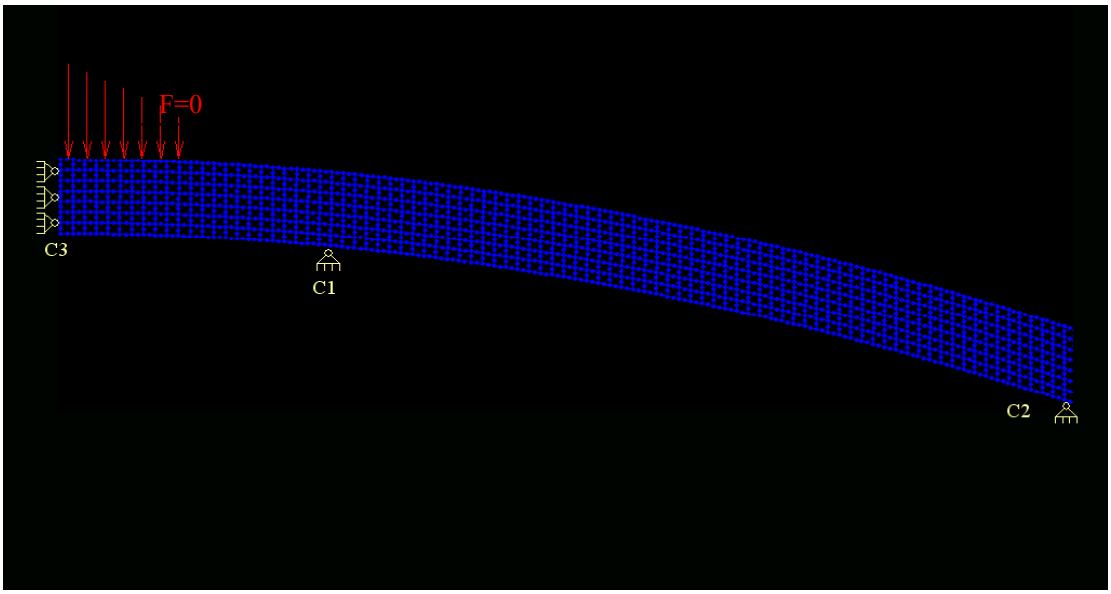

Figure 3.5. axisymmetric model with load applied from the top surface of the lens.

3.5.1 Representation of the distribution of the von Mises and hydrostatic stress when applying a load to the top surface

The result of applying a load to the top surface is shown in figure 3.6. Stresses were viewed as von Mises stress in order to evaluate the absolute value of stress concentrated on the upper and lower surfaces; the most important region being the zone were the load is applied. The von Mises stress distribution in figure 3.6 shows the lower surface under high stress compared to the top surface with the lowest stress localised at the neutral axis. Figure 3.6 shows the von Mises stress values when the load was applied to the top surface enabling the stress concentrated around the mounting point of the lens to be seen. It is interesting to note that the maximum stress occurs on the lower surface which would indicate that a crack would start from this surface when a load was applied to the upper surface. While figure 3.7 shows the distribution of hydrostatic stress where a load was applied to the top surface, it also shows whether the surface is under tension or compression. It was found that the lower surface was under tensile stress while the upper surface was under compressive stress. The compressive stress generated within the upper surface was 386 MPa and the tensile stress on the lower surface was 236 MPa. It is interesting to compare the stress values for the distribution of both of the von Mises and the hydrostatic stresses because the neutral axis disappeared in the hydrostatic stress distribution model, as shown in figure 3.7. Regions of tensile stress and compressive stress exists on the upper and lower surfaces respectively, as shown in figure 3.7. Obviously the highest von Mises stress can be observed on the lower surface but there is no indication whether it is tensile or compressive, as shown below in figure 3.6. The distribution of von Mises stress shows the absolute value of stress after a load is applied, while the distribution of hydrostatic stress indicates the relative stress

value and whether the surface is under tensile or compressive stress.

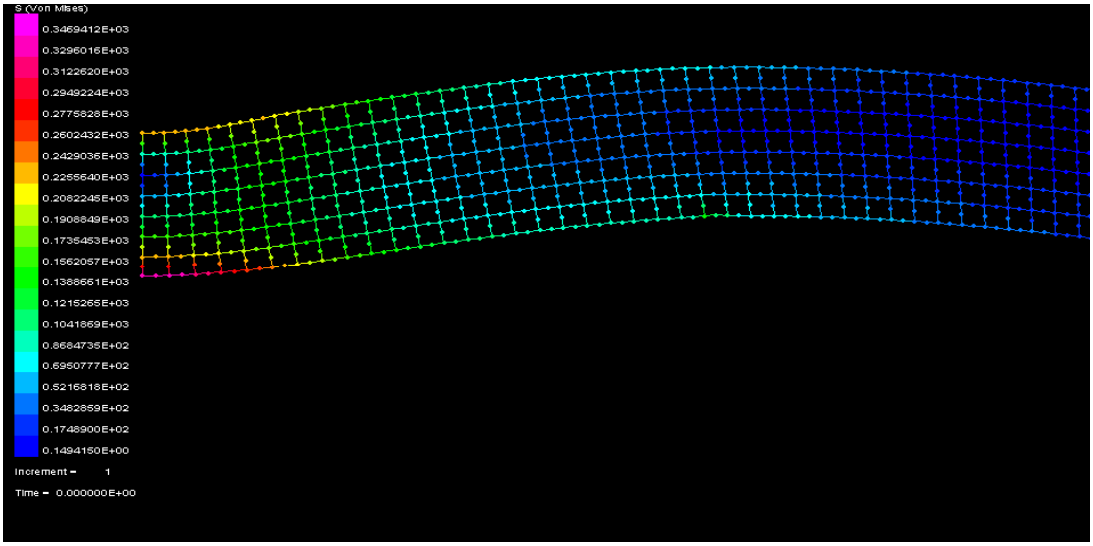

Figure 3.6. Representation of the von Mises stress values associated with the lens displacement.

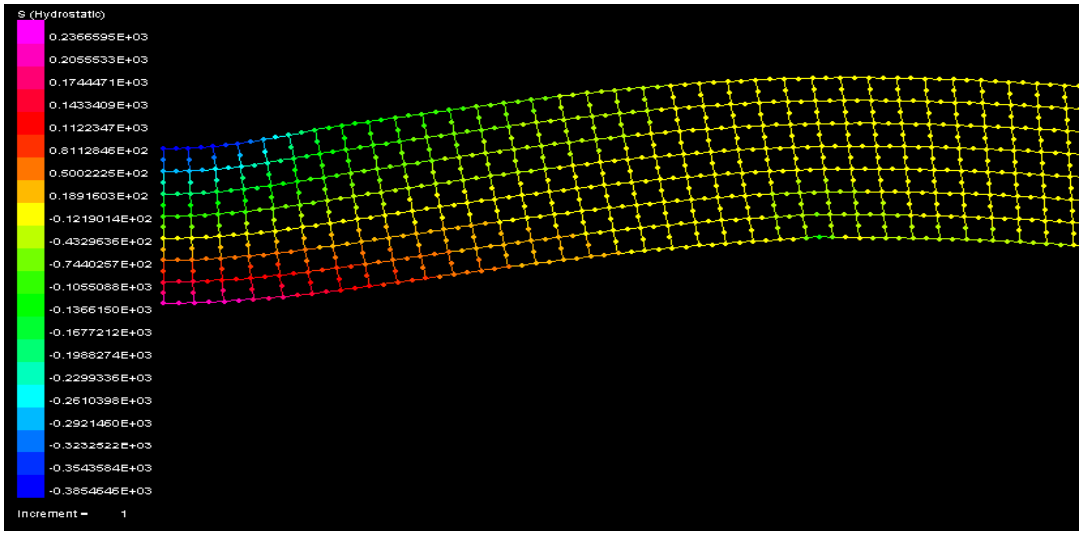

Figure 3.7. Representation of the hydrostatic stress values associated with the lens displacement.

3.6 APPLICATION OF REVERSED LOADS

The same boundary conditions were utilised for the geometry of the lens when a load was applied to the lower surface. Constraints C1 and C2 were reversed to the opposite direction to support the upper surface while C3 remained in the same position to permit the lens to move vertically. The applied loads were reversed to generate pressure onto the lower surface in a positive y-direction, as shown in figure 3.8.

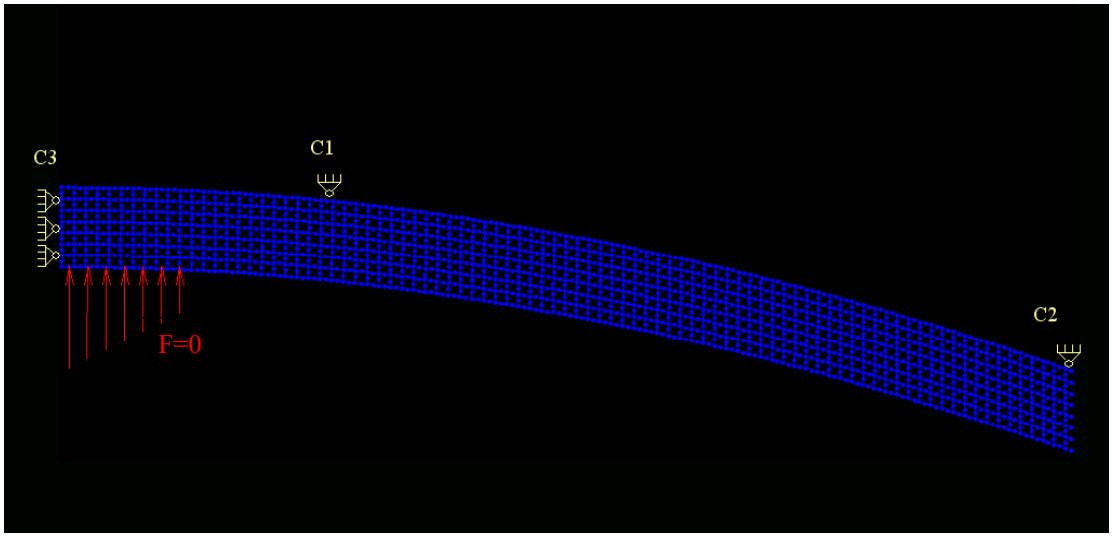

Figure 3.8. Reversed load applied to the lower surface of the lens.

3.6.1 Stress distribution with the load applied to the lower surface

The distribution of stress was changed by reversing the load and applying it to the lower surface of the modelled lens, as shown in figure 3.9. Here the neutral axis remains in the middle between the upper and lower surfaces which implies that two stress regimes exist. The highest concentration of stress was on the opposite side to that where the load was applied. In this case the highest concentration of stress appeared to be on the upper surface, as shown in von Mises stress distribution in figure 3.9 where the lens was deflected upwards. Figure 3.10 shows the hydrostatic stress distribution where the upper surface is under tension and the maximum value of stress is on the top surface. This stress gradually decreases towards the lower surface where it becomes compressive, with the highest concentration of compressive stress at the lower surface, as shown in figure 3.10.

3.7 STRESS ANALYSIS IN THE X-DIRECTION.

In reality during the manufacturing process of the ophthalmic lenses, flaws are created within the surfaces, which in turn cause fractures stemming from the stress within the flaws. Tensile stress in the x-direction (σ_x) is the stress component, which initiates fractures in the surfaces of ophthalmic lenses.

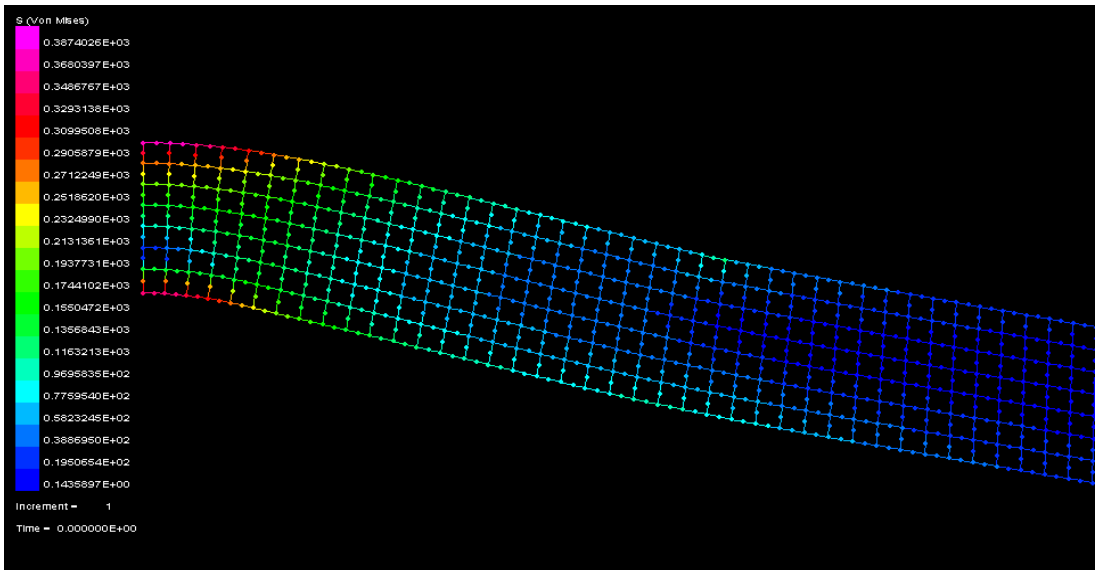

Figure 3.9. Representation of the von Mises stress distribution and displacement when a load is applied to the lower surface.

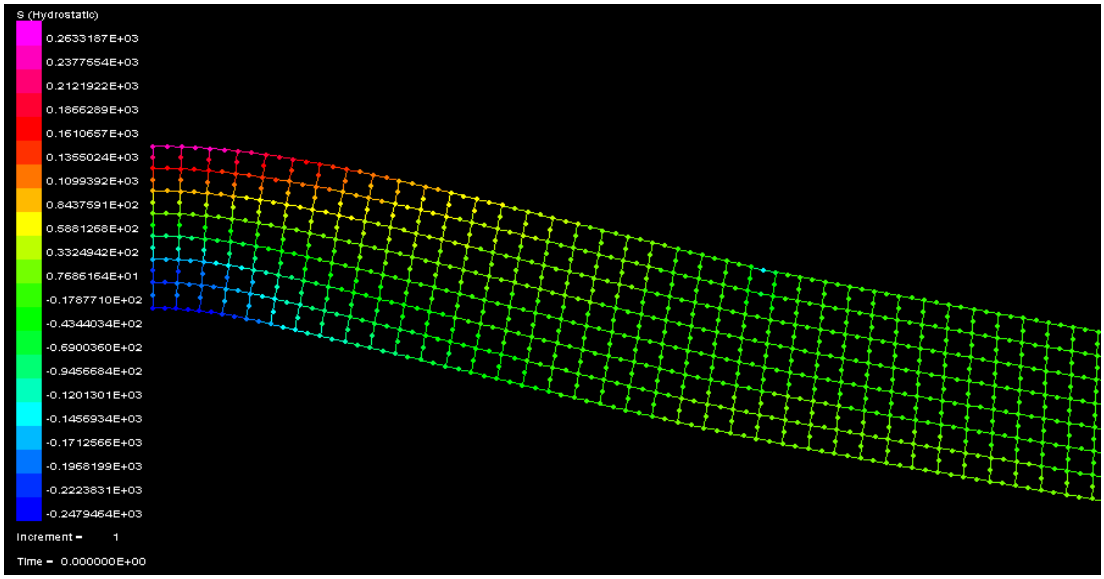

Figure 3.10. Representation of the hydrostatic stress distribution and displacement when a load is applied to the lower surface.

3.7.1 Stress analysis of the lower surface when a load was applied to the upper surface

Figure 3.11 shows the stress value in the x-direction that existed on the lower surface of the model, for both cases when a load was applied to the upper and lower surfaces. The lower surface was under tensile stress when the load was applied to the top surface. Maximum tensile stress in the x-direction (σ_{xt}) was 352 MPa in the centre of the modelled lens but this decreased on the surface towards the edges of the lens where it was mounted. Compressive stress, on the other hand, peaked where the lens was mounted and decreased towards the centre.

It can be noticed that the value of the maximum bending stress calculated using the formula of bending moment defined by Young (319 MPa) was similar to the value of maximum tensile stress in the x-direction calculated from the numerical modelling analysis (352 MPa). This is due to the introduction of the radius of the loading zone into the equation for the maximum bending stress. The other two values of the maximum stress were higher by 20% than the stress obtained from the numerical modelling analysis. Finally it can be assumed that the value of the maximum bending stress using Young's approach was more accurate than other values i.e. those of Blake and Timoshinko.

3.7.2. Stress analysis of the lower surface when a load was applied to the lower surface

The (σ_x) stress generated onto the lower surface when the load was applied to the lower surface was opposite to the stress on the upper surface, as described above. Maximum compressive stress in the x-direction (σ_{xc}) was -369 MPa. The centre of the lens was under compressive stress (σ_{xc}), as shown in figure 3.11, but this value decreased and changed to tension as the position moved away from the centre. Maximum tensile stress was concentrated in the area opposite the mounting on the upper surface (see C1 in figure 3.7).

3.7.3. Stress analysis of the upper surface when a load was applied to the upper and lower surfaces

Figure 3.12 shows the distribution of stress in the x-direction (σ_x) for the upper surface of the modelled lens. A compressive stress (σ_{xc}) was generated within the upper surface when a load was applied to the top surface. The upper surface was under tensile stress (σ_{xt}) max when a load was applied from the bottom surface. The maximum tensile stress generated on the top surface when a load was applied from the lower surface was 392 MPa, while the maximum compressive stress (σ_{xc}) max was -466 MPa on the upper surface when a load was applied to the top surface, as shown in figure 3.12.

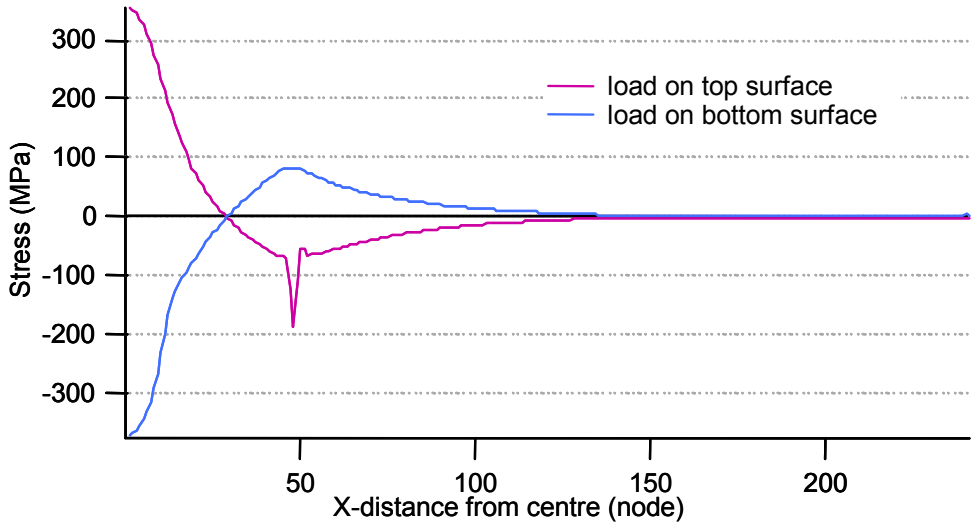

Figure 3.11. Stress in the x-direction for the lower surface.

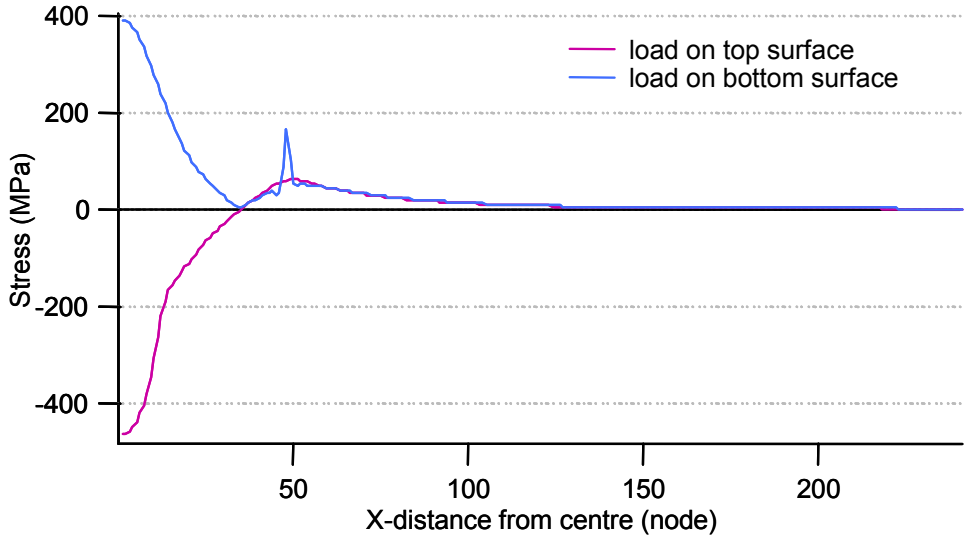

Figure 3.12. Stress in the x-direction for the upper surface.

3.8 APPLYING VOLUMETRIC SWELLING TO THE MODEL.

The volumetric swelling can be defined by increasing the size of the element or solid substance such as grains. Applying porous pressure [77] can increase the size of the solid substance or the grains. An example of such a system is a soil ground water. The mechanical behaviour of the porous medium consists of the response of liquid and solid matter to local pressure and of the overall material to effective stress. The solid substance in the absorbent medium is assumed to have a local mechanical response under pressure. The solid substance or grains response can be described by the following equation:

$$\frac{\rho_g}{\rho_g{}^o} \approx 1 + \frac{1}{k_g}(su_w + \frac{\overline{p}}{1-n-n_t}) - \varepsilon_g^{th}$$

where

$\frac{\rho_g}{\rho_g^o}$ is the grain density ratio, $k_g(\theta)$ is the bulk modulus of solid matter

su_w is the saturation and the pressure stress in the wetting fluid respectively

ε_g^{th} is the volumetric thermal strain, n is the volumetric porosity ratio, and n_t is the ratio of the trapped fluid volume.

Also $\varepsilon_g^{th} \propto \alpha_g(\theta)$

$\alpha_g(\theta)$ is the thermal expansion coefficient for the solid matter to corresponding to the expansion temperature θ .

By simplifying the above equation and neglecting the small terms, the total volumetric strain can be represented as: $-u_w / K_g + \varepsilon_g^{th}$

In ABAQUS software and for the volumetric strain that is generated using the above

equation i.e. a porous medium, it is customary for the user specify the elastic modulus and volumetric ratio for each element where swelling is required. The above equations indicate that the porous medium can generate volumetric strain. This volumetric strain is proportional to the volumetric porous ratio and pressure stress. It is important to distinguish k_g and α_g as properties of the solid grains material because as a whole, a porous medium will exhibit a much softer (and generally non recoverable) bulk behaviour than is indicated by k_g and also show a different thermal expansion.

This approach for generating volumetric thermal strain in a porous medium (swelling the soil particles with water) has been used to swell the surface of the spherical lens that was modelled. Increasing the volume of each element belonging to the spherical surface of the lens will generate volumetric strain and swell the surface. A pressure stress will be generated in each element and because the lens is spherical and concave a compressive stress will be generated on the surface (these compressive stresses can be generated onto flat surfaces as well). This compressive stress will reduce the component of stress that caused a crack on the surface of the lens, as is described in the following sections of this chapter. Another technique available in ABAQUS for generating volumetric strain is by mass diffusion into a solid state.

3.8.1 Applying volumetric swelling to the inner surface of the model.

A volumetric swelling has been applied to the lower surface of the model and the size of each element was increased 10% by volume. Each of the 176 elements have been swollen by increasing their volume which generated a residual stress within the swollen surface. Figure 3.13 shows this distribution of hydrostatic stress when volumetric swelling was applied to the lower surfaces of the model. A residual compressive stress was generated within the surface when no load was applied to the top surface. Generating compressive stress in the lower surface generates tensile stress on the upper surface of the lens, as shown in figure 3.13.

Figure 3.14 shows the hydrostatic stress pattern when swelling is applied to the lower surface and a load is applied to the upper surface. Both upper and lower surfaces are under compressive stress when a load is applied to the upper surface. The highest compressive stress is concentrated on the top surface rather than the lower surface while tensile stress is localised in the middle of the lens. This means the tensile stress zone has shifted from the lower surface to the middle of the lens when a load is applied to the upper surface, as shown in figure 3.14.

Figure 3.15 shows the distribution of hydrostatic stress when the volumetric swelling value was increased, as the modelled lens was distorted, and in this case the volume of each surface element doubled. The lens buckled inside when the lower surface was swollen to its maximum level, as shown in Figure 3.15.

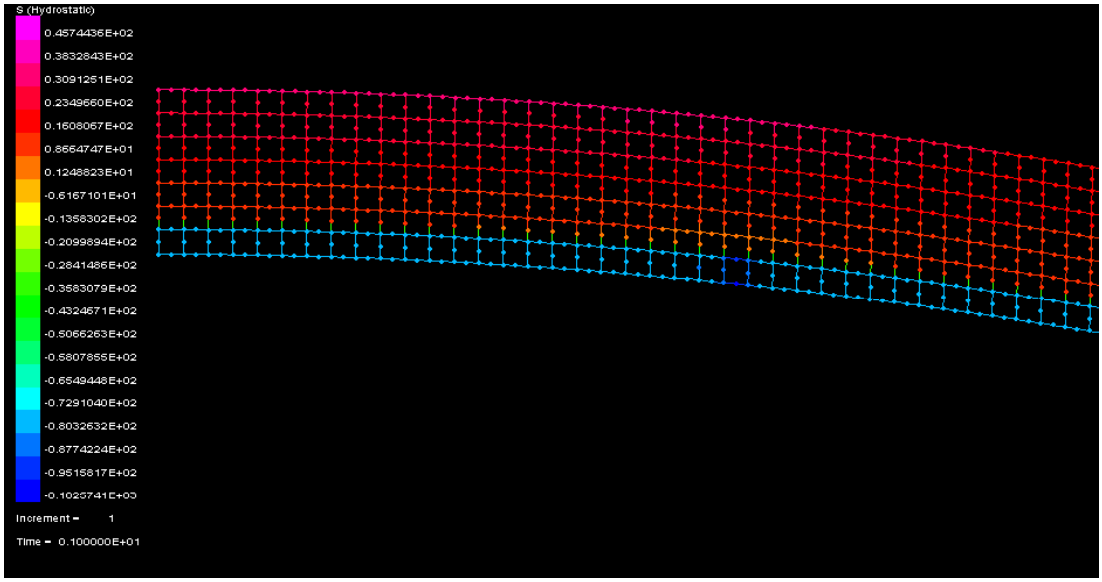

Figure 3.13 Representation of the hydrostatic stress distribution for swelling the lower surface of the lens.

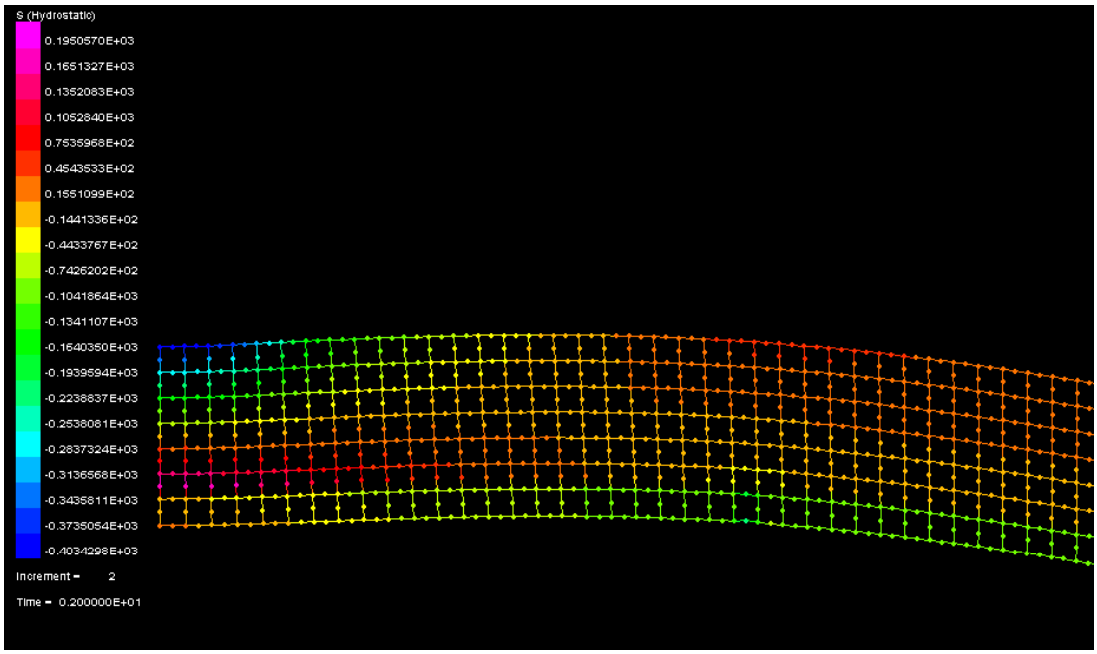

Figure 3.14. Representation of the hydrostatic stress distribution for swelling the lower surface of the lens and applying a load to the upper surface.

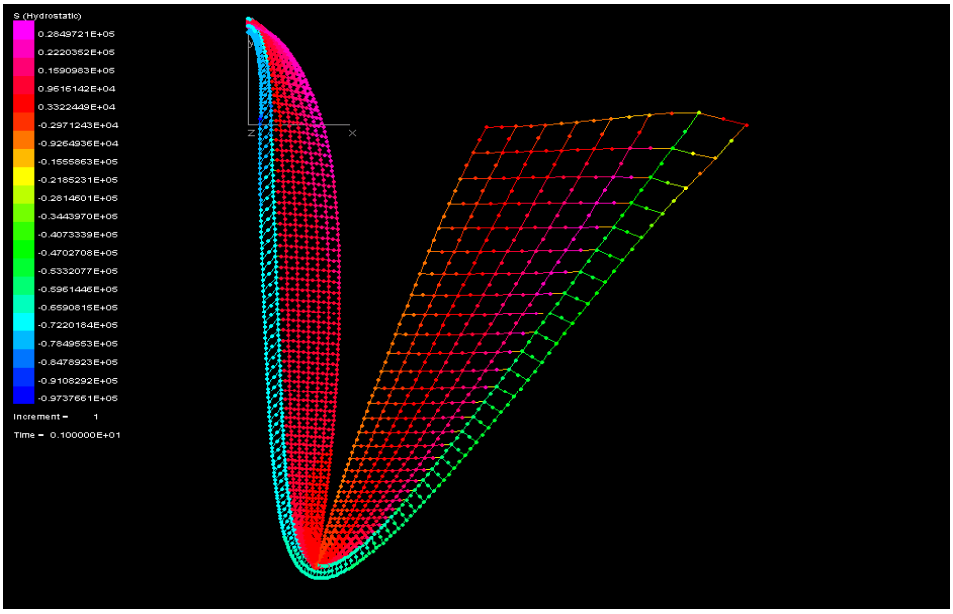

Figure 3.15. Representation of the hydrostatic stress distribution for increasing the swelling of the lower surface.

3.8.2 Applying volumetric swelling in both upper and lower surfaces to the model.

In the previous section volumetric swelling by 10% has been applied to the lower surface of the model. The same amount of volumetric swelling was applied to the upper and lower surfaces, as shown in figure 3.16. Figure 3.16 shows the distribution of hydrostatic stress after both the upper and lower surfaces of the model have been swollen. Both surfaces were under compressive stress while tensile stress dominated the neutral axis, as shown in figure 3.16. This region of compressive stress increased when the load was applied to the upper surface, as shown in figure 3.17, which shows the hydrostatic stress pattern for deformation of the model when the load was applied to the upper surface. The lower surface was still under compressive stress and the centre was still under tensile stress when the load was applied to the top surface.

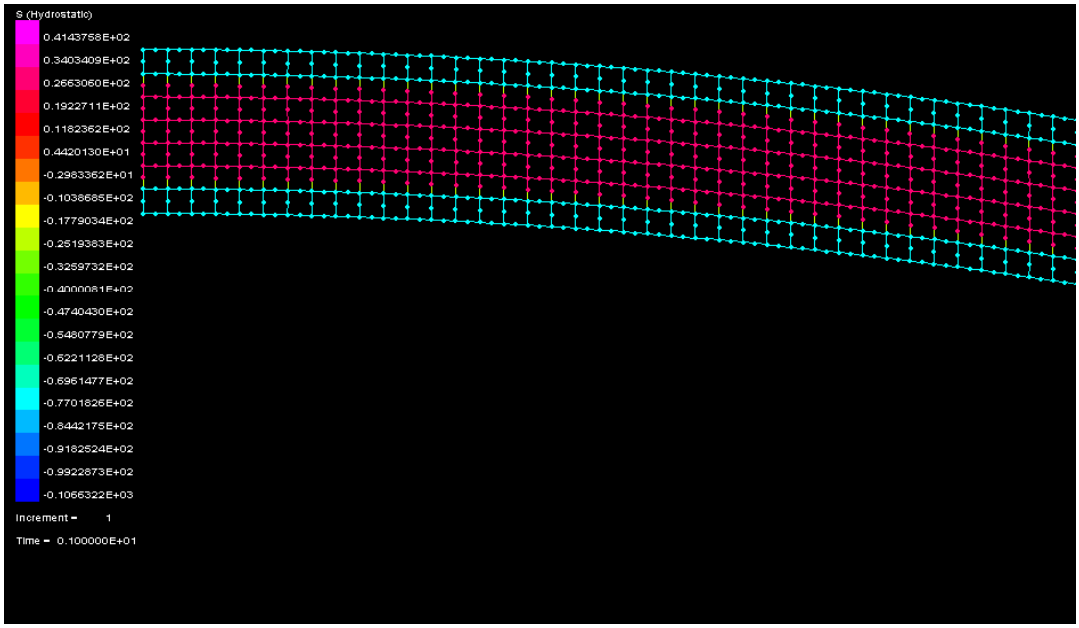

Figure 3.16. Representation of the hydrostatic stress distribution for swelling both upper and lower surfaces.

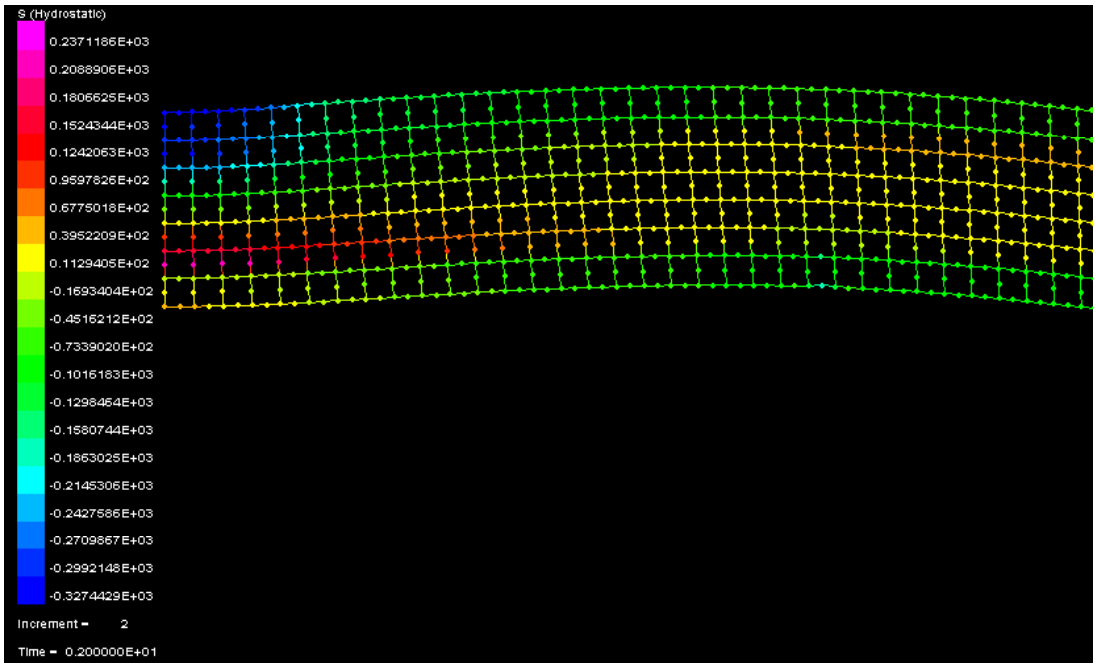

Figure 3.17. Representation of the hydrostatic stress distribution for swelling of both upper and lower surfaces when a load was applied on upper surface.

3.8.3 Effect of swelling to stress in the x-direction on the lower surface

Figure 3.18 shows the effect of the volumetric swelling on the stress in the x-direction that was generated in the lower surface of the lens. It shows that the pure swelling has generated a compressive stress in the upper and lower surfaces. The effects of only swelling the lower surface, swelling both upper and lower surfaces, and not swelling the lens with a load applied to the top surface are shown in figure 3.18.

Theoretically, swelling either the lower surface or both upper and lower surfaces reduces tensile stress generated in the lower surface in the x-direction. The compressive stress region around the mount where the lens was supported (C1) was observed as a sharp peak, as shown in figure 3.18. The maximum tensile stress in x-direction (σ_{xt}) was reduced from 352 (MPa) with no swelling effect, to 64 and 25 (MPa) with swelling on both sides and one side respectively, as shown in figure 3.17. The three sharp peaks that located in the negative stress region are an indication of the compressive stress where the lens was mounted.

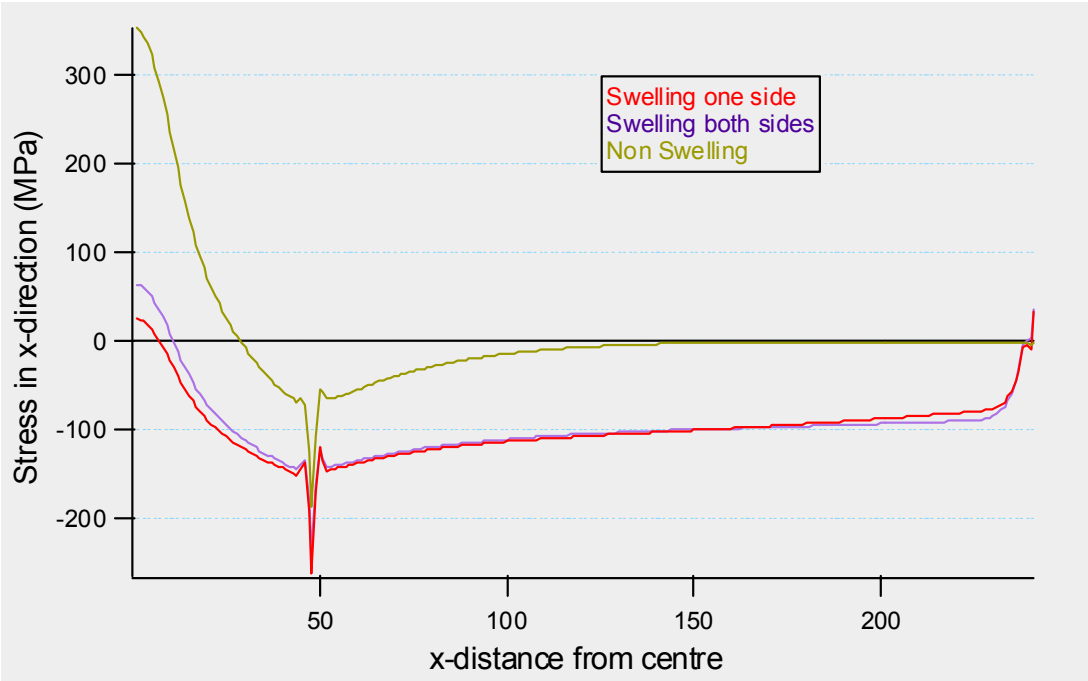

Figure 3.18 The effect of volumetric swelling to stress in the x-direction on the lower surface.

3.8.4 Effect of swelling on stress in the x-direction on the upper surface

It was shown previously that the upper surface was in compression when a load was applied to the top surface. Figure 3.19 shows the effect of the swelling on the stress in x-direction on the upper surface of the lens. Maximum stress in x-direction (σ_x) was -300 MPa when no swelling was applied. The stresses were -380 and -466 MPa when both upper and lower surfaces were subject to swelling, as shown in figure 3.19. Here the peak shifted from the region of tension to the compression zone by swelling the upper and lower surfaces.

A crack might easily start from the peak, which would indicate that the highest tension stress is in the x-direction. All three curves in figure 3.19 represent stress in the x-direction combined with the swelling and load applied to the upper surface. The swelling curve on one side has the highest tension stress peak above the constraint, which is the mount (C1) where the lens is supported.

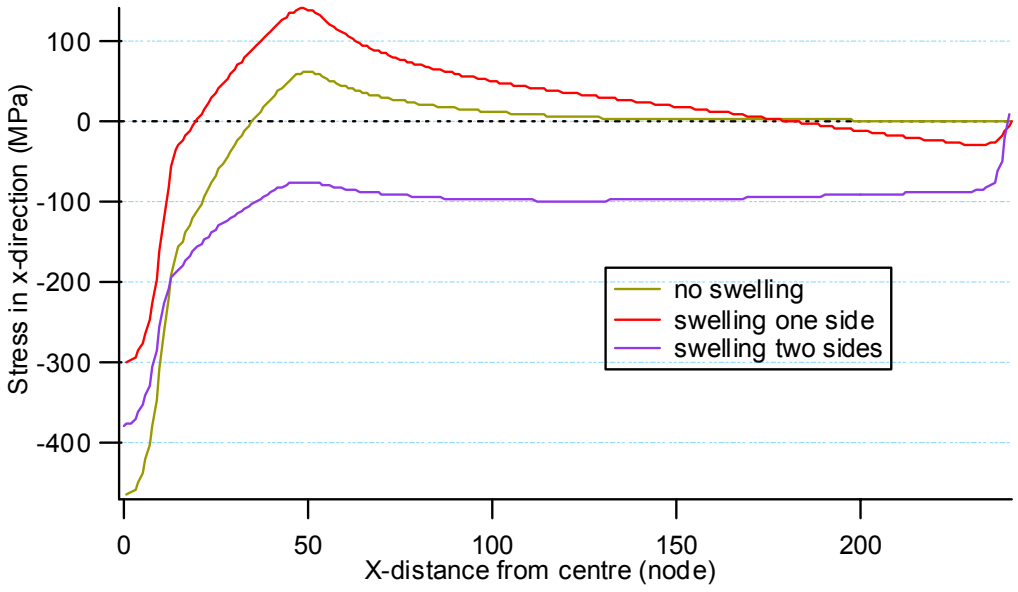

Figure 3.19 Swelling effect on stress in the x-direction on the upper surface.

3.9 CONCLUSIONS

In this chapter it has been shown that the stress pattern of the lower and upper surfaces of a spherical concave lens can be modelled. The spherical lens generated for this modelling work is considered to have the same dimensions as the real lens, i.e., 78.2 mm diameter and 2.2 mm thick.

By analysing the distribution of stress on the upper and lower surfaces, it was found that fracture is likely to start on the lower surface when a load is applied to the upper surface. The validity of the maximum stress in the x-direction obtained from the numerical modelling analysis was justified from the theoretical calculations. This permits modification to be made to the actual model in future work such as introducing the volumetric swelling into the model.

It was further found that the point(s) where the lens was mounted produces a zone of stress concentration. Two types of stress occur in this zone, compressive stress localised within the lower surface and tensile stress concentrated within the upper surface. On the other hand a crack might start on the upper surface from the lens mounting position when a load is applied to the upper surface. The stress causing the fracture (or stress in the x-direction) reaches its maximum value in the centre of the lower surface and then decreases further away from the centre. Another region where stress concentration in the x-direction increases is the upper surface where the lens is mounted which means, in a real impact test, if the lower surface is very smooth and there is no chance of a crack starting from the lower surface, it may very well start from the upper surface.

Applying volumetric swelling to the lower surface significantly reduces stress in x-direction generated on the lower surface by applying a static load to the upper surface. Stress in the x-direction was reduced by 92% from the stress generated in the lower surface in the absence of volumetric swelling. This percentage decreased to 82% when the same amount of volumetric swelling applied to the upper surface was applied to the lower surface. This applied to the model lens generated in a concave spherical shape. Applying volumetric swelling to the lower surface will only generate compressive stress on that surface which will be reduced by a small amount because of compressive stress generated within the upper surface by volumetric swelling applied to the upper surface itself. The stress in the x-direction generated in the lower surface has been increased relatively by swelling both surfaces rather than the lower surface only. Applying volumetric swelling to the upper and lower surfaces generates a multi layered stressed model. Stressed composite layers were formed within the modelled lens by generating a compressive stress in the upper and lower surfaces and the tensile stressed region between these two layers.

In the photoelasticity stress analysis chapter, similar findings of multi composite stressed layers in the modelled lens will be presented by swelling both surfaces of the actual ophthalmic lenses.

CHAPTER 4

Polymerization Process Analysis

4.1 INTRODUCTION

In the previous chapter a spherical concave lens was modelled and the volumetric swelling of each element on the surface generated a compressive stress within the surface causing it to expand. This chapter describes the experimental method used for generating the compressive stress necessary to expand the lens surface. Raman spectroscopy was used to analyse the stuffing (swelling) and polymerisation process of monomer into the surface of the CR-39 ophthalmic lenses. This chapter also demonstrates the basic principles of Raman spectroscopy, including previous work using Raman to analyse the polymerisation of CR-39 allyl resin.

Raman spectroscopy can be described as the scattering of light from a gas, liquid, or solid with a shift in wavelength from the usually monochromatic incident radiation [78, 79].

Raman intensity is measured from the following equation:

$$I_{Raman} = KI_L(\nu_o - \nu_i)^4\left(\frac{d\alpha}{dQ}\right)^2$$

where:

I_L is laser intensity

ν_o is the wave number of monochromatic beam radiation (from the laser light)

ν_i is the wave number of ith vibrational mode

$d\alpha$ is the change in polarizability

dQ is the change in the normal coordinate length of the vibration

K constant

Raman spectra are complementary to infrared spectra; both consist of lines (or bands of lines), which are images of molecular vibrations [80, 81]. The intensity of Raman lines represents the change of molecular polarisation by vibration, while the intensity of infrared lines represents the change of molecular dipole moment [81].

For polymer applications both FTIR and Raman Spectroscopy are complementary vibrational spectroscopy techniques. A combination of FTIR and Raman can yield valuable information because FTIR is sensitive to a chemical group that possesses a significant dipole moment. For example, FTIR is sensitive to C-C, and C=O groups while Raman is sensitive to highly polarisable groups such as C-C and C=C.

4.2 METHOD OF SWELLING THE OPHTHALMIC LENS SURFACE

The plano power ophthalmic lenses were made from CR-39 resin, to produce a finished product, then treated with a swelling agent and tested. Figure 4.1 shows the chemical structure of CR-39 which has two vinyl groups (C=C) at the end. The cured CR-39 polymer is a highly cross-linked polymeric material, which can not be

dissolved in any solvent. Different types of individual monomers have been diffused into the polymeric surface of the ophthalmic lens. It has been found that monomer mixed with solvent caused the CR-39 ophthalmic lenses to swell, but the first step is to diffuse the monomer into the highly cross linked polymeric surface, as shown in the schematic figure 4.2. After the diffusion process is finished, uncured diffused monomer was cured in the polymeric surface material using an Ultra Violet (UV) initiated polymerisation technique [82]. Two types of polymerisation occurred, homo-polymerisation within the monomer itself and co-polymerisation between the monomer and polymeric material of the ophthalmic lens, as shown in figure 4.2. The main purpose of this technique is to expand the surface volumetrically to place the polymeric surface of the ophthalmic lens under compressive stress. It was found that diffusing the monomer into a highly-cross linked polymeric material such as a CR-39 ophthalmic lens, caused the surface to swell and created a compressive stress within the surface of CR-39. The UV polymerisation stage ensures the monomer remains permanently close under the surface.

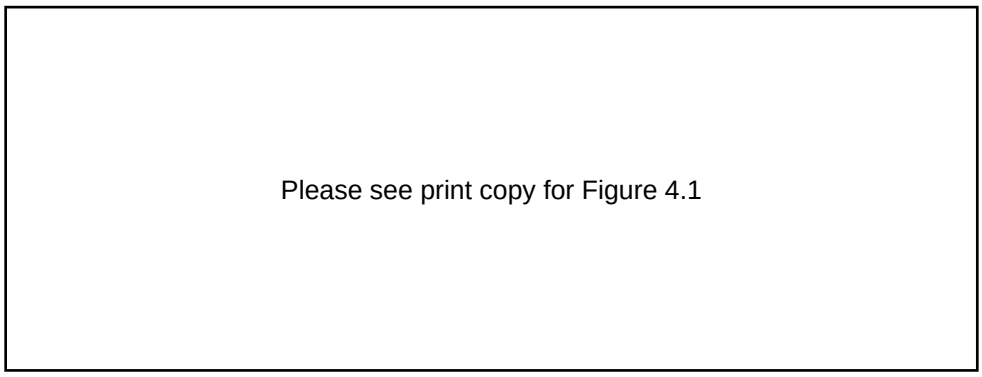

Figure 4.1. Diethylene glycol bis-allyl carbonate (CR-39).[47]

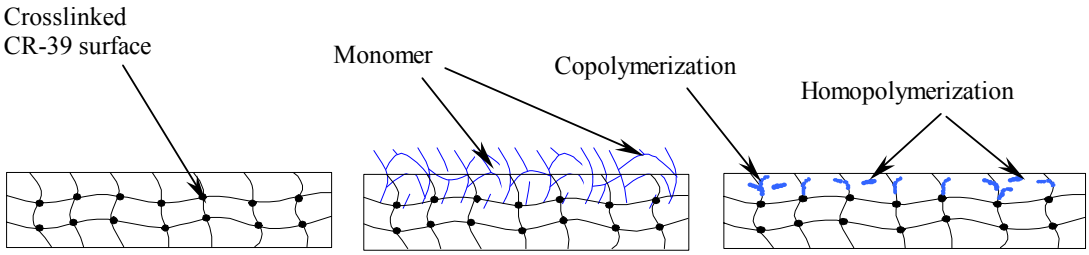

a. Crosslinked CR-39 b. Monomer diffusion process c. UV Polymerization

Figure 4.2. Swelling CR-39 ophthalmic lens by diffuse the monomer into the surface .

4.3 EXPERIMENTAL TECHNIQUE AND SAMPLES PREPARATION

Micro-Raman spectra were obtained with a dispersive Horiba-Jobin Yvon HR-800 Raman instrument. Laser light excitation was via a HeNe 20 mW laser, polarised 500:1 at a wavelength of 632.817 nm. A holographic grating with 950 lines/mm was used in conjunction with an air-cooled CCD detector. Figure 4.3 shows a schematic diagram of the dispersive Raman spectroscopy set-up used to analyse the swelling process of the ophthalmic lens. A 50x objective lens with a capture time of 150 second was used and an optimum signal with less noise from the spectrum was obtained, with a confocal hole under the detector set at 1100 μm , and the slit of the laser light set at 100 μm .

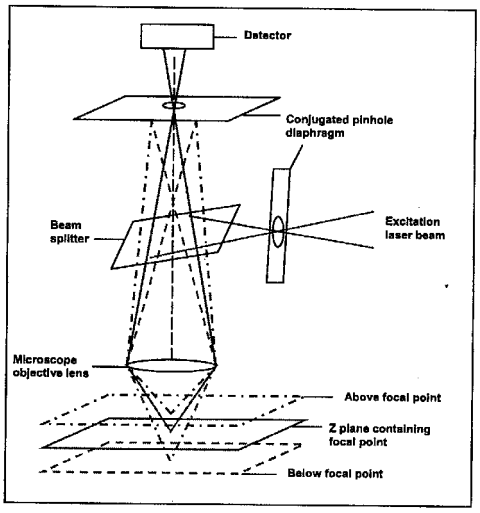

Figure 4.3. Schematic diagram of dispersive Raman spectroscopy.

Ultra Violet (UV) initiation was used to polymerise the monomers diffused into the lens. The UV system with shutter assembly was supplied by Amba Lamps Australasia Proprietary Ltd. The input power of the UV medium-pressure mercury lamp was 2 KW, and the UV light was not isolated by any filters. UV light intensity output was measured by the UV Power Puck device. The measurements of the used UV light were found to be UVA (320 – 390) nm, UVB (280 – 320) nm, and UVV (395 – 445) nm consecutively.

A review of the literature (chapter 2) showed that CR-39 polymer is a highly cross-linked material and diffusing any monomer or solvent into CR-39 polymer lenses while soaking them at room temperature is not an easy task.

Many monomers and experiments were used to evaluate whether one monomer, or a mixture of two or more, can diffuse such that a mixture of two monomers, or one monomer with solvent, can be diffused into a CR-39 ophthalmic lens. These monomers were CR-39, acrylic acid (AA), methacrylic acid (MAA), divinyl benzene (DVB), styrene (ST), and vinyl acetate (VA). The experimental solvents were chloroform, acetone, and water. Two systems for diffusing monomers into CR-39 ophthalmic lenses using Raman spectroscopy were investigated.

The spherical concave CR-39 ophthalmic lenses and a monomer of CR-39 were supplied by Sola Optics (Scientific Optical Laboratory of Australia). These lenses were made from CR-39 resin and cured in a glass mould under temperatures increasing from 35 ^{o}C to 85 ^{o}C. The glass mould produces a 10mm thick spherical concave lens with smooth upper and lower surfaces. The lower surface is ground in different stages until the lens is 2.2 mm thick, with smooth parallel surfaces. A convex lens with the outer surface parallel to the inner surface, a homogeneous thickness, and zero power is known as a plano power lens.

These plano power ophthalmic lenses were immersed into a mixture of swelling agent and photo initiator at 50 ^{o}C for 6 hours to prevent a rise in temperature above Tg of CR-39, then removed, cleaned with a tissue and washed in acetone. Photo-polymerisation was carried out by supporting each lens on a 7 cm Petri dish and placing them 10 cm below the focal point of the UV light for not longer than 1 min 30 seconds to ensure the temperature did not reach the Tg of CR-39 polymer. Each lens was weighed before and after the photo-polymerisation process.

4.4 RESULTS AND DISCUSSION

Raman spectra was used to analyse the residual vinyl group (C=C) group in the CR-39 polymer as supplied. Knowing the amount of residual (C=C) bond in CR-39 is important for evaluating the quantity of reacted (C=C) bond after conducting the (UV) initiated polymerisation process to the CR-39 ophthalmic lens. Raman spectroscopy was used to analyse diffusion and polymerisation of the monomer into the CR-39 ophthalmic lens and to map the cross section in order to identify the depth of monomer penetration. The diffusion and polymerisation of styrene mixed with vinyl acetate monomers and acrylic acid mixed with chloroform as a solvent, were investigated. Table 4.1 tabulates the chemical structures of acrylic acid mixed with chloroform and styrene mixed with vinyl acetate associated with the photo-initiators used in both mixtures.

Swelling agent	monomers and solvents		initiators
AA	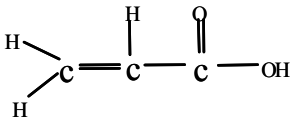	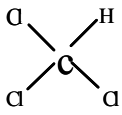	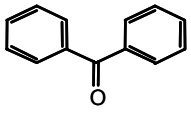
	acrylic acid (AA)	chloroform	Benzophenone (BP)
Stva	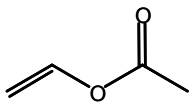	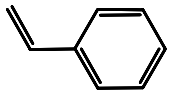	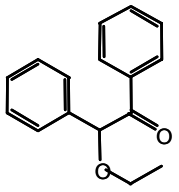
	vinyl acetate (va)	styrene (st)	benzoin ethyl ether (BEE)

Table 4.1 Chemical structures of the monomers and photoinitiators used to swell CR-39 ophthalmic lens.

4.4.1 Determination of residual C=C in CR-39 Ophthalmic lenses

Raman spectroscopy was used to identify the extent of un-polymerised allyl groups (C=C) in CR-39 ophthalmic lenses. The thermal initiator used for curing CR-39 resin was secondary isopropyl peroxide. The extent of the curing reaction in CR-39 was determined by un-polymerised residual C=C in CR-39 ophthalmic lens by measuring the intensity of the peak at 1649 cm^{-1} assigned to the unpolymerised allyl groups [83], as shown in figure 4.4. The bonds of CR-39 polymer and their assigned wave numbers are reported in table 4.2.

Table 4.2 wave numbers of CR-39 bonds

Bands	C=O	C=C	C-H	C-O
ν (cm^{-1})	1750	1649	1457	1292

A strong band in the monomer at 1649 cm^{-1} due to the C=C stretching mode, decreases in intensity during polymerisation of CR-39 resin. It was convenient to use carbonyl at ≈1750 cm^{-1} as an internal reference although it was necessary to correct the area for a subsidiary peak resulting from a fragment of thermal initiator. Some broadening of the spectrum peaks were observed and therefore these peak heights were inappropriate for quantitative measurement. The spectrum was smoothed and an appropriate baseline from which to measure peak areas for the carbonyl group in the monomer and polymer of CR-39 was established. Figure 4.5 shows the spectrum scaled to compare the C=C bond peaks with the carbonyl group, in order to evaluate the amount of un-polymerised C=C bond left in CR-39 polymer. The peak areas of the carbonyl and vinyl group were compared before and after curing the CR-39 resin, and the amount of residual C=C bond was found to be 9%.

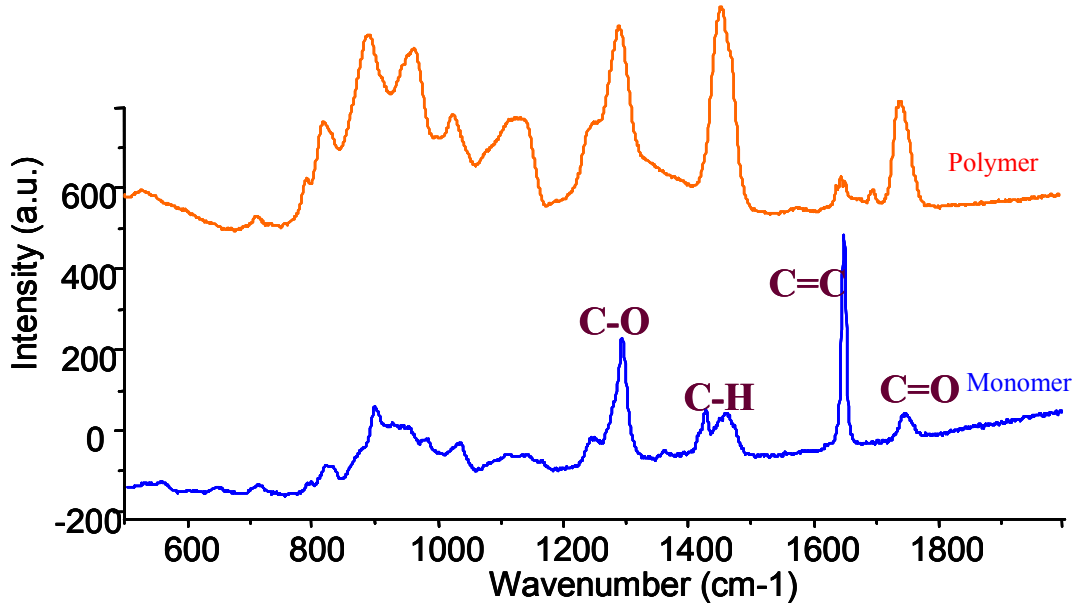

Figure 4.4. Raman spectrum for CR-39 monomer and CR-39 polymer .

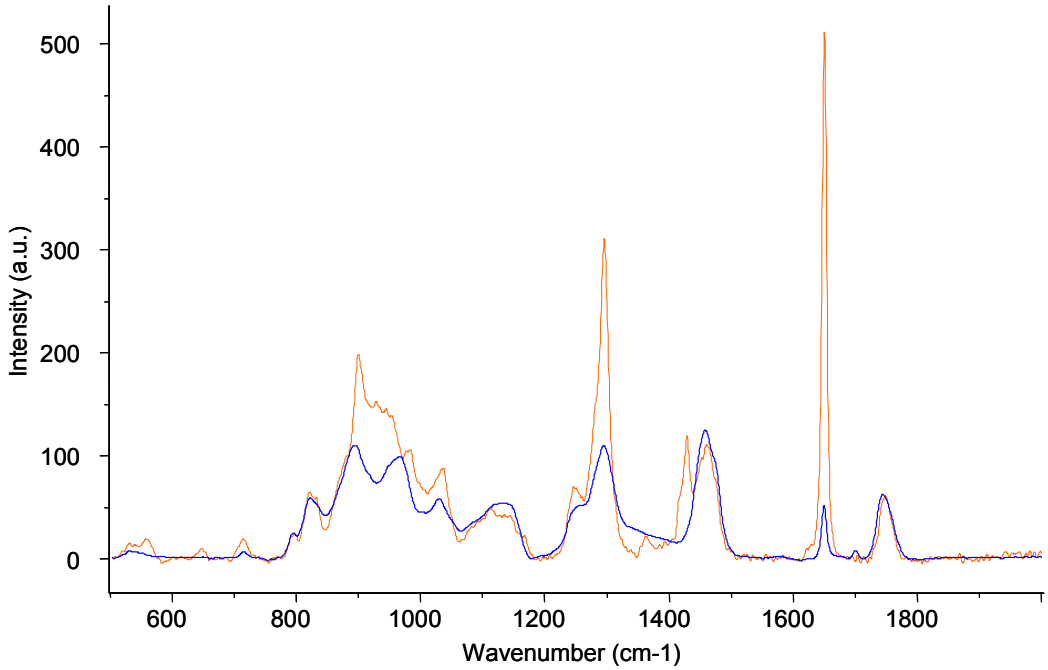

Figure 4.5. Raman spectrum for CR-39 monomer and polymer with scaling up the monomer spectrum.

4.4.2 Polymerisation of Acrylic Acid (AA) in a CR-39 ophthalmic lens

The CR-39 ophthalmic lenses were dipped in a solution containing acrylic acid (AA), chloroform, and (Benzophenone (BP) as the photo-initiator). The percentage of acrylic acid with chloroform was 1:1 by volume and the concentration of BP was 1.5% of the monomer (mol/mol). The diffusion process was carried out at 50 ^{o}C for 6 hours.

After diffusion all the samples were removed from the solution, rinsed, wiped with the acetone and placed in a fume hood for 1 min to dry. The CR-39 ophthalmic lenses were ready for photo-polymerisation when clean and dry. Each lens was weighed and then exposed to the UV light to begin polymerisation of the AA monomer diffused into the surface, and then weighed again. Figure 4.6 shows a significant weight increase during diffusion for a group of 10 lenses although the weight decreased marginally during the UV initiation process due to the chloroform evaporating from the exposed surfaces. By using the following equation the swelling ratio for diffusing the monomer into the lens can be measured:

$$\text{Swelling ratio} = \frac{wt_s - wt_{\text{int}}}{wt_s} \ \%$$

where wt_s is the swollen weight, and $wt_{\text{int.}}$ is the initial weight.

The swelling ratio for the swollen lens was evaluated using the above equation and it was found to be around 1%, this ratio was calculated based on the weight increase of the whole lens. However, this swelling ratio can be estimated to be around 4% for the swollen surfaces only.

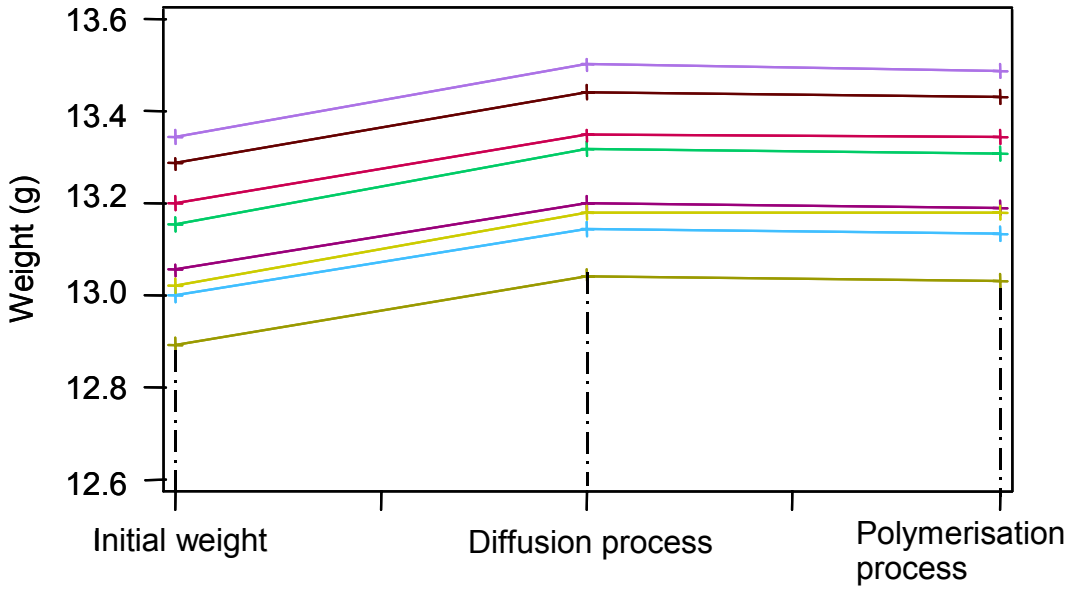

Figure 4.6. Weight of 8 samples from treating the lens with acrylic acid and chloroform.

As a solvent, chloroform proved to be an excellent swelling agent for the CR-39 ophthalmic lenses. Some experiments were carried out using UV initiation to polymerise the acrylic acid as a monomer with and without chloroform, and the photo-initiator (BP) [84, 85]. Figure 4.7 a. shows Raman spectra for poly-acrylic acid when 50g of acrylic acid monomer were placed into a glass watch and exposed to UV light in the same position and environment as the CR-39 ophthalmic lenses were grafted. Acrylic acid cured within 3 minutes partial polymerisation occurred within 1 ½ minutes, and full conversion of monomer of (AA) to poly-acrylic acid took place in the third minute.

Figure 4.7. b. shows Raman spectra for poly-acrylic acid when 50g of the swelling agent (acrylic acid mixed with chloroform and photoinitiator BP) were exposed to

UV irradiation under the same conditions AA was cured previously. Curing time remained the same, approximately 3 minutes for full polymerisation of the acrylic acid monomer, with or without mixing with chloroform and photo-initiator.

Diffusion and polymerisation of the swelling agent into the CR-39 ophthalmic lenses was analysed by Raman spectroscopy before and after polymerisation, as shown in figure 4.8. It can be seen from the diffusion of AA with chloroform that the C=C bond at 1634 cm^{-1} existed beside the residual C=C bond of CR-39 at 1648 cm^{-1}, as shown in figure 4.8. b. The absence of the acrylic acid C=C bond after exposing the CR-39 ophthalmic lens to UV irradiation shows that acrylic acid is polymerised within the surface of the ophthalmic lens as shown in figure 4.8. c. The residual C=C bond in CR-39 lens at 1648 cm^{-1} reduced from 9% to 7% when the areas of that bond were compared before and after polymerisation to the carbonyl bond as internal reference.

FTIR was used to evaluate the above process of photo polymerisation of AA into CR-39 lens. The result of the FTIR spectrum is shown in appendix I. There was no change in the spectrum before and after the polymerisation was accomplished.

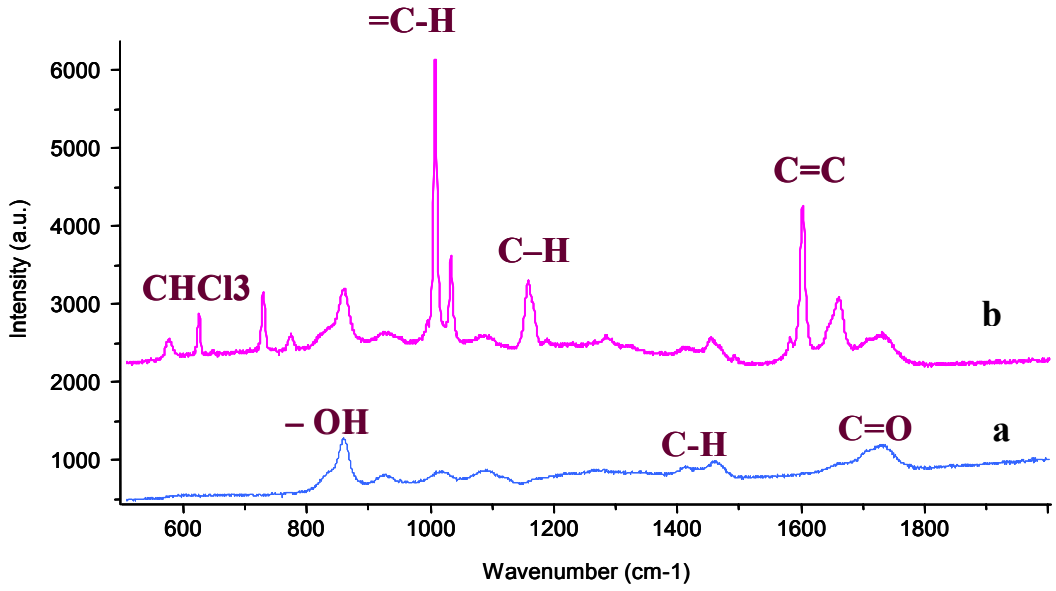

Figure 4.7. Raman spectroscopy for poly acrylic acid from (a) acrylic acid without photo-initiator, (b) acrylic acid with chloroform and photo-initiator.

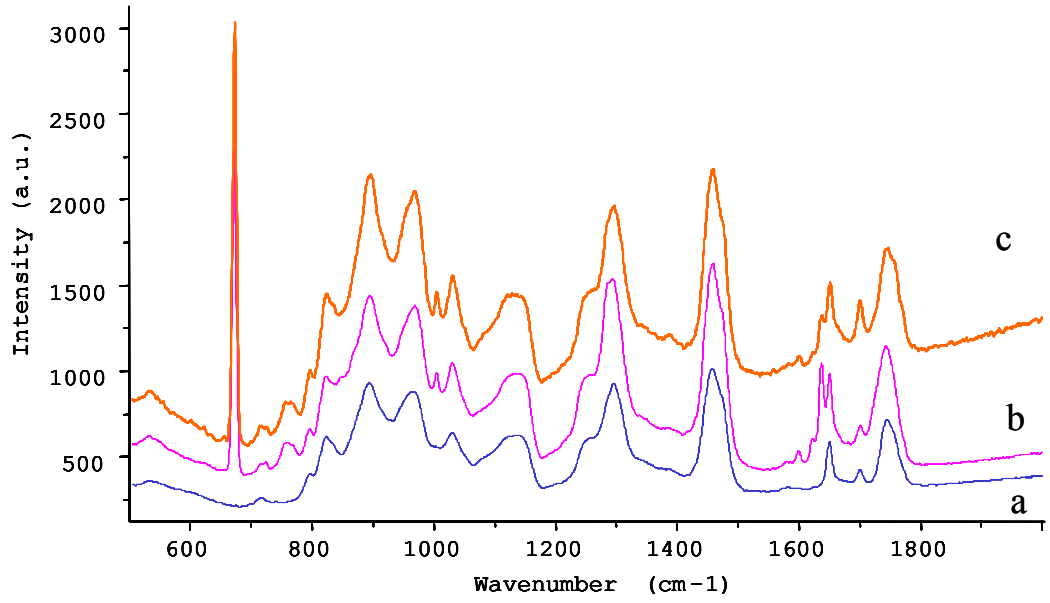

Figure 4.8. Raman spectra for CR-39 ophthalmic lens (a), diffusion process of the swelling agent AA into the lens (b), polymerisation process (c).

4.4.3 Analysing the polymerisation of styrene and vinyl acetate into the CR-39ophthalmic lens

The same procedure used to prepare the sample for diffusion of acrylic acid was also used to prepare the sample for diffusing a mixture of styrene and vinyl acetate. These two monomers were first tested to determine their ability to be diffused into the highly, cross linked CR-39 polymer. It was much easier to diffuse a mixture of both of them rather than diffusing the styrene or vinyl acetate as individual monomers into CR-39 ophthalmic lenses at 50 ^{o}C. The photo-initiator used was benzoin ethyl ether (BEE) instead of Benzophenone (BP). The concentration of PEE was 1.5 % (mol/mol) for 1:1 by volume, mixture of styrene and vinyl acetate. Figure 4.9 shows the weight patterns for 8 samples which were treated with vinyl acetate and styrene as a swelling agent.

After the diffusion process, the same environment and position for exposing the lens treated in AA were used to expose the lens treated with styrene and vinyl acetate.

Figure 4.10 shows Raman spectra of the diffusion and the polymerisation of vinyl acetate and styrene into the CR-39 ophthalmic lens. The spectrum (a) is for the original CR-39 lens, spectrum (b) is after the diffusion of styrene and vinyl acetate, and spectrum (c) is the UV polymerisation stage.

It can be seen that two peaks of C=C bonds at 1645 and 1635 cm^{-1} existed beside the residual C=C bonds of CR-39 polymer during diffusion of the swelling agent (styrene and vinyl acetate) into the lens, as shown in figure 4.10.b. The UV polymerisation process did not affect these two peaks because they existed after polymerisation was accomplished, as shown in figure 4.10.c.

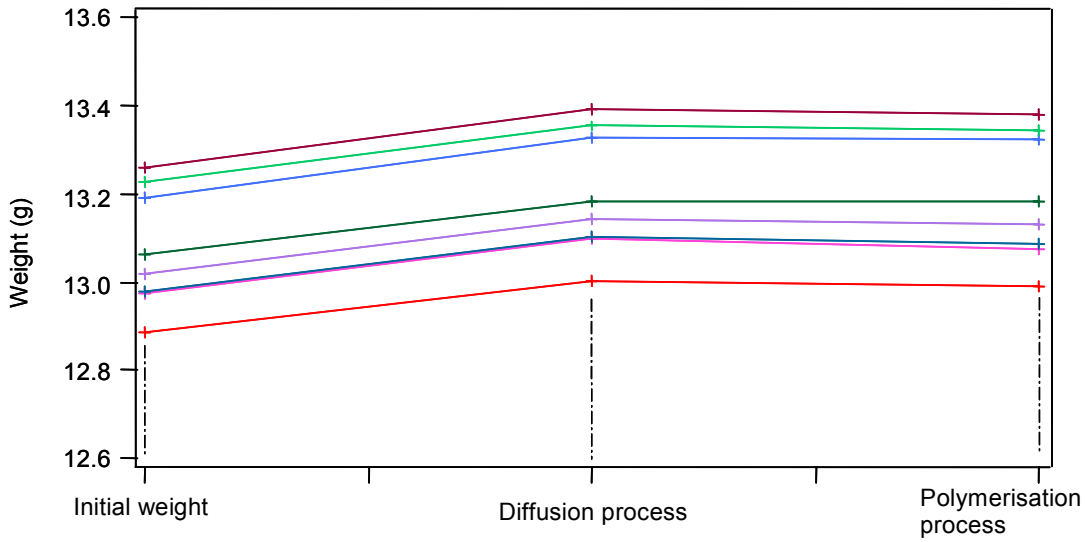

Figure 4.9. Weight of 8 samples from treated by styrene and vinyl acetate.

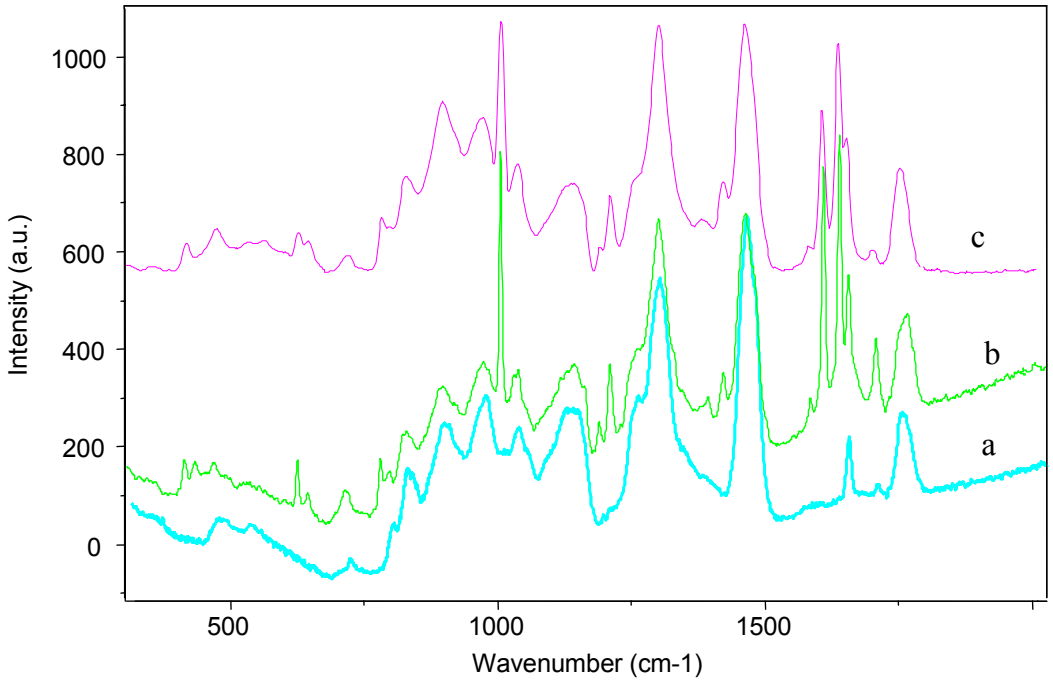

Figure 4.10. Raman spectrum for CR-39 ophthalmic lens (a), diffusion process of vinyl acetate and styrene (b), UV polymerisation process (c).

4.4.4 Determination of the depth of the grafted layer into the CR-39 ophthalmic lens.

Raman spectroscopy was used to map the edge section of the CR-39 ophthalmic lens to identify the depth of monomer penetration. This was performed after diffusing the mixture of acrylic acid and chloroform, and also after exposing the lens to the UV light. Figure 4.11 a. shows the mapped area while diffusing the monomer of AA and chloroform. The mapped area is spotted in 3×20 points and the Raman spectrum obtained at every point. The spectrum range was 1500-1700 cm^{-1} wave length to analyse the C=C bond of acrylic acid located in 1634 cm^{-1} wave length, as shown in figure 4.11 b. The three dimensional image (figure 4.11.c) represents the intensity of the C=C peak of AA through the mapped area. The highest intensity of C=C peak of AA is in the area closest to the edge of the lens, as shown in figure 4.11.c. Similar changes in peak intensity can be noticed in figure 4.11 d. The intensity lines represent all the mapping points across the scanned area. Figure 4.11.a shows a matrix of the mapping zone to identify the depth of the swelling agent into the lens, starting from the edge. All the figures (4.11.b-d) resulted from the mapped area, as shown in figure 4.11.a.

Figure 4.12 shows the intensity of the two peaks of C=C bonds from diffused acrylic acid at (1634 cm^{-1}) and CR-39 at (1648 cm^{-1}). It was observed that the C=C bond existed at the edge of the cross section where the length y=0. This peak decreases across the section of the lens until it reaches zero at a depth of 250µm. A similar cross section was made after exposing the surface of a CR-39 ophthalmic lens to the UV initiation process. It was observed that the C=C bond that existed from diffused acrylic acid (1634 cm^{-1}) disappeared while the chloroform peak still existed, as shown in figure 4.13. The chloroform did not fully evaporate from the surface and

also diffused 250µm deep because the swelling agent mixture was diffused.

It was not obvious that the acrylic acid and chloroform would diffuse to approximately the same 250 µm depth but they did. Perhaps an explanation is that the chloroform is a good solvent for acrylic acid and an excellent swelling agent for CR-39 lens, and the extra free volume caused by the presence of the chloroform will increase the diffusion of the acrylic acid. This depth can be accurately measured by increasing the mapping points for the same area.

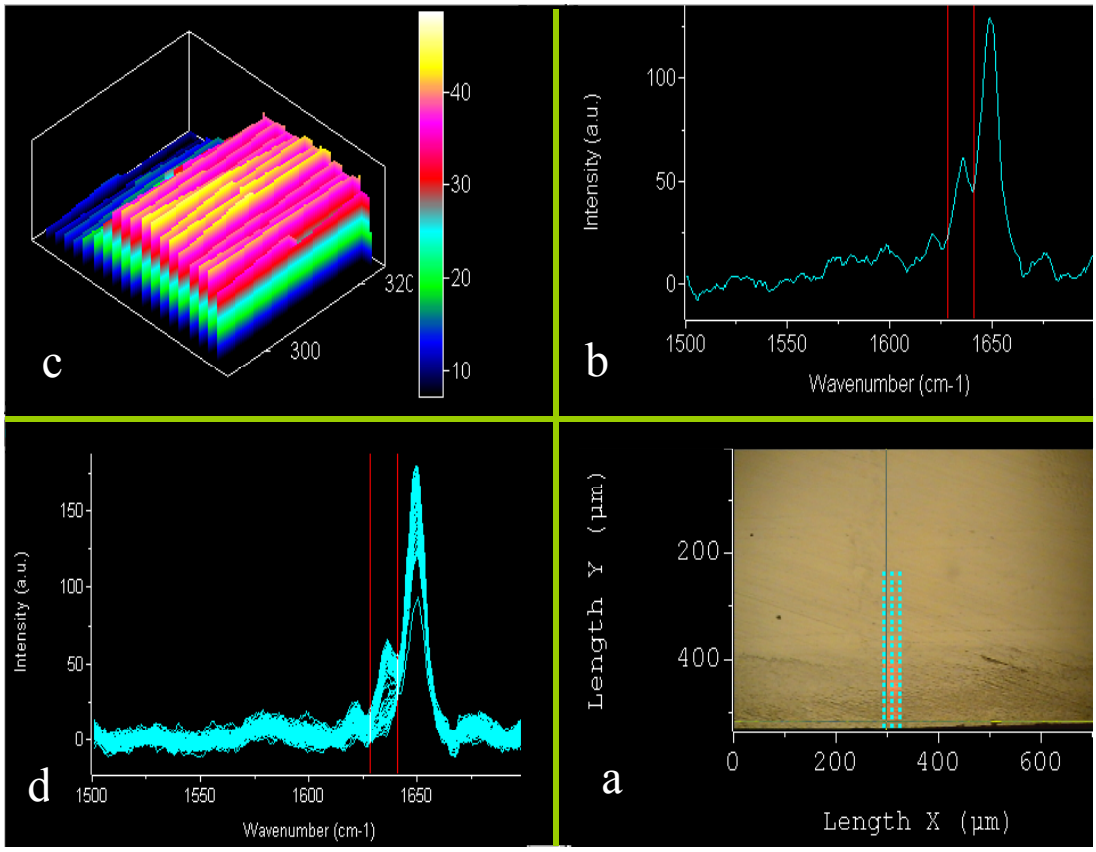

Figure 4.11. Mapping of cross section of CR-39 ophthalmic lens during the diffusion process of acrylic acid.

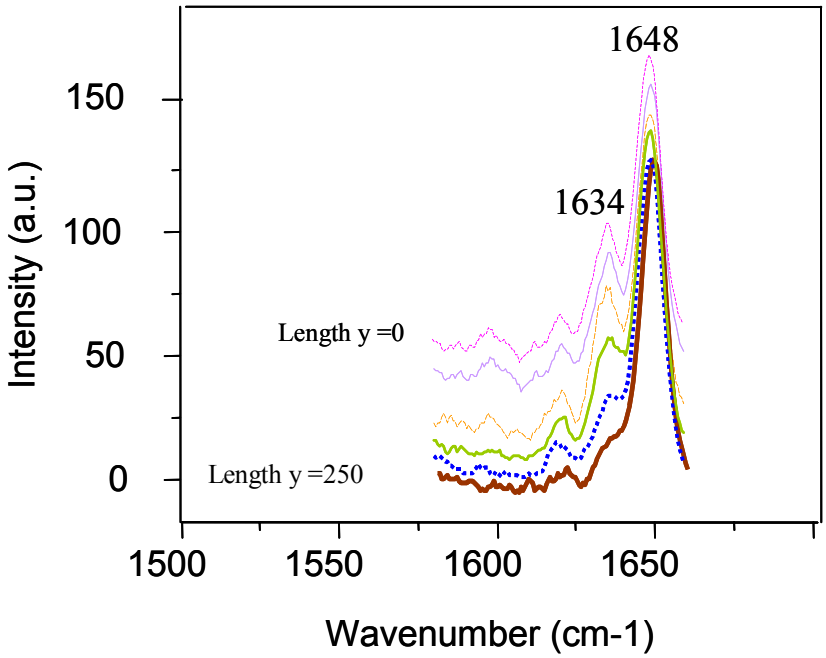

Figure 4.12. Diminishing of C=C bond after diffusing acrylic acid into CR-39 ophthalmic lens, (50µm steps).

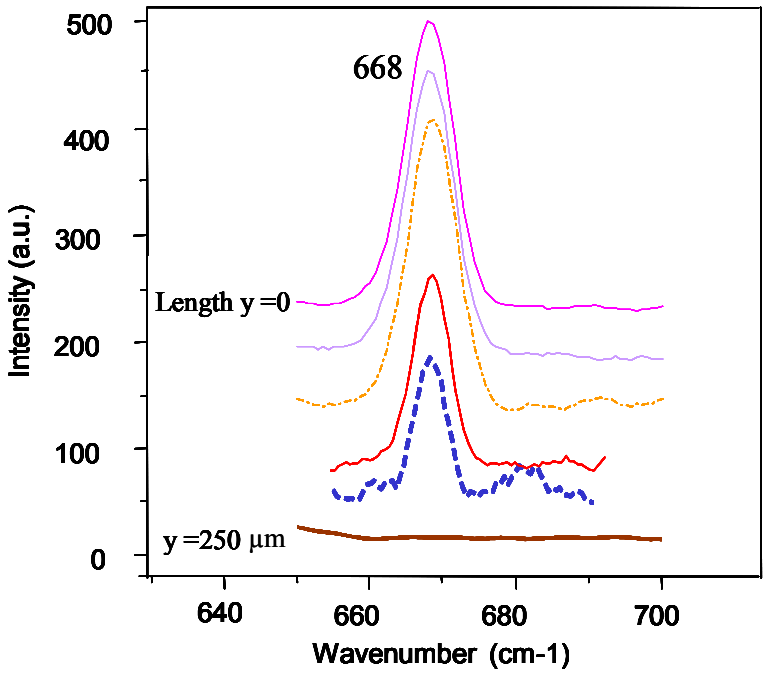

Figure 4.13. Diminishing chloroform peak after exposing CR-39 ophthalmic lens to UV irradiation, (50µm steps).

4.5 CONCLUSIONS

Laser Raman spectroscopy provides a convenient method for quantitative measurements for polymerising CR-39 polymer. Laser Raman was more sensitive to CR-39 polymer than FT-IR because of the polarisable C=C bond end group in CR-39, however the ν(C=C) vibration does involve a large change in polarisation, making it Raman intense. The consumption of C=C bond in the CR-39 polymerisation process depends on two factors, first the temperature profile required to polymerise the resin of CR-39 and second, the amount and type of thermal initiator used in the curing process. By using laser Raman spectroscopy the residual un-polymerised C=C bond was 9% of the total amount of C=C bond in the CR-39 resin when using secondary isopropyl peroxide as a thermal initiator.

A mixture of vinyl acetate with styrene can be diffused into the surface of a CR-39 ophthalmic lens but it is very difficult to achieve polymerisation within the surface or polymerise the mixture by itself. The diffusion of acrylic acid (AA) with chloroform as a solvent is more efficient than other monomers such as a mixture of styrene and vinyl acetate. Acrylic acid as a monomer can be photo-polymerised with or without the photo initiator (BP).

The C=C bond from diffusing acrylic acid into a CR-39 ophthalmic lens was fully polymerised into the surface after exposure to Ultra Violet light radiation. No polymerisation occurred from diffusing a mixture of vinyl acetate and styrene into the CR-39 ophthalmic lens. The consumption of a residual C=C bond of CR-39 by treating the lens with acrylic acid was 2%, but there was no consumption when the lens was treated with styrene and vinyl acetate.

The depth of diffusing the monomer into the surface for 6 hours at 50 ^{o}C was approximately 250μm. Not all the chloroform evaporated from the CR-39 ophthalmic lens surface, some remained in the lens at the same depth as the acrylic acid. This retained solvent in the surface may have some effect on the mechanical properties of the lens such as reducing the surface modulus as discussed further in chapter six.

The weight of the CR-39 ophthalmic lenses increased significantly while the swelling agent diffused into them. The swelling ratio was 1% for diffusing the monomer into the lens and based on the weight increase of the entire lens. Considering the monomer diffused to a depth of 250μm only on both upper and lower surfaces, this swelling ratio can be estimated to be around 4% for the swollen surfaces only.

While the weight decreased marginally during polymerisation due to the swelling agent evaporating from the surface, the average weight increased by 1.16% for diffusing acrylic acid with chloroform and 0.7% for diffusing a mixture of styrene with vinyl acetate in the same time and at the same temperature. These effects refer to chloroform because it is the best solvent for CR-39 ophthalmic lenses, as mentioned earlier. Chloroform as a solvent can be diffused into CR-39 polymer at room temperature.

CHAPTER 5

Mechanical Testing

5.1 INTRODUCTION

The experimental method used for generating the compressive stress to expand the surface of CR-39 ophthalmic lens was discussed in the previous chapter. The effect of residual compressive stress to the fracture load and fracture energy of CR-39 ophthalmic lens is described in this chapter.

The first section of this chapter describes the methodology of measuring the residual stress that was generated into the surface of the ophthalmic lens caused by diffusing and polymerising the monomer into the surface. The second section of this chapter presents the effect of swelling the surface on the fracture energy of the ophthalmic lens.

5.2 PHOTOELASTICITY EXPERIMENT

Ordinary light consists of a wave motion in which the vibrations of the electric field are normal to the direction of propagation. A special filter, the polariser, is able to select only those rays which are vibrating in a particular plane, so producing "polarised" light [86, 87]. On entering a transparent model subjected to stress, polarised light can only vibrate along two perpendicular planes coinciding with the

planes of principal stress. The speed of propagation of each component light ray depends upon the refractive index in that direction and hence on the stress acting in the plane. Consequently, the two rays emerge from the model out of phase, the difference in phase depending on the difference between the two principal stresses, the wavelength of the light that is used, and the thickness of the model.

The main two components of a polariscope are defined by the polariser and analyser as shown in figure 5.1. When the polarizer and analyser are crossed so that no light exits from the analyser, the set up is called a dark field. Light will only be transmitted due to effects resulting from birefringence in the model. Placing a quarter wave plate after the polariser will convert the incoming linearly polarised light to a circular polarized light [88]. While the second quarter wave plate converts the light emerging from the model back into linearly polarized light before it passes through the analyser to configure the polariscope into a circular polariscope as shown in figure 5.1.

One of the important uses of photoelasticity is obtaining knowledge of the stress and strain fields over a large area of a model. With the overall stress field available, regions of particular interest can be identified, e.g., regions of high stress gradients or residual stress.

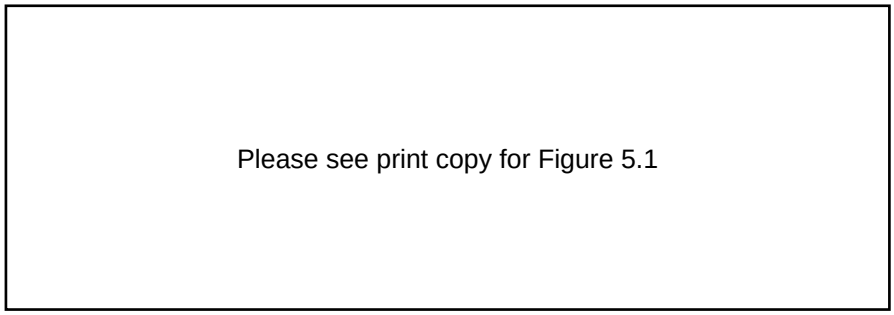

Figure 5.1. Layout of a circular polariscope.[88]

A circular polariscope configuration was used for determining the magnitude of principle stress difference in the treated samples. A circular polariscope was employed by inserting two perpendicular quarter wave plates in the crossed polariscope type Leitz Orthoplan research microscope from Ernst Leitz GMBH Wetzlar as shown in figure 5.2.

Figure 5.2. Leitz Orthoplan polariscope used in the photoelasticity experiment.

5.2.1 Sample preparation

A thin section of 50 micron thickness was made from a CR-39 ophthalmic lens. A special sectioning technique was employed to control the thickness of the thin section.

Three samples were made to examine different treatment conditions. The first sample was un-treated and was used as a reference. The second sample was treated with the swelling agent in the inner surface of the lens, while the treatment for the third

sample was in both inner and outer surfaces. The swelling agent used was a mixture of acrylic acid and chloroform as described in section 4.4.2. Sections of these samples were mounted in a plastic mould of 20 mm diameter and 20 mm height by placing a clipper inside the mould and inserting the sample sections inside the clipper vertically as shown in figure 5.3 a. A florescence resin type Epofix Struers was pre-mixed with Epofix hardener in a mixing ratio of 3:25 by weight. This mixture was poured into the plastic mould containing the specimens. After 24 hours of curing at room temperature, the whole mounted sample was pulled out from the mould as a one cylindrical rigid sample contains the different sample sections for a different treatment conditions of CR-39 ophthalmic lenses as shown in figure 5.3 a. The cylindrical moulded resin sample was ground from one side and polished in three steps to obtain a surface roughness of 0.06 micron. The grinding and the polishing process are as follows:

- Grinding using a range of silicon carbide paper from the coarsest grit of 180, 280, 400, 800, to the finest grit of 1200.
- Polishing with a suspended solution of 0.5 micron diameter of alumina particle.
- Polishing with a suspended solution of 0.05 micron diameter of alumina particle.
- Polishing with a suspended solution of 0.06 micron diameter particle of colloidal silica (oxide polishing solution OPS).

The sample was ground and polished in a circular pattern on the grinder and polisher surface to obtain a smooth shiny surface for the sample.

A frosted glass slide of 47mm x 26mm dimension was glued on the polished surface by using transparent super glue. A thin section of 1 mm thick was sectioned from cylindrical rigid sample by clamping the sample from the glass slide side into a cutting machine type Petro_thin / Buehler cutting machine using a diamond cutting

blade. The cut surface of this thin section was ground and polished in the same manner described above until the thickness reached 50 micron approximately as shown in figure 5.3 b. At this stage the sectioned samples were ready for the microscopic experiment.

The above procedure was useful for sample handling in order to control the required thickness, and during the polishing procedure. It also facilitates the sample movement on the polariscope's stage to distinguish the birefringence bands of each sample. All the above operations from the initial cutting to the final polishing were carried out in the presence of water or coolant liquid to ensure that the samples were not affected by temperature increases during the specimen preparation. The use of a thin section may help to relieve some of the constraint within the mounted samples and thus influence the accuracy of the residual stress measurements. It may reduces the residual stress by factor of $(1-\nu)$.

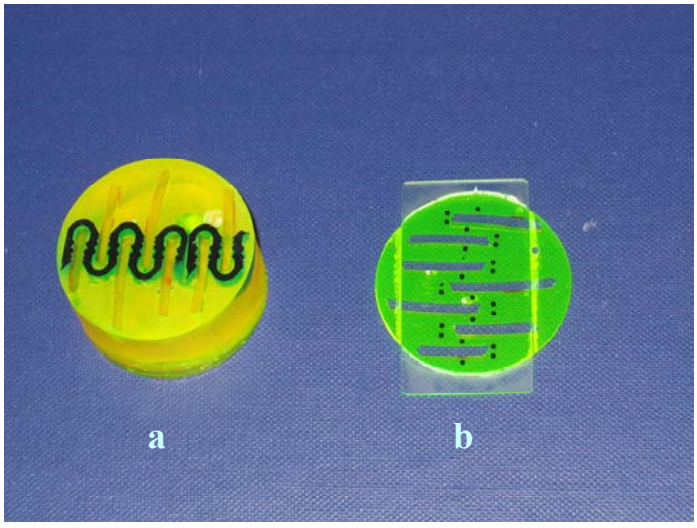

Figure 5.3. Thin section of CR-39 samples, (a) cylindrical cured resin sample mounting clippers holding different sections of CR-39 lenses having different treatment conditions, (b) 50 micron thickness thin section glued from one side with a glass slide.

5.2.2. Discussion of Residual Stress

Residual stress is one of the most important characteristics of glass articles from the point of view of their strength and resistance [89]. In the case of optical glass, birefringence caused by the residual stresses characterises the optical quality and toughness of the articles. The phenomenon of generating the residual stresses is applied in optical polymer and it can be evaluated by placing a thin section of a stressed sample into a polariscope light zone. This section presents the technique used in this project to evaluate the residual stresses that was generated into the surface of CR-39 ophthalmic lens.

5.2.2.1 Evaluation of residual stress

Each sample (prepared from the above section 5.2.1) was placed in the circular light zone of the circular polariscope and a film camera was attached to the polariscope to take images of each sample. It was found that no birefringence pattern observed in the untreated sample as shown in figure 5.4. While the birefringence patterns observed in the other samples where the treatment applied from the inner surface only and both the inner and outer surfaces as shown in figure 5.5 and figure 5.6 respectively. It was found that the birefringence resulting from the photoelastic residual stress corresponded to the second fringe order.

Figure 5.4. untreated sample, no birefringence band was observed .

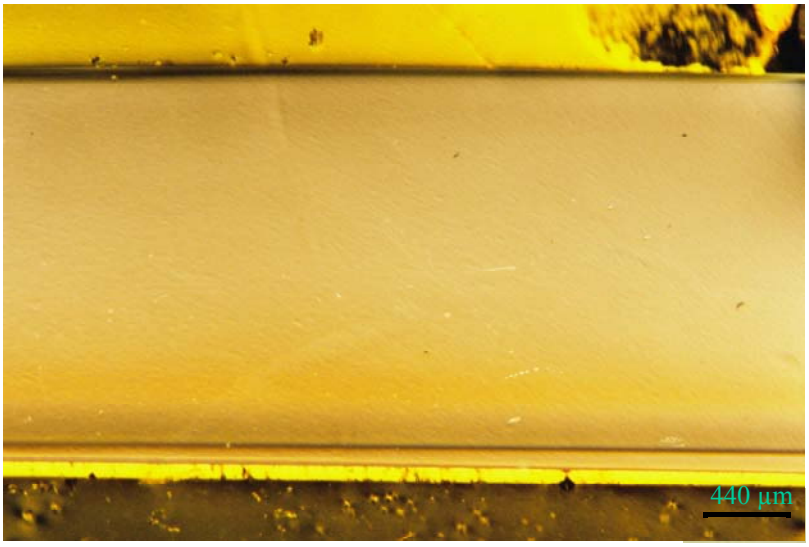

Figure 5.5. Treated sample from the lower surface of the lens, birefringence bands were observed from the lower surface only.

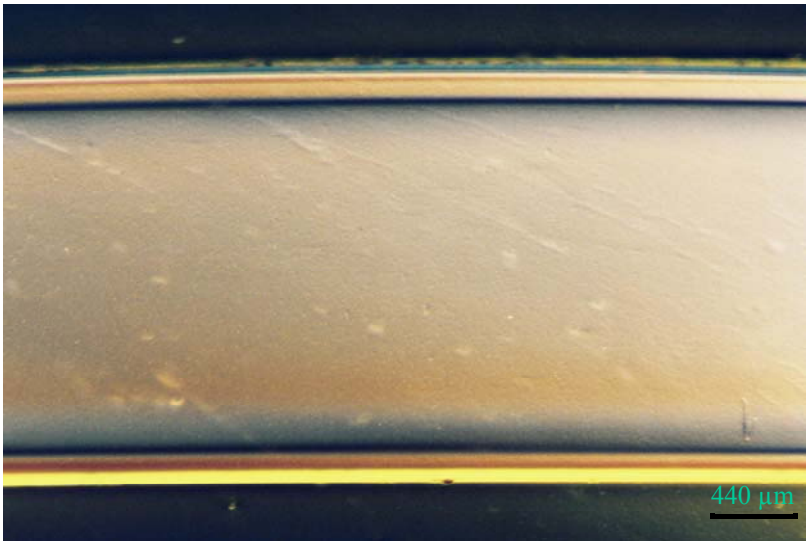

Figure 5.6. Treated sample from the both lower and upper surfaces of the lens, birefringence bands were observed in both surfaces.

5.2.2.2 Stress optical coefficient measurement

An apparatus was designed for this part of the photo-elasticity experiment with the aim to quantify the observed birefringence with incremental applied load. A three point bending test device was developed as shown in figure 5.7, and fixed on the rotatable stage of the circular polariscope field. The 3-point bending tester was designed to be adjustable in the x and y directions. Two adjustable pins can be moved and tightened in the x-direction and the whole set up can be moved in the y-direction as shown in figure 5.7. A load cell manufactured by Transducer Technique (USA) with maximum load capacity of 1000 grams was attached to the top of the moveable pin of the 3-point bending tester. The load was applied by incremental increases in downward displacement by turning the top lever in clockwise direction as shown in figure 5.7. This load cell was connected to an electronic reader where the load can be recorded.

An Accutom 50 precision cutting machine was employed to cut a thin section of untreated CR-39 ophthalmic lens by using a 357 CA cutting disc at 3000 rpm cutting speed. The same grinding and polishing procedure as discussed above was used to prepare a 50 micron thick and 2.2 mm width strip sample of untreated lens. As an unconstrained sample was required in the testing process, some difficulties were found in holding the sample in the grinding and polishing process. Extreme care was necessary in both the grinding and polishing process since the lens chipped very easily.

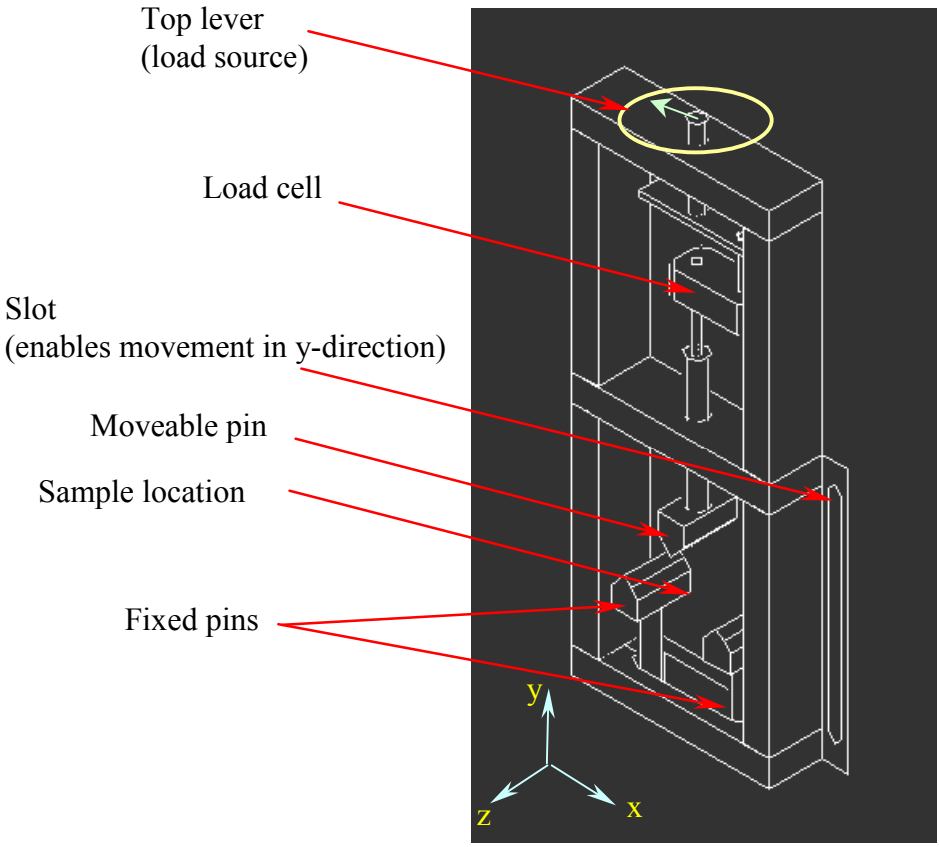

Figure 5.7. Three point bending device for thin section of CR-39.

5.2.2.3 Three point bending test load application.

A polished sample of 50 micron thickness and 2.2 mm wide was positioned horizontally on the two fixed pins of the attached 3-point bending device (see figure 5.7). The sample thickness (50 micron) was aligned in the z-direction of the 3-point bending tester. A photographic sequence method was employed to capture the change of the birefringence order when the bend specimen was loaded in the field of the circular polariscope that was configured. The load was applied gradually from the moveable pin located on the top of the thin section where the load cell was attached. The light from a 100-watt mercury vapour lamp passing through the specimen was picked up by a digital camera type DC 100 controlled by Leica DC Twain software mounted on the polariscope bench. The 30 micron gauge length was magnified 2.5 times by the lens system. The moveable pin was moved down to the sample in 1 mm increments with a 10-second time interval between each increment. One second after the application of each increment a photograph was taken of the specimen. A photograph of the specimen before the displacement process was started gave the measurement which, together with the load measurement from other exposures, made the calculation of the principle stress for each of various values of load possible.

Figure 5.8 shows the direction of the load and displacement applied to the thin section of the lens, no birefringence was observed when the sample was unstressed. The dispersion of birefringence was observed when the first load was applied as shown in figure 5.9. Figure 5.10 shows the emergence of the birefringence bands in the case of maximum load. Optical creep was observed during the unloading of the

sample after the 13 photograph was taken as shown in figure 5.11. A photograph of the fringe pattern shown in figure 5.11 was taken immediately after the load was removed. In pure bending test, the optical creep shown in figure 5.11 obtained from a total incremental strain load of 13 mm displacement, with approximate loading time of 2 minutes. The main purpose of the current photoelasticity experiments was to measure the optical stress and stress-optical coefficient relevant to the residual stresses that were generated into the surface of CR-39 ophthalmic lens. The optical creep of CR-39 had been investigated in details else where [53].

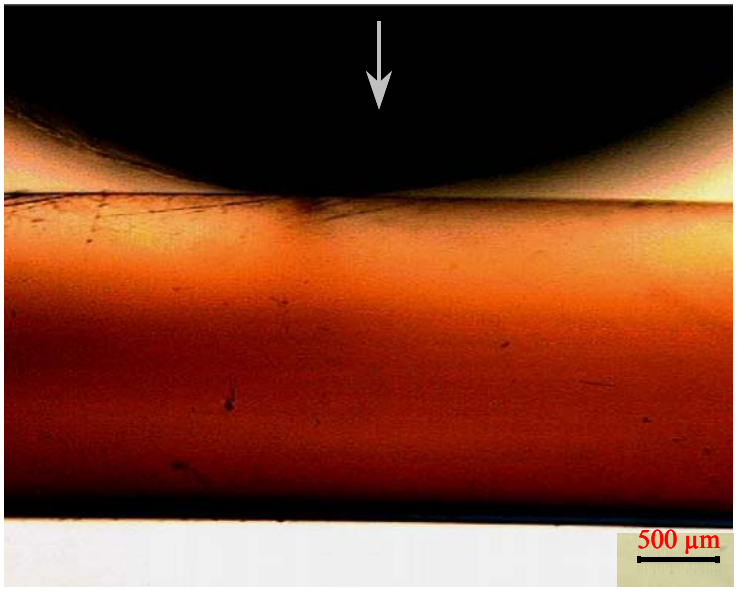

Figure 5.8. The movement direction of the moveable pin no load was applied no birefringence was observed.

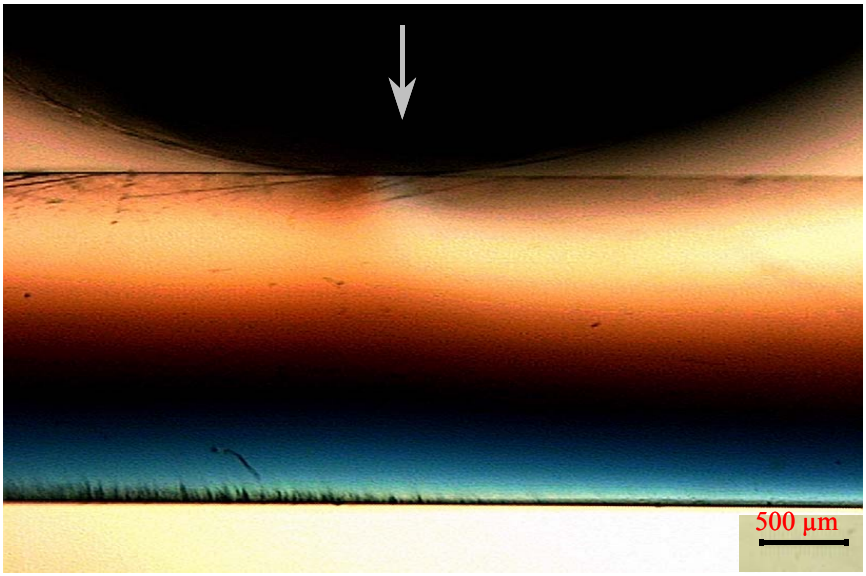

Figure 5.9. Birefringence was observed at the first load applied to the thin section.

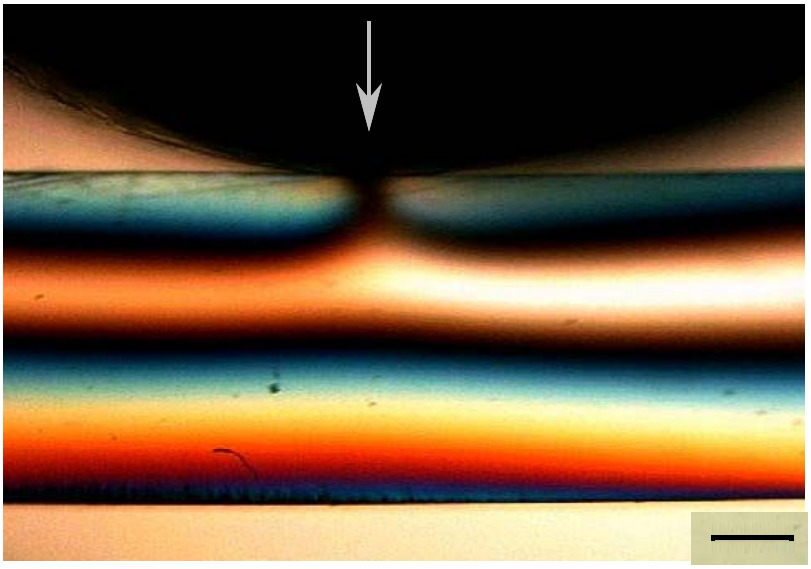

Figure 5.10. Interference of the birefringence bands under maximum applied load.

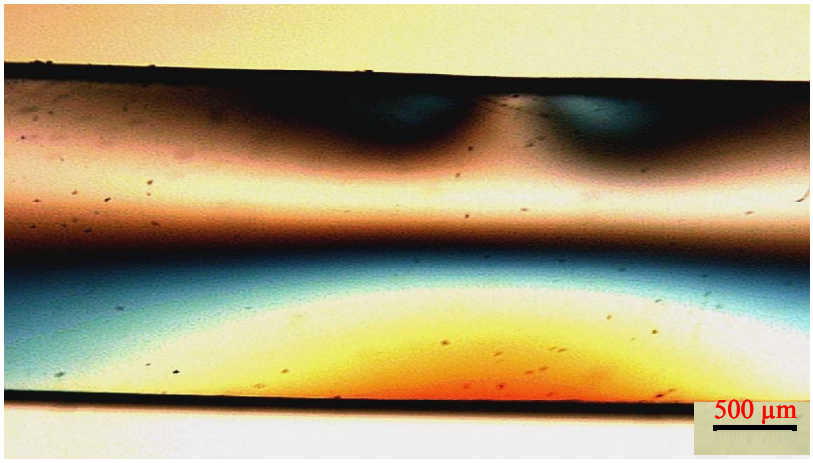

Figure 5.11. Optical creep when the sample was un loaded.

5.2.2.4 Measuring of residual stress and stress optical coefficient

The measured load for the observed fringe order, which was similar to the treated sample, was found to be 1.2 N, and relative retardation of 500 nm [90] respectively.

The applied stress was obtained from the measured load using the following equation:

$$\sigma = \frac{3Fl}{2bh^2}$$

where

F is applied load

l is distance between two fixed points of 3-point bending test fixture

b is specimen thickness

h is specimen width

The stress optical coefficient was obtained using the following equation:

$$(P-Q) = R / C_g \times t$$

where

$(P-Q)$ is the difference in the principle stresses

R is relative retardation

C_g is stress optical coefficient

t is thickness of the strip

The measured value of the residual stress was found to be 14 MPa with a stress optical coefficient value of 21 Brewsters for this stress. This residual stress was measured for the treated sample from both lower and upper surfaces. The residual stress in the treated sample from one surface was found to be same as the treated sample from both sides. Comparing the observation of the optical residual stress to the compressive stresses generated by the volumetric swelling in chapter3, it can be noticed that the residual compressive stress that was generated by swelling the lower surface was relatively reduced when both surfaces were swollen for the same volumetric swelling ratio applied in both lower and upper surfaces. This discrepancy of the residual stress generated from the treatment effect and applying the volumetric swelling (chapter 3) can be related to the limitation of the polariscope used in the photo-elasticity experiments.

5.3 IMPACT TESTING

The first part of this chapter described the measurement of the residual stresses obtained in the treated sample by means of birefringence. This second part describes the evaluation of the fracture load and fracture energy of the lenses on two treatment conditions compared to untreated CR-39 ophthalmic lens. The fracture energy was also evaluated for these two treatment conditions when the scratch-resistant coating layers were applied to the lenses and compared to the untreated lenses covered with same scratch-resistant coating layers.

5.3.1 The Safety Aspect of Lenses – An Introduction

The safety of dress eyewear depends on many factors: the nature of the hazard, qualities of the frame, and the fracture characteristics of the lens [15]. At the time of adoption of a standard for lens impact resistance (1972), glass was the most common lens material used in the eyeglass industry, and much research had been done regarding the fracture resistance of glass. At that time a fracture test would involve mounting a lens in a frame, mounting it on a dummy head, and subjecting it to impact by different real-life objects. Objects impacting lenses may be separated into two categories: low mass high velocity and high mass low velocity. This distinction is important because the results of these two types of test will be presented in this chapter.

Several testing procedure have been used or proposed to evaluate the resistance of ophthalmic lenses to breakage. The most common is the drop-ball test, which measures the height from which a ball must be dropped to break a lens. As an alternative static-load testing has been used to measure the load required to break a

lens. In actual use, eye glass lenses break under a variety of conditions; however, when eye injuries occur as a results of lens breakage, the failure is most often caused by an impact incident.

Crazing and shear yielding are the two primary localised deformation mechanisms intrinsic to glassy polymers. Shear yielding is plastic deformation in the form of shear bands which is intimately tied to the material softening that is observed right after yield. Crazing nucleates at the crack tip during the elastic regime or a head of the crack. As the craze extends, plasticity develops until an unstable crack propagation takes place when craze fibrils start to break down. Both processes have to be avoided in a properly designed component made of glassy polymer [91, 92]. CR-39 polymer is a glassy, highly cross linked material, in which crack propagation on fracture is controlled by plastic deformation at the crack tip. Increasing the plastic zone near the crack tip helps to slow down crack propagation and improve fracture energy. (hence, toughness improvement).

5.3.2 Static load impact test

The finished CR-39 ophthalmic lenses were provided from Scientific Optical Laboratories of Australia (SOLA). The plano power* type lenses were provided with a base curve of +6.0 D. All these lenses were round with a diameter and thickness of 78 mm and 2.2 mm respectively. The use of an Instron static load test in this type research was very useful to evaluate the fracture energy improvements for different treatment conditions. The instrument consists of range of load cells that can be attached to a crosshead that moves at preset speed determined by the operator. The load cell that was used in the static load experiment has maximum load capacity of

10 KN. The load cell was factory calibrated once every year. Attached to the crosshead is 15.9 mm steel ball mount. A steel ring of 25.4 mm inside diameter and 3.2 mm thick was mounted on the fixed part of the instrument as shown in Figure 5.12. The crosshead speed was set at 12.7 mm/min, as this speed was suitable for a quick test such as impact.

In the static load impact test, three groups of five lenses in each group were prepared. The first group was untreated to represent the reference and to be compared to the other two groups. The second group of the ten lenses, the treatment condition was on the lower surface only while the third group both of the lower and upper surfaces have been treated. Each lens was centred on the mount using the quarter cylindrical block to keep the centre of the lens and the centre of the mount on same vertical axis as shown in figure 5.13. The crosshead was then lowered onto the lens until the fracture was attained. The peak of the load displacement curve indicated fracture load; fracture energy was determined by measuring the area under each curve, up to lens fracture.

The static impact test was carried out as a preliminary test to the dynamic impact test to evaluate the effect of the treatment to CR-39 lenses. However, the literature [11, 12] have shown that the dynamic impact test is appropriate for testing the fracture energy of the ophthalmic lenses and this dynamic impact tester instrument was only available at the SOLA laboratories in Adelaide. Therefore, the static test was first used in Wollongong because it quickly yields a quantitative result for any given lens and then the dynamic test was employed at SOLA to confirm the effect of the treatment to the fracture energy of CR-39 ophthalmic lenses.

*Plano power lens is a lens which technically has no refractive power because the front and back surfaces of the lens are of equal curvature

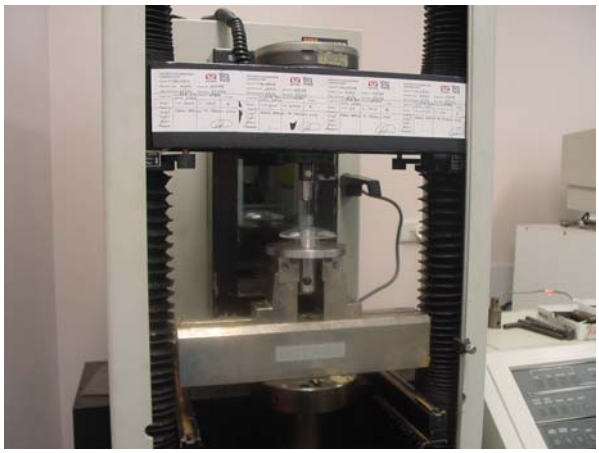

Figure 5.12. Static impact test.

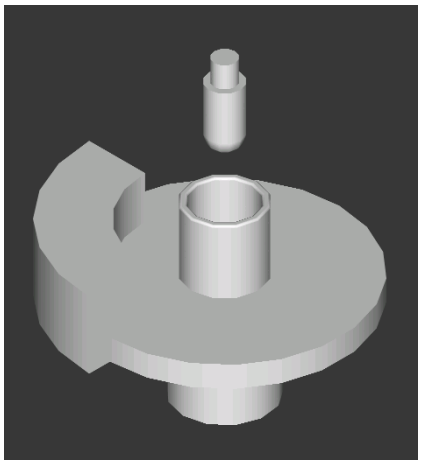

Figure 5.13. Steel ring lens mount.

5.3.3 Dynamic load impact test

The impact resistance of the polymeric ophthalmic lenses is generally measured directly on lenses by means of the drop ball impact test. In this test a ball of known weight and size is dropped on the lens from a given height. Figure 5.14 shows the standard drop ball impact test. This test is conducted by dropping the smallest ball size from the lowest position of the ball holder. The same ball is used on the same lens while gradually increasing the height of the ball holder position until maximum height or lens failure is reached. If the lens did not fail from the first test the ball size will be increased and the same test will be repeated. Multiple tests are conducted to obtain the size of ball and exact height that cause failure. The results obtained from a standard drop ball impact test depends on two chief factors. Firstly, impact resistance depends on the inherent resistance of the material to brittle fracture, which is usually measured by the material's fracture energy. Secondly, the result of the impact test also depends on the flaw distribution in the material which can be a complex function of the material microstructure and manufacturing parameters. Surface flaws play a potentially critical role in fracture mechanics, as fracture will begin at the weakest point within a tension field. The size of the flaws is increased by multiple impacting of the lens. This is the main disadvantage of using the standard drop ball test. The strength of lens materials is explained by the flaw theory which states that fracture occurs when the tensile stress acting on any flaw in the material reaches a critical value, which itself depends on the size and shape of the flaw. When this criterion is met a crack propagates rapidly through the material. The fracture-initiating flaws can be either intrinsic material inhomogeneities or surface flaws. For

ophthalmic lenses in practice, however, surface flaws resulting from grinding and polishing or from abuse in handling normally initiate fracture.

The standard traditional impact test instrument gives a fail or no fail answer only. It does not provide any more information such as the fracture load – displacement plot. The standard drop ball test was employed in this project to evaluate the effect of the treatment to the CR-39 ophthalmic lenses. Inconsistent and not significant results have been reported using the traditional drop ball test as presented in appendix II, thus more attention was paid to the use of the static and dynamic impact tests.

The Instron Dynatup 8200 (figure 5.15) was pioneered at SOLA Optics based in South Australia / Adelaide to evaluate the dynamic load impact resistance of the ophthalmic lenses. A load cell with end shaped as a steel ball is attached to upper part of the instrument. The upper part of the dynatup is a height and weight controllable type of instrument. The mounted lens is fractured by one fast drop of the upper part of the instrument as shown in figure 5.15. The weight of the upper part is preset to be 4.7 Kg and height to be 1.2 m to be appropriate for testing CR-39 ophthalmic lenses.

Figure 5.14. Standard drop ball test instrument.

Figure 5.15. Dynamic impact test instrument Instron Dynatup 8200.

5.3.4 Test Results

5.3.4.1 Static load test

The peak of the load displacement curve indicated fracture load; fracture energy was determined by measuring the area under each curve up to lens fracture.

Figure 5.16 shows the load displacement curves for five untreated lenses. The load increased from zero until the fracture occurred with increasing of the displacement.

The untreated load-displacement curves show a fracture load that varies from 600 to 2000 N with a corresponding displacement range of 3 to 7 mm respectively.

The static impact test for the group of lenses to which the treatment was applied into both lower and upper surfaces showed better fracture resistance results than the group of lenses that was treated in the inner surface only. There was no significant improvement in the fracture load of the group of lenses that was treated in the inner surface only compared to the untreated lenses.

The statistical results of the fracture loads and fracture energies for the untreated lenses and the treatment of both inner and outer surfaces will be presented in this chapter. Figure 5.17 shows the fracture load curves for the lenses treated from both sides. The treatment clearly has the effect of increasing the range of the fracture load and the range of the corresponding displacement. The maximum fracture load was 2800 N for the displacement of 9.0 mm. The treatment has increased the apparent ductility as displayed by the load-displacement curves in figure 5.17.

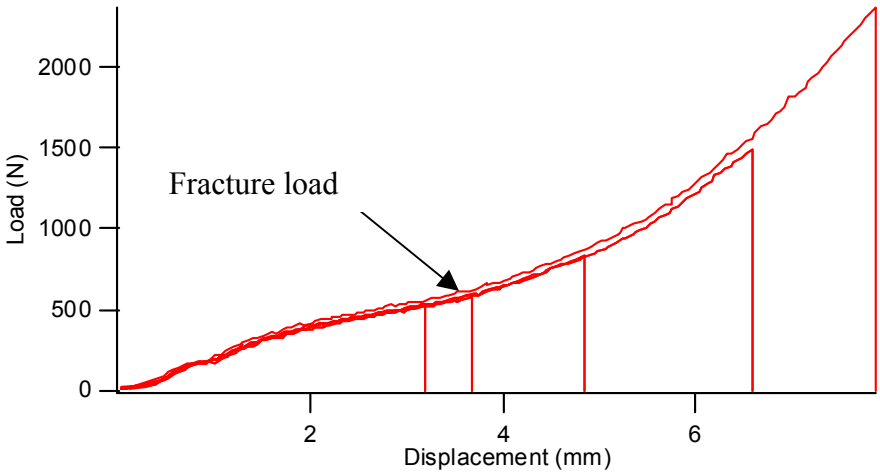

Figure 5.16. Typical static load-displacement curves for untreated lenses.

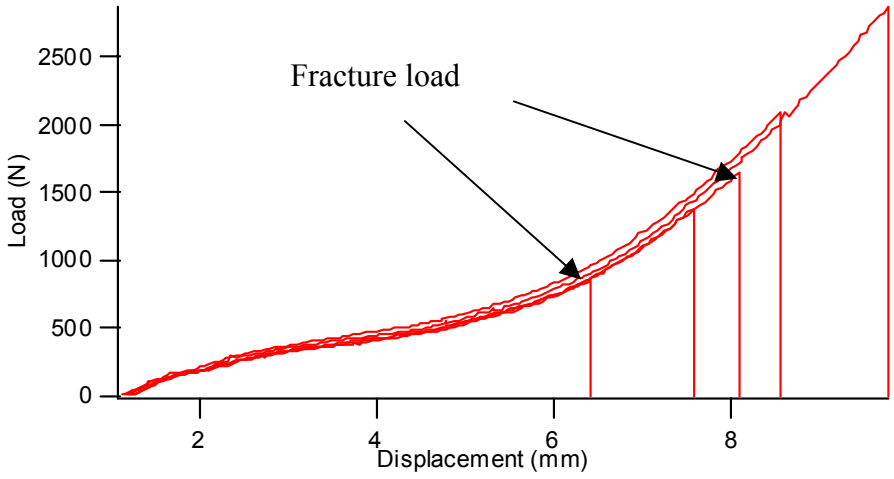

Figure 5.17. Typical static load-displacement curves for treated lenses.

5.3.4.2 Dynamic load test

All lenses used in both of the static and dynamic impact tests were collected from one manufacturing batch that gave an almost constant thickness of about 2.2 mm. Thus, the effect of the lens thickness on the fracture load and fracture energy was considered to be insignificant for both the static and dynamic impact tests. In addition, the thickness of the untreated and treated lenses was measured prior to the dynamic impact test. The average thickness of 10 untreated lenses was found to be 2.18 mm with standard deviation of 0.04, and 2.22 mm with standard deviation of 0.04 for the treated lenses. It was therefore reasonable to conclude that the improvement in fracture resistance of CR-39 ophthalmic lenses was due to treatment rather than the insignificant increase in lens thickness.

The results that were obtained from the dynamic load test are showing in Figure 5.18. Load – deflection curves are shown for ten untreated lenses, with the load increasing until the fracture occurred. It can be observed that of the ten untreated lenses, one lens is relatively ductile with a deflection of 4.6 mm approximately.

A significant effect of applying the treatment in both upper and lower surfaces of the lens can be noticed in Figure 5.19. Ten lenses were treated by the swelling agent as described earlier, generating compressive stresses in both lower and upper surfaces of the ophthalmic lenses. A higher fracture load with deeper deflection was observed by applying the treatment into the both inner and outer surfaces of the ophthalmic lenses as shown in Figure 5.19.

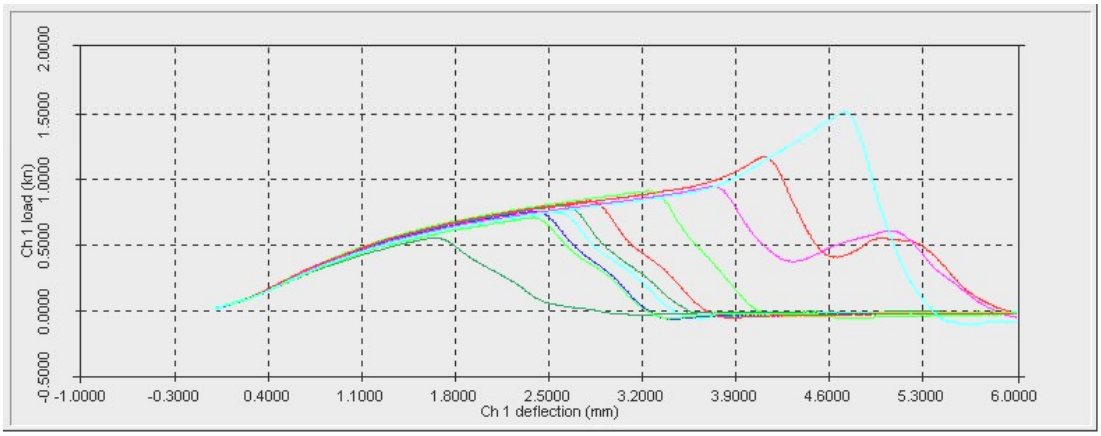

Figure 5.18. Dynamic impact curves for untreated lenses.

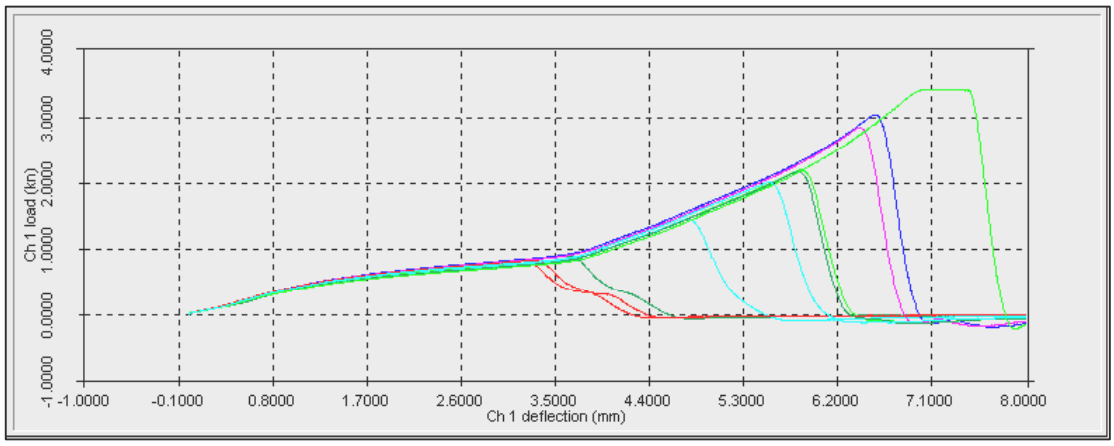

Figure 5.19. Dynamic impact curves for the treated lenses.

5.3.5 A Results of the Impact Tests

From the above experimental static and dynamic impact tests, analysis can be made to compare the results of each test and to evaluate the effect of the treatment on the fracture load and fracture energy of CR-39 lenses. Three groups of five lenses each have been tested in the static load impact test. The group of lenses to which the treatment was applied on both top and lower surfaces produced better impact resistance. The relation between fracture energy and load is useful. Figure 5.20 shows the mean fracture energies and the fracture load together with their average standard deviation for the static load impact test. It can be seen that the fracture energy has significantly improved by 53% in the presence of the treatment of both top and lower surface.

The fracture load is slightly increased over that of the untreated lenses by the inner surface treatment. The standard deviation is also relatively reduced due to the swelling treatment procedure. Lower value of the mean standard deviation can be achieved by increasing the sample size, but the importance of doing the static load test is to identify if the treatment has a beneficial effect on the impact resistance.

When a central load impacts a spherical lens in the centre of the convex side, the lens deforms. This deformation causes stress in the lens, and when the stress reaches the failure stress of the lens material, the lens will break. Because the CR-39 lens material is relatively brittle, the failure occurs by fast fracture. Fracture occurs when the stress reaches a level where a flaw or crack that is already present in the sample is able to grow so that the sample breaks. As shown previously in the numerical modelling chapter (figure 3.19), a tensile stress concentration zone was generated in the upper surface in the case of the mounted lens and loaded from the upper surface

with swelling of the lower surface only. This highly localized stress concentration in the upper surface may cause fracture to be initiated from the existing flaws in the upper surface and to propagate towards the lower surface so that the lens breaks faster than the case of swelling both surfaces. The surface flaws may have existed in the substrate material itself or be formed during the manufacturing process [16]. The surface flaws in the lower side of the lens can be reduced as a result of the swelling as discussed further in chapter six, while the existing flaws that remained in the upper surface promoted crack initiation. In the static impact test, this argument seems to apply as there was no significant improvement in the fracture loads and fracture energies found by swelling the lower surface only.

The dynamic impact test was carried out for two groups of 10 lenses each. The first group was the untreated and the second group consisted of lenses treated on both lower and upper surfaces. Another two groups of 10 untreated lenses and 10 lenses treated on both lower and upper surfaces were also tested after application of a scratch-resistant coating.

The average of fracture energies and fracture loads with their standard deviations for the four test groups are presented in table 5.1 and graphically in figures 5.21 and 5.22 respectively. The fracture energy and the maximum fracture load have significantly improved by 160% and 100% respectively compared to the untreated lenses.

A scratch-resistant (SR) coating has been spin coated and cured on both upper and lower surface of the treated lenses and prepared for the dynamic impact test.

Figure 5.22 shows the improvements in both of fracture energy and fracture load after applying the (SR) coating on the lens surfaces. The fracture energy and the fracture load have increased by 48% and 38 % respectively in the presence of (SR) coating layer on the treated lens surfaces. This drop of the fracture energy is due to

the (SR) coating layer; a coating which is harder than the lens will crack more easily than would the uncoated substrate. If the coating is well adhered, energy is concentrated at the initial crack and then propagates through the lens, resulting in fracture. Average fracture energy, fracture loads, and standard deviations, with the presence of the treatment and (SR) coating are given in table 5.1.

Table 5.1. Mean fracture energy and fracture load with their standard deviations SRtreated: hard coat applied on both sides of the treated lenses, SR untreated: hard coat applied on both sides of the untreated lenses

	Energy (J)	Stdve (J)	Load (N)	Stdve (N)
untreated	1.7	0.9	0.9	0.3
treated	4.6	2.4	1.9	0.9
SR untreated	1.6	0.4	0.8	0.1
SR treated	2.4	1.3	1.2	0.5

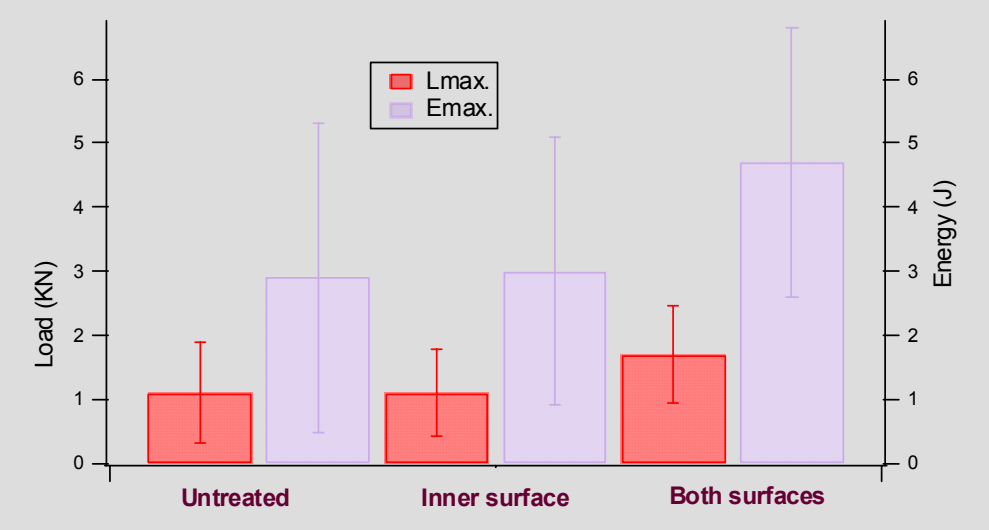

Figure 5.20. Static test results of average maximum load and fracture energy with their associated standard deviation of the presence of the treatment.

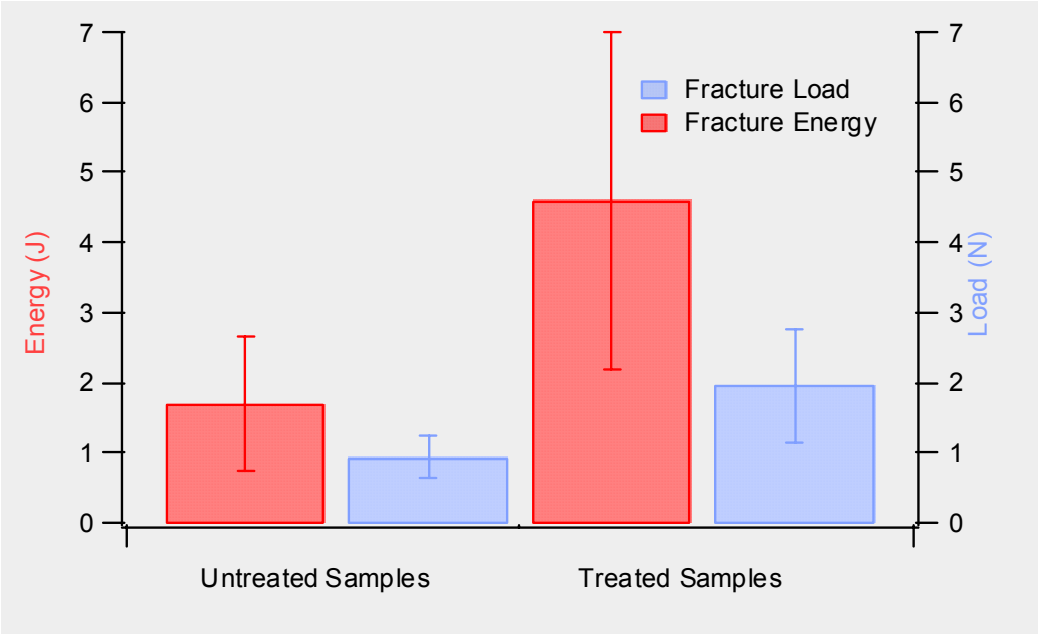

Figure 5.21. Dynamic load test results.

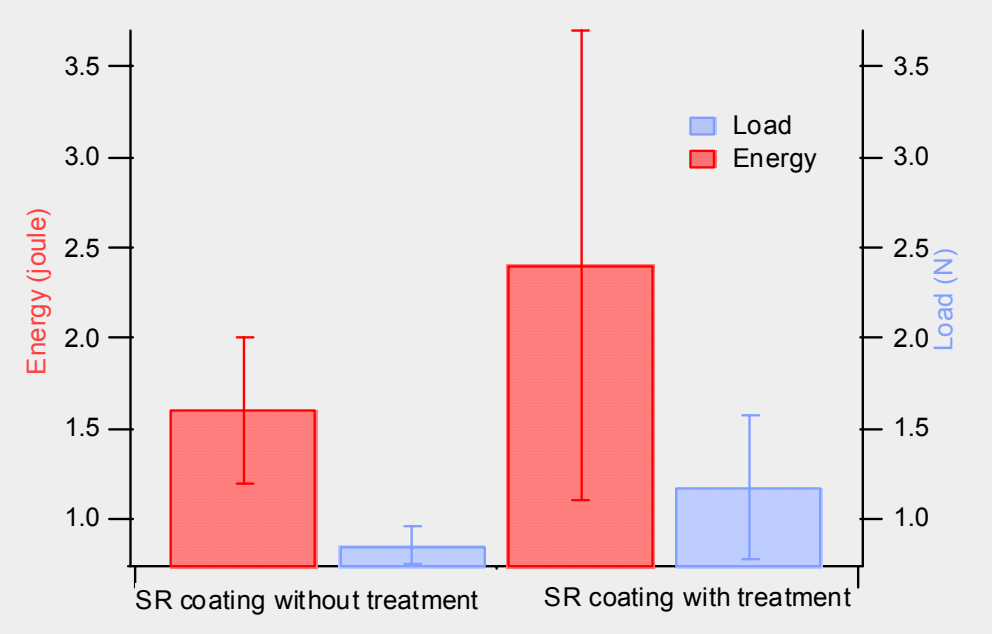

Figure 5.22. Dynamic load test results for the (SR) coating.

In the static impact test, the mean fracture energy increased by 53% and a statistical t-test between groups showed that the difference between the means was not statistically significant (with p*< 0.28), whereas in the dynamic impact test the mean fracture energy increased by 160% and this increase was found to be statistically significant (with $p < 0.004$). This is an indication that the results obtained from the dynamic impact test are much more statistically significant than those obtained from the static test. This difference between the level of significance of the two tests can be attributed partly to the difference of sample size used in both tests. The small sample size was chosen for the static test because of limited supply of the virgin CR-39 lenses from the manufacturer. Whichever testing method is used, the fracture energy of CR-39 ophthalmic lenses was shown to increase by treating both the lower and upper surfaces.

Applying the treatment to both upper and lower surfaces caused a significant change in dynamic test results, as can be seen in figure5.19. The improvement in toughness was reflected in the deflection-to-maximum load results, that were increased from the range of 2.5 – 4 mm for the untreated to 3.5 – 7 mm for the treated lenses as shown in figures 5.18 and 5.19 respectively. Also, the peaks of fracture loads were considerably increased because the treatment permitted the deflection to be extended to a steeper pert of the load-deflection curve.

*_P-value,_ sometimes referred to as observed significance level is a number between 0 and 1 that reflects the strength of the data that are being used to evaluate the null hypothesis. The _p-value_ defines the smallest value of alpha for which the null hypothesis can be rejected. A small p-value is an indication of strong evidence against the null hypothesis, while a large p-value indicates weak evidence against the null hypothesis.

An f-test showed that the swelling treatment increased the standard deviation of the failure energy significantly (with $p < 0.001$), comparing the control untreated group to treated lenses, while the toughness of CR-39 lenses was increased significantly. This may be partly attributed to sampling a steeper region of the load-deflection curve. The f-test is an appropriate tool in testing hypothesis of two population based on the sample variance rather than a mean (t-test) or portion of a population [93]. John et al.[16] used the f-test in their research on the effects of coatings on the fracture resistance of ophthalmic lenses to compare the variance of the coated and uncoated lenses.

5.4 CONCLUSION

The following conclusions, based on the experiments and tests carried out and described above, are given below.

CR-39 is the constituent polymer most used worldwide for ophthalmic applications, with better optical properties, cosmetic quality and being slightly cheaper than other ophthalmic lenses polymers such as polycarbonate. The need for tough, thinner optical lenses has become increasingly apparent for the last five years. CR-39 polymer is a brittle, high cross linked substrate, in which crack propagation on fracture is controlled by plastic deformation at the crack tip. Increasing the plastic zone near the crack tip helps to slow down crack propagation, leading to fracture energy improvement. It has been shown that swelling the surface of the CR-39 ophthalmic lens generated a residual compressive stress within the surface of the lens. The residual stress can be evaluated by the photoelasticity stress measurement.

The residual stress was found to be 14 MPa and the stress optical coefficient was found to be 21 Brewsters. It has been found that the stress optical coefficient for CR-39 cannot be considered as a constant because the optical creep was relatively high. It was found to be useful to compare the measured stress optical coefficient value of CR-39 to that of other polymers used for optical lenses such as the polycarbonates. The measured stress optical coefficient (Cg) value of CR-39 was found to be within the range of the various values of polycarbonates, of 20-70 (Brewster). The measured value of Cg (21 Br) for the residual stress value of 14 MPa was found to be relatively reasonable compared to Cg value obtained from the literature, which was found to be 37 Br for the tensile stress of 17 MPa.

It has been shown that the CR-39 polymer can be toughened by swelling the surface and placing it under compressive stress. The plano CR-39 lens can be considered as multi layered residual stressed composite substrate, after swelling both top and lower surfaces. The plano CR-39 ophthalmic lens can be toughened by swelling both inner and outer surfaces. The static load test and the dynamic load test have shown consistent overall fracture energy improvement of the layered composite structure of the CR-39 ophthalmic lens.

The fracture energy was improved by 48% after applying the SR coating on the treated ophthalmic lenses, as a result of the residual compressive stress that was generated on the outer and inner surfaces of the CR-39 ophthalmic lens. The fracture energy has been improved considerably in the absence of the SR coating layer. SR coating is a hard brittle substrate that allows the crack to initiate and be injected to the bulk material of the ophthalmic lens. The presence of residual surface compression on both lower and upper surfaces not only reduces the crack injection but also strengthens the overall ophthalmic lenses.

CHAPTER 6

Surface Characterization

The purpose of this chapter is to provide a picture of the effect of the treatment on the surface properties employing the ultra-micro-indentation system (UMIS), the atomic force microscope (AFM), and the dynamic mechanical analysis (DMA). UMIS was employed to analyse the mechanical properties of CR-39 surface during the treatment using a polystyrene sample as a reference. AFM was used to evaluate the degree of the surface roughness during the treatment process. Finally, DMA was used to analyse the dynamic mechanical properties of the surface and bulk of CR-39 before and after the treatment.

6.1 INDENTATION EXPERIMENTS (UMIS)

Traditional micro-hardness testing has been regularly employed as a fast and accurate method to determine localised material properties such as hardness and elastic modulus. This technique was found to be invaluable for determining the mechanical properties of thin coating layers on the substrate surface. It was found that a substrate has no influence on the measurements of the mechanical properties due to the small penetrations that were possible using such techniques combined with a limitation on the depth of indentation to be less than about 30% of the film thickness [94, 95].

The ultra-microindentation system (UMIS-2000) developed by the CSIRO, Australia, was employed to evaluate the mechanical properties of the surface of CR-39 ophthalmic lens. The main components of the instrument are shown schematically in figure 6.1 [96]. This instrument has a depth and load resolution of 1 nm and 0.01 mN, respectively.

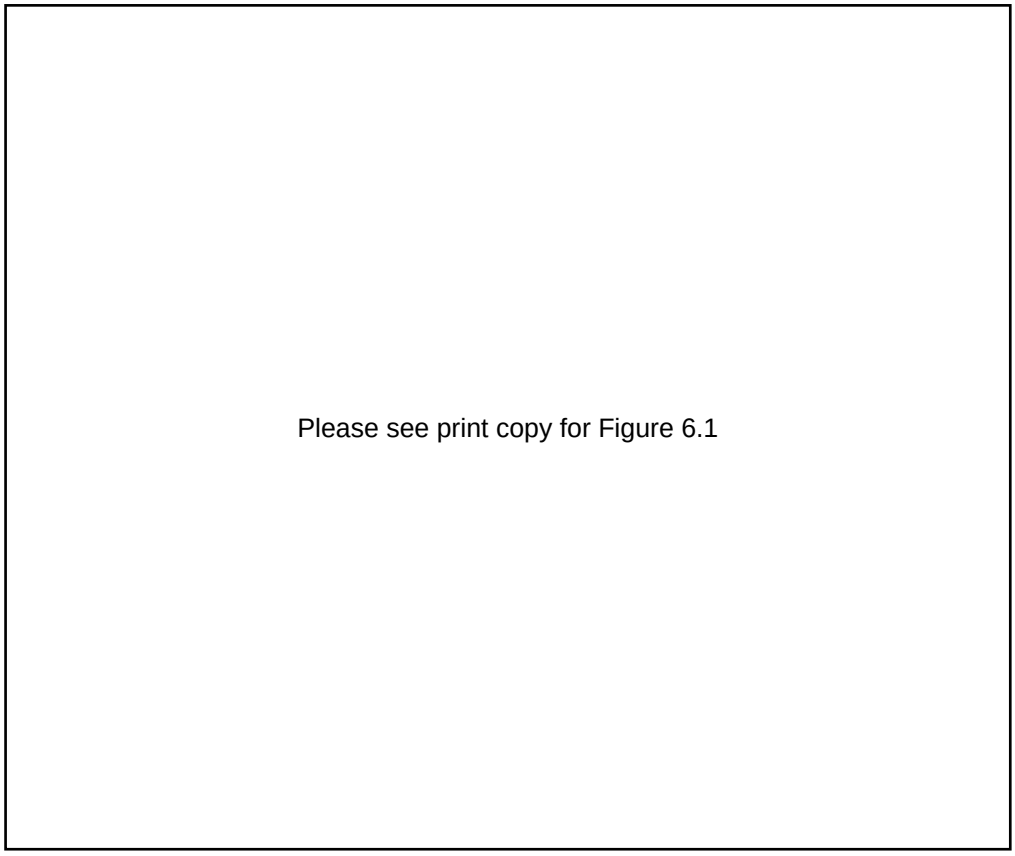

Figure 6.1. Schematic diagram of the basis of UMIS system.[96]

6.1.2. Theoretical background

Microhardness testing is a well established technique for assessing the resistance of material to deformation. Although the stress field developed in the material during indentation is more complex than conventional tests, certain features in an indentation test such as strength, brittleness and viscoelasticity can be related to the mechanical properties of materials. In this test, the spherical and Berkovich indenters were allowed to penetrate vertically downward into the tested sample under two different applied loads to form a plastically deformed indentation in the sample surface. In this section the main formulas are presented for using the spherical and Berkovich indenters. The analysis is available automatically within the UMIS 2000 operating software such that the substrate modulus and the surface hardness were calculated.

6.1.2.1. Spherical indenter test

The determination of the elastic modulus was measured by Hertz's relationship between force and displacement as described from the following equations [96]:

$$E^* = F\left[\frac{9}{8}\right]^{1/2}\left[\frac{1}{D_i} - \frac{1}{D_m}\right]^{1/2} \delta_e^{-3/2}$$

and

$$\frac{1}{E^*} = \frac{1-\nu_m^2}{E_m} + \frac{1-\nu_i^2}{E_i}$$

where

E^* is the composite modulus

D_i, D_m diameters of the spherical indenter and the residual spherical impression respectively.

δ_e is the elastic displacement for the force F

ν_m, E_m are the Poisson's ratio and the elastic modulus of the material being tested.

ν_i, E_i are the Poisson's ratio and the elastic modulus of the indenter

The hardness of CR-39 was measured using the following formula:

$$H_{sph} = F / A$$

where:

H_{sph} is the hardness using the spherical indenter

F is the force applied

A is the contact area measurement

6.1.2.2. Berkovich test

A sharp conical diamond indenter (Berkovich) was attached to the microhardness testing instrument to evaluate the mechanical properties of the same specimens used in the hemispherical indentation test. The indentation test was monitored by the

relationship between load and displacement (or indentation depth) depending on the fact that the displacements recovered during unloading was primarily elastic. By assuming the contact area between the indenter and the specimen remaining constant during the initial unloading, the analyses of Sneddon (1965) [97] could be used. Sneddon's analysis ends up as a simple relationship between applied load P, and the indentation displacement. The analysis, which was derived for the indentation of an elastic half space by a flat cylindrical punch, could be used to approximate other indenter shapes, through the use of appropriate geometric factors [98]. Oliver and Pharr developed an expression for load frame compliance as a function of contact area, assuming the load frame and specimen as two springs in series [99]. Combining Sneddon's analysis with Oliver and Pharr's developments, and considering the indented material stiffness equal to the slope of the unloading curve at the maximum load, the elastic modulus can be expressed by the following formula [99]:

$$E^* = \left[\frac{dP}{dh}\right]_{F\max} \times \frac{1}{2K\ h_{p\max}}$$

where:

E^* is the elastic modulus of the indented material

$\left[\frac{dP}{dh}\right]_{F\max}$ is the unloading slope at maximum load

$h_{p\max}$ is the plastic penetration at maximum load

K is a geometric factor constant

Berkovich hardness (Hb) can be defined as the load divided by the projected area of the indentation or by the mean pressure that a material will support. Berkovich hardness can be obtained from the indentation curve at the maximum load as:

$$H_b = F_{\max} / A$$

where $F_{\max}$ is the maximum indentation load and A is the projected contact area at the peak load.

6.1.3 Experimental preparation

The polystyrene (Austrex 103, granules, supplied by Polystyrene Australia) sheet used as a reference sample was prepared by compression moulding in a hot press at 165 ^{o}C. The resultant 3mm thick bulk material was cut into approximately 1 x 1 cm squares, then ground and polished to 1 μm surface finish without any intermediate grinding and polishing steps. Three samples were cut out from three different lenses, the first was untreated, the second lens was treated with the swelling agent but was uncured, and the third sample was UV cured. Indentation experiments were carried out at room temperature and ambient atmosphere using an instrument built by CISRO / Australia.

A standard tungsten carbide R50/60 μm spherical indenter was attached to the indenter holder of the UMIS-2000 instrument. The technique involved incremental loading and partial unloading cycles with a maximum load of 50 mN. Unloading at

each cycle was set at 50% of the load employed for the particular cycle. The following parameter set up was employed for the spherical indentation test:

- Initial contact force was 0.015 mN
- 20 increments to a maximum load of 50 mN
- Holding time at each step of 60 seconds and pausing 0.1 second at each load increment
- Each indentation was set at 100 μm apart.

A standard Berkovich diamond indenter was used to evaluate the mechanical properties of the same samples prepared for the spherical indentation test, using different indentations areas. A different technique was used for the Berkovich indentation test because the indenter geometry was different from the spherical indenter. The technique involved incremental loading, holding, and unloading. The following conditions were used for all indentations:

- Initial load of 0.015 mN and maximum load of 3 mN. A small load was used to minimise the substrate effect on the treated samples.
- 20 increments of loading and unloading steps, respectively.
- Holding time at each step was 10 seconds and a longer holding time of 10 minutes at maximum load.
- Each indentation was set at 50 μm apart.

6.2 SURFACE ROUGHNESS MEASURMENTS (AFM)

The atomic force microscope was invented by Binning, Quate, and Gerber [100]. A typical commercial AFM consists of a piezoelectric scanner which controls scanning

motion, an optical head which senses cantilever deflection, and a base which supports the scanner and the head, and includes a circuit for the deflection signal. Figure 6.2 shows the main parts of a commercial AFM (NanoScope III). The beam from a laser beam diode is focused onto the back of the cantilever and reflected off the back of the cantilever onto a split photodiode. The differential signal from the split photodiode provides a sensitive measure of the cantilever deflection. The feed back signal is used to control the height of the piezoelectric crystal as the sample is scanned. The height of the piezoelectric crystal is related directly to the topography of the sample surface. The advantage of using an atomic force microscope is that it can image non-conducting samples such as polymers and ceramics and can produce three-dimensional images of solid surfaces at very high resolution.

A digital instrument multimode AFM was employed to image the changes to the surface topography while treating CR-39 ophthalmic lenses. Imaging was performed using a contact mode with a standard silicon nitride cantilever. In contact mode, cantilever deflection was kept constant with the height of the sample stage being adjusted by the feedback loop. The deflection set point was adjusted using a force ramp to keep the applied force at a minimum whilst still being positive. A scan size of 20 μm was used for all scanned images. Dinanoscope version 6.11 controller software was used to operate and process the images that were scanned by the AFM instrument. Five images were obtained for each sample, each from a different spot.

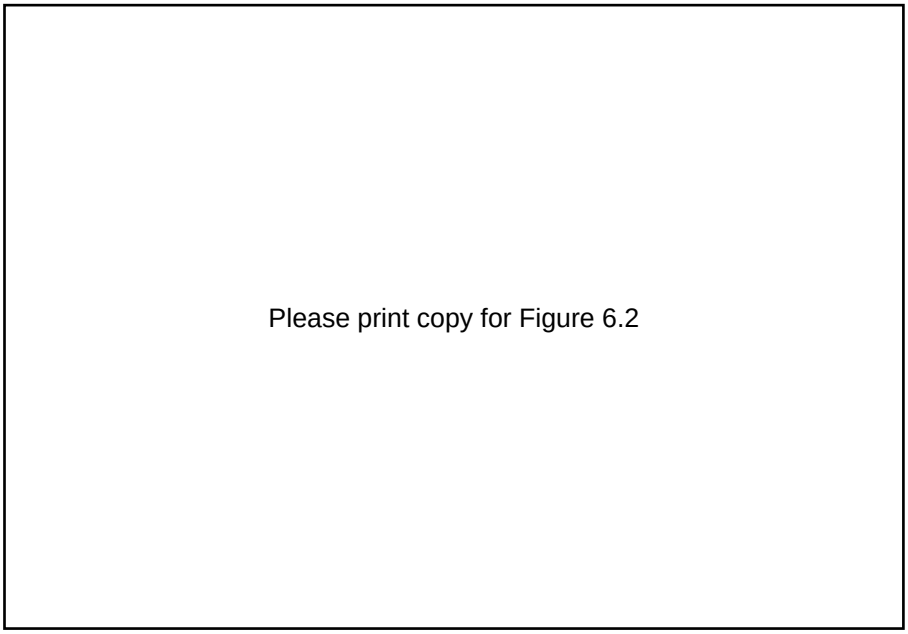

Figure 6.2. Schematic representation of AFM sensing system.[100]

6.3 DYNAMIC MECHANICAL ANALYSIS (DMA)

DMA can be simply described as applying an oscillating force to a sample and analysing the material's response to that applied force [101]. A TA series instruments DMA Q800 was employed for the dynamic mechanical analysis (DMA). The DMA system possessed a liquid nitrogen cooling facility that allowed testing to be accomplished over the temperature range –145 ^{o}C to 600 ^{o}C. Two modes of operation were used, controlled force and multi-frequency strain. The sample was clamped between two parallel arms and deformed at a defined load pattern stress and on an oscillating strain, depending on the experimental mode.

6.3.1 Controlled force mode

In controlled force mode, the penetration clamp of DMA Q800 was employed to apply a load or stress to the sample and measure the resulting deformation, as shown in figure 6.3.a. The spherical indenter of 440µm radius was controlled by the association of the driver motor and air bearing, as shown in figure 6.3.d. The main advantage of using an air bearing was to reduce noise. The optical encoder was attached to the DMA instrument to measure the resulting displacement of the moveable block where the load was applied. A squared sample 10 mm long and 2.2 mm thick was mounted on the fixed arm of the DMA Q800 and a preload of 0.01 N was applied. The ambient temperature was equilibrated at 35 ^{o}C and a 2 N maximum load was applied with a ramp force rate of 0.1 N/min. A creep of 5 minutes holding time at the maximum load was configured before the unloading cycle of 0.1 N/min was started.

6.3.2 Multi frequency strain mode

In this mode the DMA instrument can be configured to have multiple frequencies in range of 0.001 to 10 Hz. A sinusoidal stress forces the sample to undergo oscillatory motion at a fixed frequency. Energy dissipation in the sample causes the resulting strain to be out of phase with the driver signal. This difference of phase was defined as phase lag as shown in figure 6.3.a.

A typical sample, 35 mm long by 10 mm wide by 4 mm thick was mounted in the single cantilever configuration. The sample was subjected to a sweep strain at a

frequency of 1 Hz with an amplitude of 15 μm and a preload force of 0.01 N. The test was operated over various temperature ranges 30 ^{o}C and 100 ^{o}C with a ramp temperature rate of 5 ^{o}C/min.

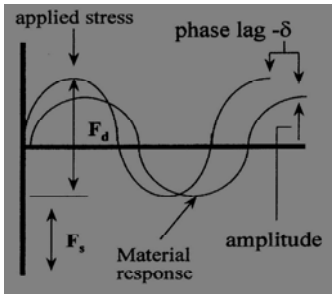

(a) Basic principle of DMA

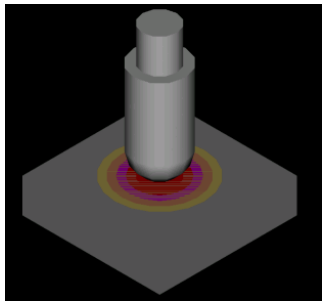

(b) Penetration mode of DMA

(d) DMA Q800 series

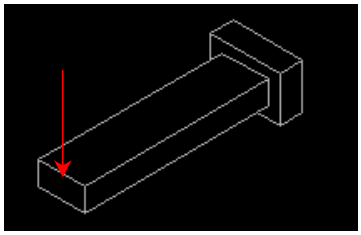

(c) Single cantilever mode

Figure 6.3. Dynamic Mechanical Analysis (DMA) test.

6.4 RESULTS AND DISCUSSION

There are two distinct sections of results involved in this chapter. The first section describes the surface characterisation of CR-39 ophthalmic lenses during the treatment process. The mechanical properties of the surface are compared to the polystyrene surface as a reference sample using the ultramicroindentation system (UMIS-2000). The effect of the treatment on the surface roughness of CR-39 are analysed by employing the atomic force microscopy (AFM) instrument. Three groups are used in the AFM experiment; untreated, uncured, and uv treated samples respectively. The second section covers the dynamic mechanical analysis of CR-39 ophthalmic lens with and without applying the treatment into the surface. Two groups of samples are tested, untreated and uv treated, to evaluate the effect of treatment to the virgin sample.

6.4.1 Surface characterization

6.4.1.1 Mechanical properties characterization

The UMIS indentation results displayed excellent consistency in the acquired load displacement curves of the tested samples. The mechanical properties of the surface of the CR-39 ophthalmic lens were examined before and after the polymerisation process (uv treatment) was accomplished. The load-displacement curve was usually acquired during indentation testing and used to determine the elastic modulus and hardness [102]. The elastic modulus and hardness of the treated surface were evaluated using the spherical and sharp indenters (Berkovich). Figure 6.4 illustrates an average of five tests for twenty loading and partial unloading cycles for four

different samples, using the spherical indenters. Four pairs of loading, partial unloading cycles were obtained at a maximum load of 50 mN for different samples. It should be noted that the transition from elastic to plastic behaviour occurred where the load, partial unload data points began to diverge, as shown in figure 6.4. It can be seen from figure 6.4 that the upward arrow was the direction to the loading point, while the downward arrow was the direction to the partial unloading point.

The surface of the uncured, treated sample had more penetration than the other samples. This implies that diffusing the swelling agent into the surface softens the polymeric surface of CR-39 ophthalmic lens. UV initiated polymerisation decreases penetration for the maximum load applied of 50 mN. Surface softening of CR-39 polymer during the diffusion process of the swelling agent can be noticed using the Berkovich test, as shown in figure 6.5. A maximum load of 3 mN was configured in the Berkovich test due to the sharpness of the conical indenter. Figure 6.5 shows an average of five tests of twenty incremental loads, holding at maximum load, and then twenty unloading indentations. More penetration occurred during 10 minutes of holding the indenter at maximum load for the uncured sample than for the others. It can be noticed from figures 6.4 and 6.5 that a similar trend of higher penetration occurred after the diffusion process of the swelling agent, causing surface softening. The softened surface became harder after exposure to the UV light and initiation of the polymerisation process, however, it remains softer than the original untreated surface. The surface of the polystyrene sample was found to be much harder than the treated and untreated samples in both tests.

Table 6.1 summarises the substrate modulus and hardness values associated with their total penetrations to the maximum load. The apparent elastic modulus and surface hardness had been obtained on the basis of the unloading curve [96]. It was

observed that the total penetration at the maximum load for the uncured sample was increased over that of both of the spherical and Berkovich indentation tests, while the modulus and hardness decreased. The measured modulus values of the original untreated sample as well as the treated sample were found to be relatively accurate compared to the modulus value of the reference sample (polystyrene) using the spherical indenter test. The composite modulus value of polystyrene using the spherical indenter was found to be 3.4 GPa, this value was relatively close to the range of measured values found from the literature[96] which were in range of (3.7 - 4.4) GPa for different indenter radius and different surface finished samples. The measured modulus values using the Berkovich test were found to be significantly higher than the measured values using the spherical indenter test, due to the instrumental calibration requirement (other users had higher modulus than the expected values using the Berkovich indenter), loading rate or test temperature. The uncured sample had a lower surface modulus than the untreated and the uv treated samples in both indentation experiments. The tabulated values of the modulus, hardness and maximum penetration were the average of five repeated tests.

Table 6.1. Modulus and surface hardness results using the spherical and Berkovich indentation tests.

	Polystyrene			Untreated			Uncured			UV treated		
Indenter type/ Load at max.	E GPa	H GPa	δ_{max} μm	E GPa	H GPa	δ_{max} μm	E GPa	H GPa	δ_{max} μm	E GPa	H GPa	δ_{max} μm
Spherical R50/60 50 mN	2.9	0.13	1.5	1.8	0.1	2.0	1.1	0.06	3.0	1.5	0.08	2.3
Berkovich 3 mN	5.8	0.4	0.6	3.7	0.2	0.8	1.9	0.1	1.2	3.5	0.2	0.9

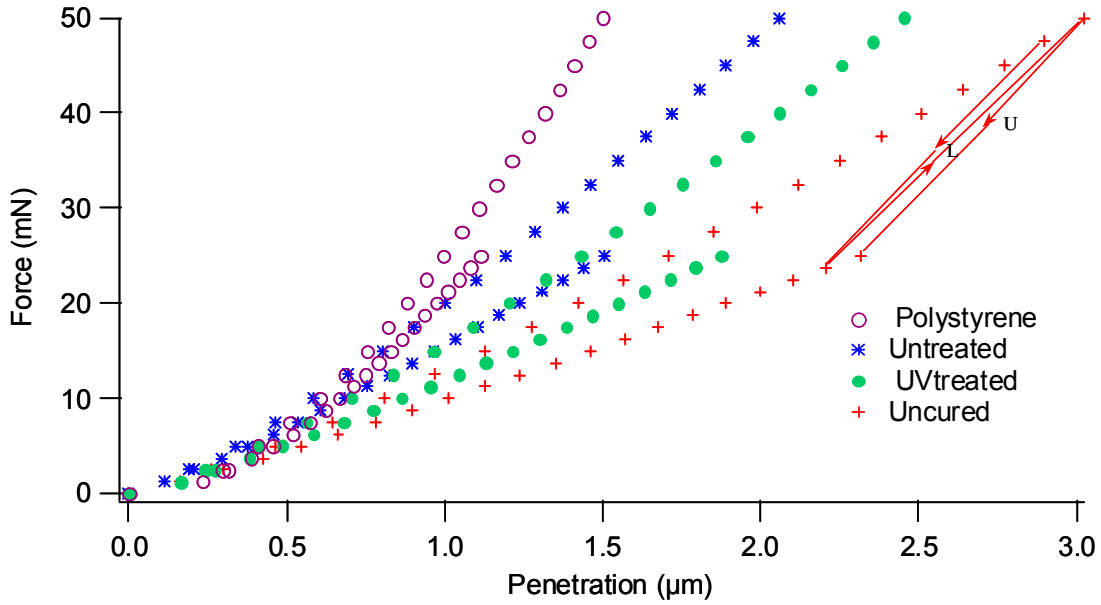

Figure 6.4. Load – displacement curves of hemispherical indentation test. (L) Loading, (U) Partial unloading.

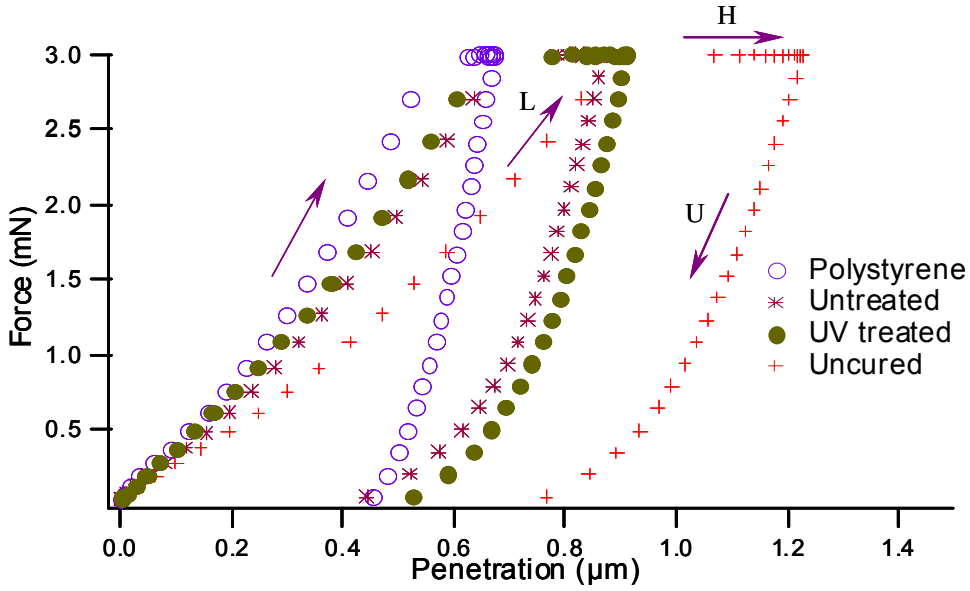

Figure 6.5. Load – displacement curves of Berkovich indentation test (L) loading, (H) holding, (U) unloading.

Figure 6.6 shows the elastic modulus values and the maximum penetrations and their associated standard deviations for the spherical indentation test. A maximum load of 50 mN was applied to all the samples. It can be observed that the polystyrene sample was harder than the other three samples in that it showed higher modulus and lower penetration at a load of 50 mN than the other samples. It was found that the uncured sample had a softer surface than the uv treated and even the untreated samples and showed a lowest modulus and highest penetration. It can be seen from this figure that the standard deviation was relatively small. The standard deviation value is an indication of the test repeatability showing that the sample was homogeneous with a uniform surface treatment. Figure 6.7 shows the ratio of elastic modulus to surface hardness for the untreated, uncured, uv treated, and polystyrene samples respectively, using the spherical indenter.

The elastic modulus E, is a direct measurement of the elastic deformation of the material, whereas the hardness value H, gives an indication of the extent of plastic deformation in a material. Therefore the ratio E/H should in general be a fair indicator of the general deformation characteristics of the material, i.e., the higher the ratio, the more likely the material will behave in an elastic manner.

It can be seen that the E/H ratio for the uv treated sample was relatively increased compared to the untreated sample. This indicated an improvement in elastic deformation as the hardness decreased, which is the measurement of a material's resistance to localised plastic deformation. The polystyrene sample exhibited the highest E/H ratio, as shown in figure 6.7.

In figure 6.6, the polystyrene sample exhibited higher elastic modulus and lower penetration than all the CR-39 samples for the maximum penetration load of 50 mN.

In figure 6.7, the E/H ratio of polystyrene was higher than the CR-39 samples due to more elastic deformation for polystyrene. From the literature review (2.2.5.2), the tensile strength and flexural modulus of CR-39 were 38 MPa and 2.2 GPa [25] respectively, while, for polystyrene they were found to be 55 MPa and 2.9 GPa, as reported in the technical information sheet of the polystyrene where the polymers were supplied (Polystyrene Australia Pty Ltd). All these findings indicate that the polystyrene (reference sample) shows more elastic deformation than CR-39.

Figure 6.8 shows the E/H ratios for the untreated, uncured, uv treated, and polystyrene samples respectively, using the Berkovich indenter for the maximum load of 3 mN. In this case, the E/H ratio for polystyrene was lower than that of all CR-39 samples. These contradicts the earlier results shown for the spherical indenter and could be attributed to the use of Berkovich indenter for such material i.e. CR-39, as found from the literature that a sharp indenter is not recommended to use for CR-39 due to excessive creep [62]. The inaccuracy of the elastic modulus measurements using a sharp indenter may due to the recovery of CR-39 that was found to be almost entirely elastic [66]. The relationship between load and depth of penetration for the Berkovich indenter employed here and derived by Oliver and Pharr assumed a combination of the elastic plus a significant plastic deformation for the indented materials. Thus, the very significant creep and small plastic deformation that have occurred during loading of CR-39 may lead to complication and inaccuracy in the calculation of hardness as well as the estimation of the elastic modulus.

Alternatively, the inaccuracy of the elastic modulus obtained using a sharp indenter could be attributed to the imperfect shape of the indenter. Previous experiments carried out on polystyrene standard samples had shown that the values of elastic modulus of polystyrene obtained were 1.6 times the correct value for the relevant

penetration depths. This imperfection in the indenter was verified microscopically using scanning electron microscope (SEM).

Although, the previous work has shown that the surface fracture energy can be evaluated using a sharp indenter such as Berkovich where the cracks are observed [103], [104], the attempt of determining the surface fracture energy of CR-39 samples was unsuccessful for two reasons: the inconsistency of the value of elastic modulus due to creep, and the instrument limitation of measuring the crack length immediately after the load removal.

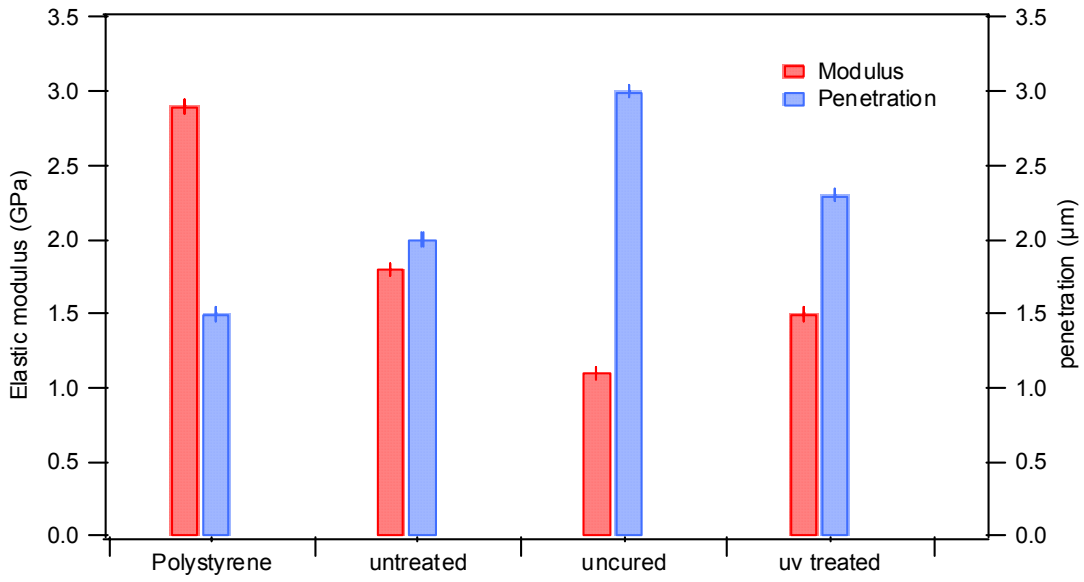

Figure 6.6. Elastic modulus and maximum penetration at the maximum of 50 mN load for the sperical indenter.

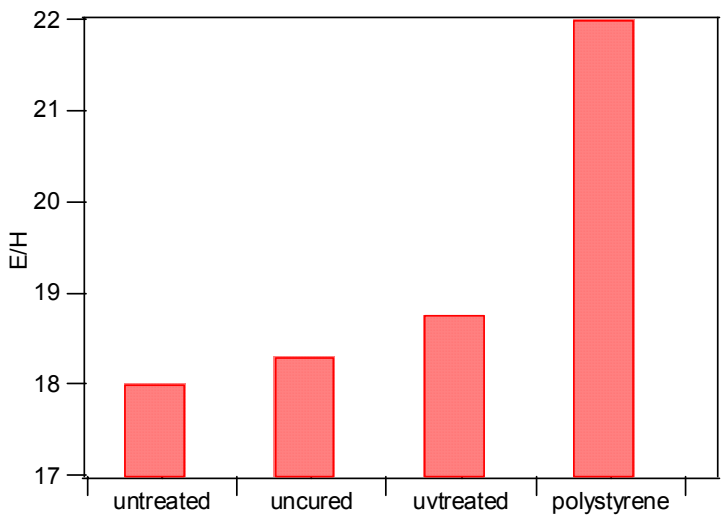

Figure 6.7 E/H ratio for the CR-39 ophthalmic lens with different treatment and polystyrene using a spherical indenter.

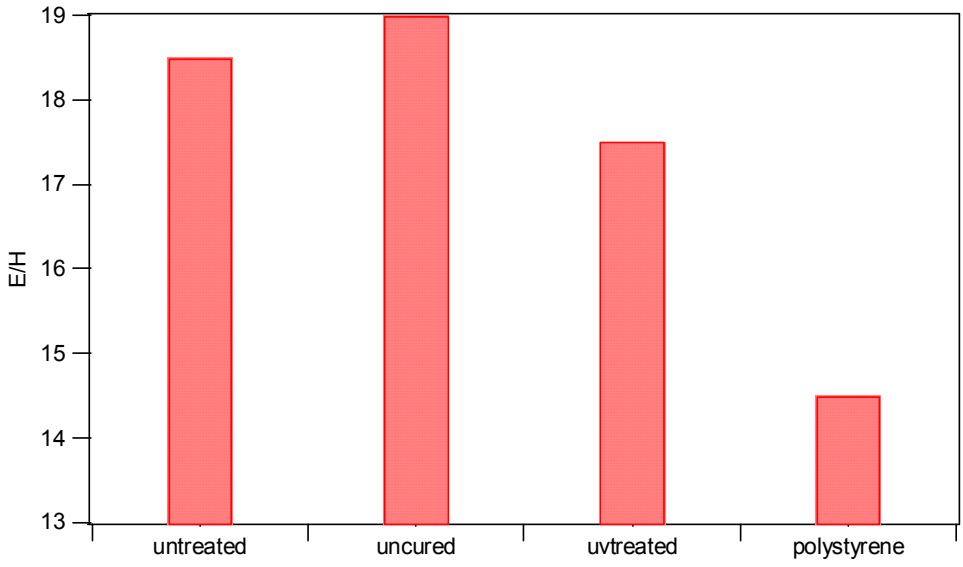

Figure 6.8 E/H ratio for the CR-39 ophthalmic lens with different treatment and polystyrene using a Berkovich indenter.

6.4.1.2 Surface roughness characterisation

The surface roughness was measured using atomic force microscopy (AFM) in contact mode. AFM imaging was carried out using a scan size of 20 μm. All the scanned images were 'flattened' using a plane fit procedure to remove the large-scale waviness from the roughness analysis. The scanned images were flattened and viewed in the three dimensional plot.

Figure 6.9 shows the topography of the untreated surface of CR-39 ophthalmic lens. It was noticed that the uncured sample has a relatively smoother surface than the untreated one, as shown in figure 6.10. Figure 6.11 shows a scanned image of the UV treated sample that appeared significantly smoother than the surface of untreated and uncured samples respectively. The value of average roughness and standard deviation of five scanned images of each sample were tabulated in table 6.2. It was observed that the average roughness value was decreased from 1.37 nm to 0.84 nm for the untreated and UV treated samples respectively.

The scanned surface depth was analysed by accumulating depth data within a specified area, and applying a Gaussian low-pass filter to the depth data to remove noise from the data curve and average the curve profile. The histogram filter cut-off parameter was provided in the input configuration of the dinanoscope software to control the amount of data entering the Gaussian low-pass filter. The larger the filter cut-off, the more data is filtered into a Gaussian low-pass filter. The scanned images were flattened and plane fitted before the depth procedure was operated.

Figure 6.12 shows the depth histogram curve of three samples of CR-39 ophthalmic lens.

The untreated, uncured and uv-treated samples were represented in figure 6.12 a, b, and c respectively. The raw data histogram was represented by a red curve and the correlation histogram (Gaussian-filtered data) by a blue line. It can be noticed that the depth peaks were not showing on the histogram curve as discrete, isolated spikes, they were contiguous, with lower and higher regions of the sample with other peaks. The number of data points and the histogram cut-off filter were configured to be maximum, which permitted more data to be filtered into the low pass-Gaussian filter. The depth histogram was defined by the percentage of peaks in the y-axis and depth values in the x-axis. The depth histogram also showed the values of the two largest peaks marked by two separate cursors. It can be observed that the maximum depth value was reduced from 16 nm in the untreated sample to 10 nm in the treated sample.

This an indication of a reduction in the roughness of the surface of CR-39 lens after applying uv treatment on the surface. Some noise can be observed in the correlation histogram curve due to the configuration of the cut-off filter size. It was found that decreasing the size of the cut-off filter can effectively reduce the noise. The least-squares calculations were automatically run by the dinanoscope software to determine the roughness values (RMS) for the scanned areas.

Table 6.2 summarises the average roughness and depth values with their associated standard deviations for the five scanned images. It was found that treating the surface of the uncured and uv treated samples reduced the surface roughness and depth. .

Table 6.2. Roughness and depth values before and after the treatment of CR-39 ophthalmic lens.

Samples	Untreated	Uncured	UV treated
RMS_{ave} (nm)	$1.37^{\pm.18}$	$1.02^{\pm.09}$	$0.84^{\pm.08}$
$Depth_{ave}$ (nm)	$16^{\pm.27}$	$11^{\pm.12}$	$10^{\pm.09}$

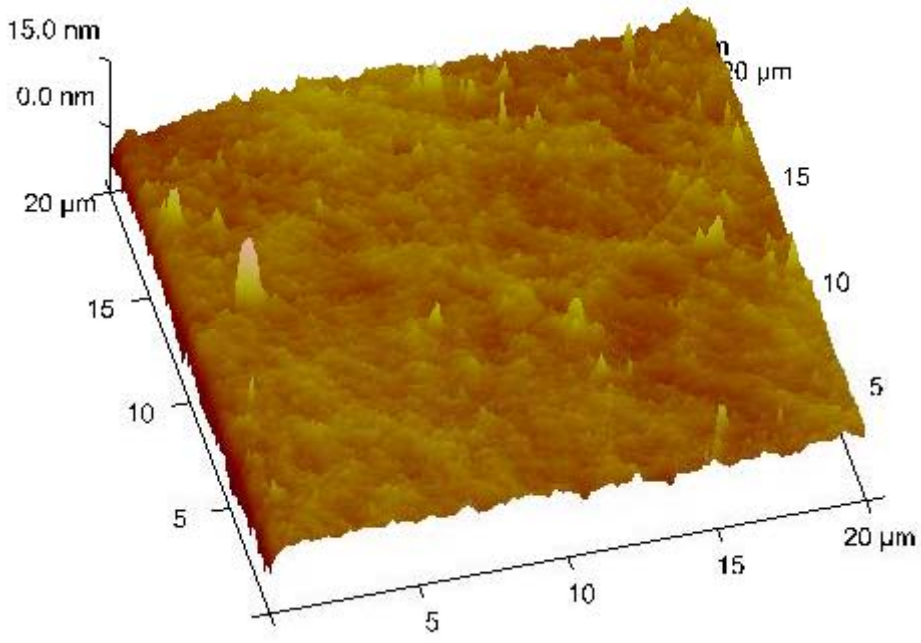

Figure 6.9. 3-dimensional scanned image of the untreated sample.

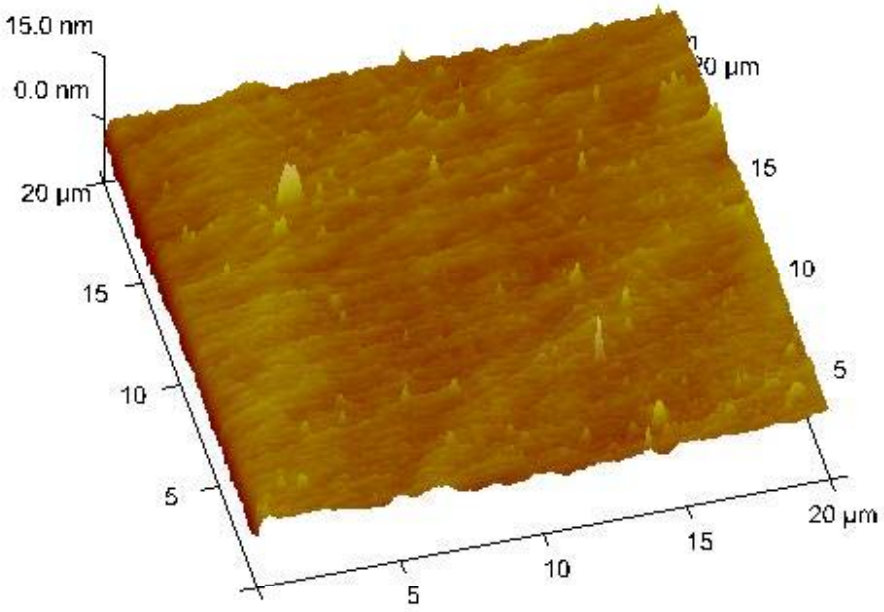

Figure 6.10 3-dimensional scanned image of the uncured sample (smoother surface than the untreated sample.

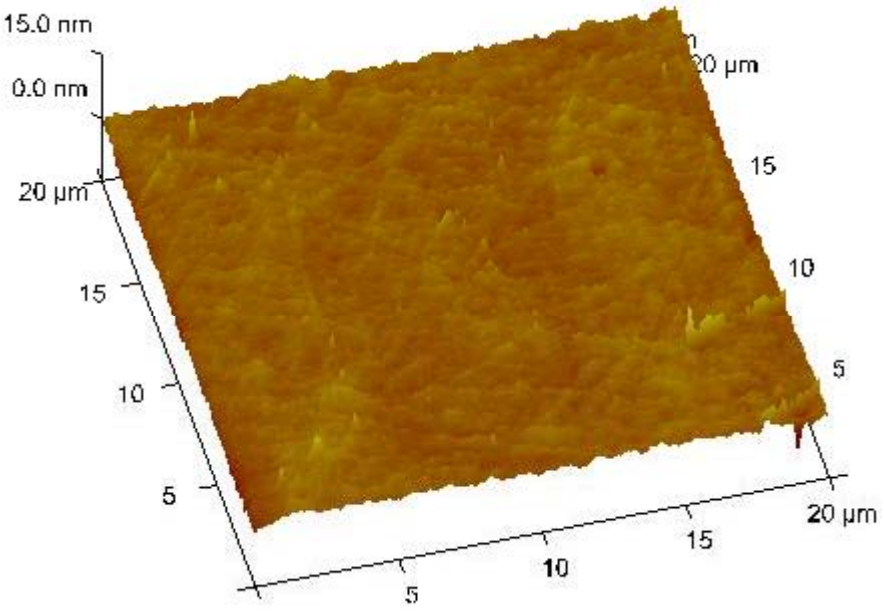

Figure 6.11. 3-dimensional scanned image of the uv treated sample (smoother surface than the uncured sample).

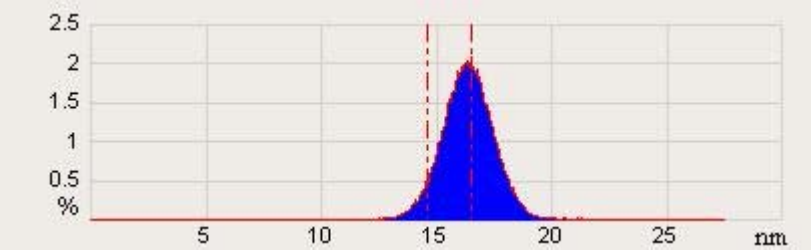

(a) Untreated sample

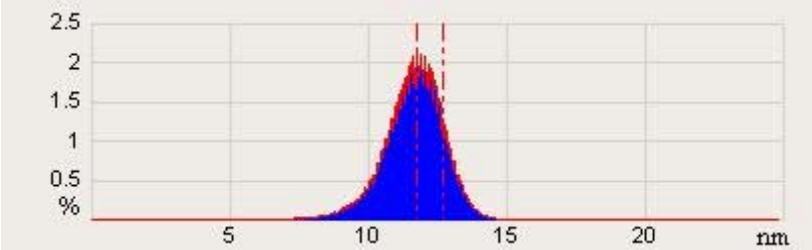

(b) Uncured sample

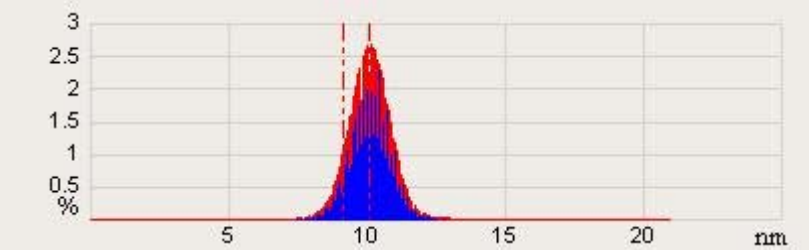

(c) UV treated sample

Figure 6.12. Depth histogram using a maximum cut-off filter.

6.4.2 DMA results

DMA penetration and single cantilever modes were employed to evaluate the effect of the treatment to the CR-39 ophthalmic lenses. The penetration mode was performed to correlate the accuracy of the results obtained from the UMIS experiments. The DMA single cantilever mode was performed to evaluate the dynamic mechanical properties of CR-39 polymer before and after the treatment was applied.

6.4.2.1 Penetration mode

Penetration DMA tests were performed on the untreated and uv-treated CR-39 ophthalmic lenses. Figure 6.13 shows the force versus penetration of the untreated sample. The force application parameter was configured to be a loading and unloading cycle with a 5 min holding time at maximum force. An identical profile of the controlled force was applied to the uv-treated sample as shown in figure 6.14. The displacement was plotted as a negative value due to the compressive force and the zero point was set up on the sample surface. It was observed that the uv-treated sample exhibited a higher penetration of 15μm and a creep of 1.5μm compared with a maximum penetration of 11μm and a creep of 0.5μm for a holding time of 5 minutes for the untreated sample. It was observed that the total area under loading, creep, and unloading curves was significantly larger for the treated sample than the untreated one. Another penetration experiment was performed on the same samples with the same loading cycle by offsetting the sample in the y-direction (different spot) to ensure a new penetration area. Figure 6.15 shows the strain versus static load relationship of the untreated sample. The strain-force relationship of the treated

sample is presented in figure 6.16. The plotted strain values in figures 6.15 and 6.16 were defined based on a change of sample thickness. A kink was observed in the first part of the curve due to instrument stability but that was not important as the main concern was to measure the slope of the straight part of the curve. As mentioned above, displacement was plotted in the negative direction, which resulted a negative strain and lead to a negative value of slope in the strain-static force curve. This negative slope was measured as 0.2 and 0.3 for the untreated and uv-treated samples respectively. It was found from the elastic contact that the magnitude of the strain was proportional to the contact pressure divided by the elastic modulus [105]. In the other word, the magnitude of the elastic strain divided by the contact pressure was proportional to the elastic modulus. Therefore, the slope of the strain-force curve for the treated sample was higher than the untreated sample, which indicated a lower elastic modulus for the treated sample than the untreated. The following equations were used to determine the elastic compression modulus of the treated and untreated surfaces. The equations used for contact of two elastic bodies are as follows [105]:

$$\frac{d_1}{a}+\frac{d_2}{a}=\frac{a}{2}\left(\frac{1}{R_1}+\frac{1}{R_2}\right)$$

and

$$P_m \alpha \frac{a(1/R_1+1/R_2)}{1/E_1+1/E_2}$$

where

a is the contact radius

d_1, R_1, E_1 are the penetration, radius and elastic modulus of the first body of contact

d_2, R_2, E_2 are the penetration, radius and elastic modulus of the second body

P_m is the average contact pressure

The elastic modulus of the surface can be determined by assuming that one of the two contacted bodies was a rigid body and the second solid was an elastically deformed body. The indenter of the DMA penetration device was considered the rigid body while the lens sample was the deformable body. The elastic compression modulus was measured at a maximum load of 2 N. The elastic compression modulus was found to be 2.1 *GPa* for the untreated and 1.5 *GPa* for the treated samples respectively. As shown previously in section 6.4.1.1, the UMIS experiments revealed that the elastic modulus for the untreated and uv treated were 1.8 and 1.5 GPa respectively, using the spherical indenter. However, the measured values of elastic modulus obtained using the DMA penetration mode and the UMIS spherical indentation test were found to be relatively consistent. This indicated that the elastic modulus of CR-39 ophthalmic was reduced due to the uv treatment applied.

6.4.2.2 Single cantilever mode tests

Single cantilever DMA tests were performed on the flat sample cured from CR-39 resin provided by SOLA Optics to ensure that it had relatively similar properties as the spherical lens. It was found that the modulus measured from DMA was not exactly the same as the Young's modulus measured from the classic stress-strain curve. In DMA, a complex modulus such as the storage modulus (E') can be measured, which can be defined by the ability of the material to return or store energy and loss modulus (E"), which can be defined by the ability to dissipate energy. Figure 6.17 shows the dynamic mechanical spectrum for an untreated sample. The dynamic mechanical spectrum was represented by three curves of the storage modulus, loss modulus, and tan delta as a function of temperature, as shown

in figures 6.17, 6.18 for the untreated and uv treated samples respectively. It can be seen that the tan δ curve for the uv treated sample exhibited a broader peak than the untreated one. The Tg value was taken at the maximum point of the tan δ peak. It was found that the uv treated sample exhibited a substantial loss modulus and a large drop in the storage modulus with a drop of Tg. Thus, the network chain mobility was changed by uv treatment as indicated by the presence of change in the tan δ curve width.

Table 6.3 tabulates the results measured by the DMA test using the controlled force and multi frequency strain methods. It was found that the ratio of loss modulus to the storage modulus had been increased from 0.07 to 0.09 at 30 ^{o}C for the untreated and treated samples respectively. This ratio is known as the damping capacity of the material. It was found that the damping capacity of CR-39 sample increased as it was influenced by the treatment. The ductility of the virgin sample was improved by increasing the damping capacity of the material. The measured compression elastic modulus ($E_{comp.}$) using the DMA penetration mode, and elastic modulus using the UMIS indentation tests (E_{sph}), were also listed in table 6.3. It can be seen from all the measured values listed in table 6.3 that the elastic modulus of the treated surface decreased with an increase in the ductility of the treated sample, as a result of the uv treatment to CR-39 ophthalmic lens.

Table 6.3. Summarizes the result obtained from DMA using the penetration and single cantilever modes.

Treatment condition	$E_{comp}(GPa)$	$E_{Storage}(GPa)$	$E_{Loss}(GPa)$	$Tg(^{o}C)$	$E_{Sph}(GPa)$
Untreated	2.1	4.25	0.3	89	1.8
Treated	1.55	3.9	0.34	84	1.5

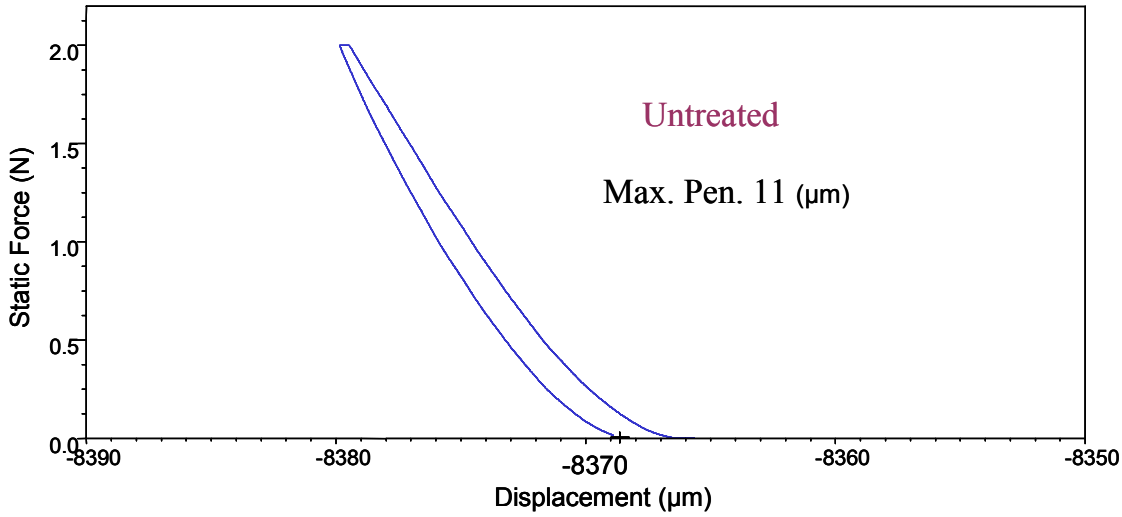

Figure 6.13. Loading – unloading static force versus displacement of untreated sample during the DMA penetration mode.

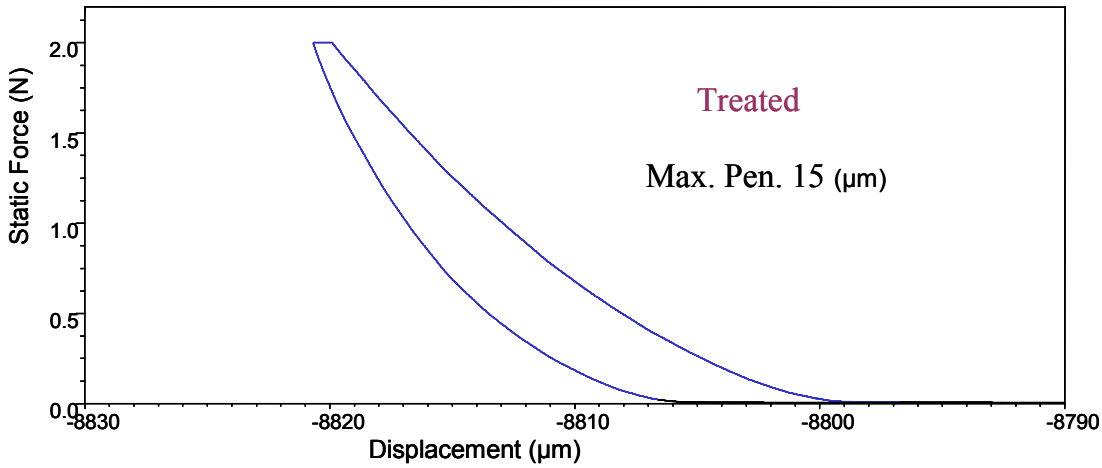

Figure 6.14. Loading – unloading static force versus displacement of uv treated sample during the DMA penetration mode.

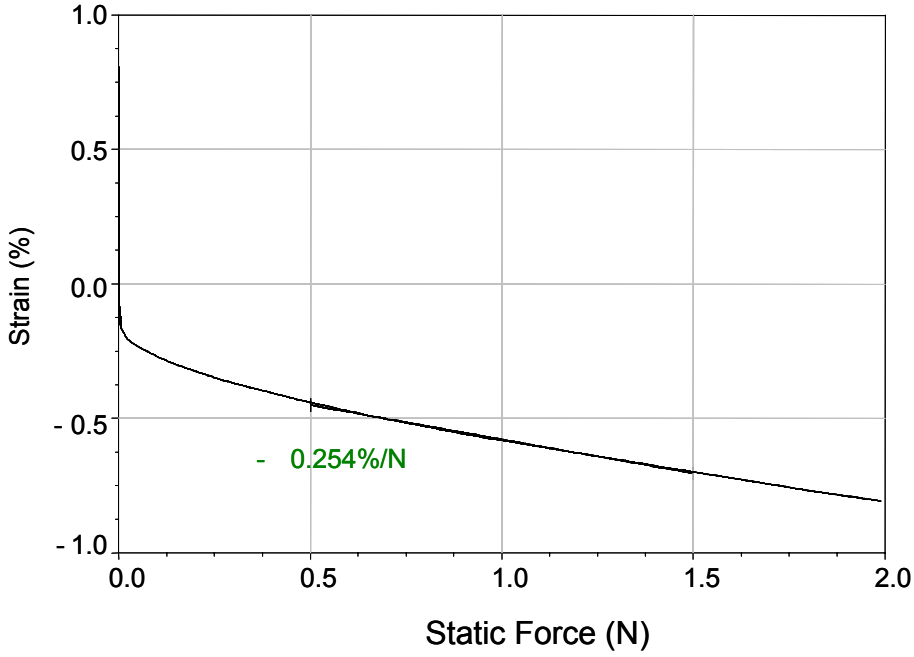

Figure 6.15. Strain versus static force curve of the loading cycle of the DMA penetration mode for untreated sample.

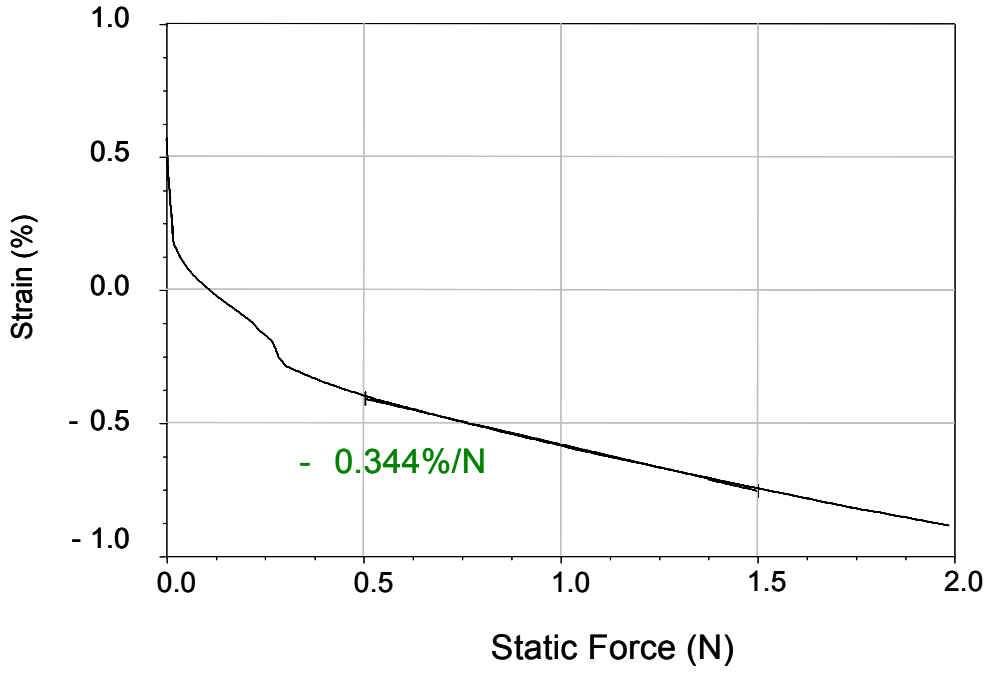

Figure 6.16. Strain versus static force curve of the loading cycle of the DMA penetration mode for uv treated sample.

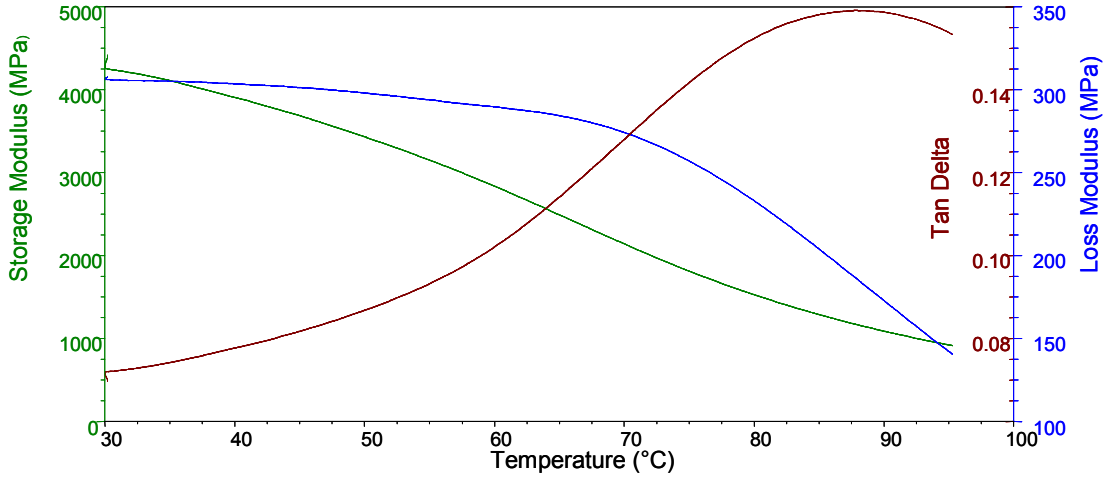

Figure 6.17. DMA test in the single cantilever configuration for the untreated sample.

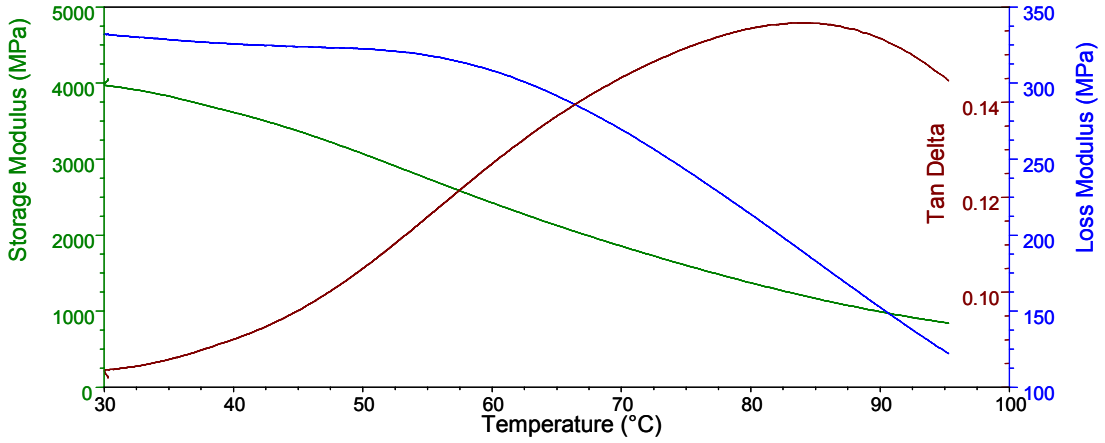

Figure 6.18. DMA test in the single cantilever configuration for the uv treated sample.

6.5 CONCLUSION

It was found from the UMIS experiments that the elastic modulus of the CR-39 surface was reduced by 38% by diffusing the monomer into the surface. By diffusing the swelling agent at 50^{o}C into the polymeric surface, the surface of treated CR-39 lens was softer than untreated lens. The modulus of the same surface was increased by exposing the lens to uv light. The elastic modulus of the uv treated surface sample remained lower than the untreated sample by 16%. The present observations showed that spherical indentation using the load-partial-unload procedure was a simple and efficient method for determining the elastic and elastic-plastic response for the CR-39 polymer sample. It was found that the results obtained from the hemispherical indenter were more accurate than using the Berkovich indenter with the polystyrene surface as a reference sample. AFM showed that the topography of the surface of CR-39 ophthalmic lens was smoother than the untreated lens. The mean squared roughness and the average depth was reduced by the influence of the uv treatment to the surface as shown by the AFM experiments. The values obtained for the elastic modulus were in good agreement comparable to the values measured using a controlled force method of DMA penetration mode. It was found that the elastic modulus was decreased by the treatment. It can be concluded that the energy absorption of the sample was improved by the treatment.

CHAPTER 7

Discussion

In the preceding chapters individual techniques, experiments, discussions and conclusions are presented. This chapter describes the correlation of all the previous chapters with an adequate discussion, a final conclusion, and some useful recommendations for further research.

7.1 SUMMARY OF KEY WORK AND RESULTS

Optical materials such as spectacle lenses need to be colourless and transparent. Transparent synthetic resins are extending their range of application as materials for lenses to replace inorganic optical materials because they are lightweight, have excellent impact resistance, and are readily processed and dyed. Various characteristics such as a suitable refractive index and sufficient impact resistance are required of transparent synthetic resins for use as ophthalmic lenses.

Diethylene glycol bis allyl carbonate (CR-39) is one of the common plastic materials used by the ophthalmic lense industry. It is considered to be brittle compared with other ophthalmic polymers such as polycarbonate and urethane acrylates. Diethylene glycol bis allyl carbonate resins have become more popular than other materials for ophthalmic lenses, having 50% of the market world wide, because of their lower cost and better optical properties than their competitors.

It has been found that the fracture resistance of CR-39 lenses is greatly affected by surface characteristics and coatings may decrease the fracture resistance of

ophthalmic lenses. Anti-reflective (AR) coatings were shown to reduce the fracture energy by 63% and the scratch resistance (SR) coating reduced the fracture energy by 57%. Through further investigation and research it was found that the fracture energy of cured ophthalmic lens can be improved by applying a soft rubbery interface between the lens surface and coating layers. Crazing the surface of the ophthalmic lens before applying the coating layers was found to be another alternative for improving fracture energy.

The main goal of this project was to develop a new technique of toughening ophthalmic lenses. A highly cross linked material such as CR-39 was chosen for toughening because it is a brittle material compared to other ophthalmic polymers. The aim of this project was to produce a thin, tough, ophthalmic lens without introducing an interface such as a thin rubbery layer into the surface.

In our study compressive stresses were generated on both the upper and lower surfaces of CR-39 plano ophthalmic lens using a volumetric swelling technique. Static load and dynamic load tests were employed to investigate the effect of the surface treatment on fracture energy.

A major aim of this project was to develop a system of diffusing a monomer into the surface of the ophthalmic lens to generate a compressive stress and polymerise the monomer to ensure that these compressive stresses are permanent. Indeed, the numerical modelling results showed how the stress causing fracture (tensile stress in x-direction) can be reduced by generating compressive stresses within the convex surfaces, while the mechanical test results showed how the fracture energy was improved in the presence of the treatment.

A substantial part of this project was concerned with modelling a thin section of the spherical lens to examine the stress distribution within the lens surface under load. It

was found that a crack can be initiated from stress in the x-direction (parallel to the surface) where the load was applied straight into the surface. For the concave modelled lens it was shown that stress in the x-direction was generated in the lower surface when the load was applied straight down onto the upper surface. It was confirmed that the stresses generated in the x-direction can be reduced by swelling the surface i.e. applying a compressive stress within the surface. The actual amount of reduction depends on size of swelling and load applied. It was found that stress in the x-direction was reduced by 92% from the original modelled lens by swelling the lower surface only. This percentage was decreased by 10% when the same amount of volumetric swelling was applied onto the upper and lower surfaces. In the model volumetric swelling was applied to the lens based on a technique for generating thermal volumetric strain in a porous medium i.e. swelling the soil particles with water. The modulus of the swollen medium was inversely proportional to the thermal volumetric strain, as implied in the porous medium equation used to apply the volumetric swelling. However, the volumetric swelling in the lens model was found to be more efficient in generating compressive stresses when the modulus of the swollen surface was less than the elastic modulus of the bulk material of the lens.

In addition to the modelling part, a large section of this project has been concerned with the experimental work in four areas; swelling and polymerisation of the CR-39 lens, photoelasticity, impact testing, and surface characterisation. After confirming by the modelling that volumetric swelling generated compressive stresses within the surface which resulted in a reduction in stress in the x-direction, an experimental procedure was designed to evaluate the appropriate monomer that can be diffused onto the surface of a CR-39 lens.

Combining the modelling result with the experimental work was the crucial part of

this project for two reasons. Firstly, it was difficult to find a monomer that can be diffused into a highly cross linked network such as CR-39 polymer, and secondly, there was a lack of certainty that fracture energy would be improved by swelling the surface of the CR-39 ophthalmic lens. It was found that diffusing the swelling agent into the surface helps to generate residual compressive stresses and plasticise the surface, resulting in a softening of the surface. It was found that acrylic acid mixed with chloroform was a good swelling agent for diffusing into the surface and polymerising during exposure of the lens to uv light, and hence, fracture energy was improved. The experiments showed that other swelling agents such as a mixture of styrene and vinyl acetate could be diffused into the surface but could not be polymerised during exposure to uv light. In this case the diffused swelling agent acts as a plasticiser because of the absence of polymerisation of the swelling agent after the uv initiation process. Further experimentation using Raman spectroscopy was employed to determine the depth of the swelling agent diffused into the lens. The depth was found to be in the range of 200-250 micron.

It was found from the photo-elasticity experiments that polymerising the swelling agent (acrylic acid and chloroform) into the lower surface, or both upper and lower surfaces, generated residual stresses within the surface. It was also found that the measured stress optical coefficient (Cg) was relatively consistent with the value obtained from the literature, and was within the range of Cg values for polycarbonates.

The modelling chapter revealed that applying a compressive stress into the lower surface, or both upper and lower surfaces, can be expected to improve the fracture resistance of the lens. The photoelasticity experiments showed that applying this treatment onto the lower surface, or upper and lower surfaces, generates a surface

residual stresses within the lens.

The numerical modelling work (chapter 3) have shown that the tensile stress in the lower surface was reduced from 350 to 25 MPa approximately, when the load was applied to the upper surface and 10% volumetric swelling was applied to the lower surface. From this we can deduce that the volumetric swelling generates stresses around 300 MPa, while the photo elastic measurement of the residual stress in chapter 5 showed that the residual stress generated by the treatment of the CR-39 lens was around 14 MPa. These discrepancies of the residual stress measurement generated from the volumetric swelling can be attributed to two reasons. Firstly, the percentage of volumetric swelling chosen for the numerical modelling was 10% to decrease the tensile stress in x-direction that was generated from applying a static load of 1.35 KN in order to qualitatively produce a compressive stress in the lower surface directly under the applied load. On the other hand, the residual stress measured by the photoelasticity experiment was the stress generated by the surface treatment in the unloaded condition. Secondly, the numerical modelling analysis did not take into account some of the material properties of CR-39 such as the plastic deformation and viscoelasticity properties. These material properties will reduce the stresses generated from these predicted by the modelling analysis. Therefore, the purpose of the numerical modelling work was only for qualitative analysis to understand the stress distribution in the loaded spherical lens, and was not meant to be used for quantitative comparison to the experimental measurement produced in this project.

Static and dynamic impact tests were employed to examine the effect of the treatment on the fracture resistance of the lens under the above conditions. The values of fracture energies obtained by the static and dynamic impact tests on the

untreated lenses were consistent to the experimental and calculated fracture energies obtained by McAuliffe et al. [12] in their research in modelling the impact testing of prescription lenses.

The results from the static load test were qualitatively consistent with the dynamic impact test, showing that applying the treatment to both upper and lower surfaces significantly increases the fracture resistance of CR-39 lenses. This effect is presumably because converting the lens into a multi composite stressed layer, while generating compressive stress into the lower surface only, produced just two regions of residual stresses. The first region was one of compressive stress within the lower surface zone where tensile stress dominated the region above the compressive stress zone due to the equilibrium. In this single sided system a crack can easily be initiated from the upper surface because of surface flaws. In general, the mechanical properties of spectacle lenses are sensitive to surface flaws so that development of a compressive surface stress for a layered composite produced by swelling the CR-39 lens makes them resistant to failure from surface flaws, which is an attractive feature, as long as the compressive residual stresses dominate the upper and lower surfaces. The presence of residual surface compressive stress is expected to not only enhance resistance to damage but also strengthen the lens, assuming the thickness of the residual stress layer exceeds the flaw depth.

The static load test and dynamic impact test have shown a consistent overall improvement in fracture resistance of the layered composite structure of the lens. It was also found that applying SR coating layers dramatically decreases fracture resistance of CR-39 lenses, presumably because the harder coating cracks with flexure before the softer substrate would, and injects a crack into CR-39 substrate.

Fracture energy was improved considerably in the absence of the SR coating layer

and was improved by 48% by applying the SR coating onto the treated ophthalmic lenses, as a result of residual compressive stress generated on the upper and lower surfaces. The SR coating is a hard brittle substrate that allows a crack to initiate and be injected into the bulk material of an ophthalmic lens. The presence of residual surface compression on both upper and lower surfaces reduces crack injection and there by strengthens the overall ophthalmic lenses.

Duckworth et al. [15] have shown that the failure load is proportional to the lens thickness squared (figure 2.4). This is an indication that the fracture load and fracture energy can be improved by increasing the lens thickness. Although the fracture energies of treated CR-39 lenses can also be positively affected by increasing the lens thickness, in our study it was doubtful that a slight increase in the lens thickness (0.04 mm average of 10 treated lenses) would have any significant effect to the improvement of the fracture energies of the treated CR-39 lenses.

The current study was not designed to evaluate the validity of static testing of ophthalmic lenses or to compare between static and dynamic testing of CR-39 lenses. In this study, static load testing was used to investigate qualitatively the effects of swelling the lower surface only, or swelling both lower and upper surfaces on the fracture resistance of CR-39 lenses. Despite the sample size of the static test being relatively small due to the difficulties of obtaining the virgin lenses from the manufacturer, the results of the average fracture energy and fracture load for the untreated lenses were consistent with the trend of the results obtained by John et al. [16] in his research on the effects of coatings on the fracture resistance of ophthalmic lenses. Alternatively, even if the results of the static test are considered to be insignificant, the dynamic impact test showed that swelling both lower and upper surfaces significantly increases the fracture resistance of CR-39 lenses. In addition,

the fracture resistance of CR-39 lenses was dramatically decreased in the presence of scratch resistance coatings, this was consistent to the findings of John et al.[16], presumably because the harder coating cracks with flexure before the softer substrate would. In the industry, the dynamic impact test is considered preferable to the static test, presumably because of the behaviour of the plastic is rate-dependent, being more brittle with high-speed impact and more flexible under static conditions. Whichever method is used, the fracture resistance was significantly improved by swelling both the lower and upper surfaces CR-39 ophthalmic lenses.

The final experimental study in this project was concerned with surface characterisation of the treated lens. It was found that the surface modulus of the treated sample was decreased after diffusion of the swelling agent, presumably because of plasticisation. The surface modulus increased again after the swelling agent was polymerised into the surface using the uv initiation process. However the surface modulus of the uv treated sample was still lower than the untreated sample, an effect which can be attributed to some degradation that occurred during the uv initiation which raised the temperature of the exposed surface to about 70 ^{o}C, in addition it may be caused by the plasticisation effect. These results were obtained using the ultra microindentation technique employing both spherical and sharp indenters. The same trend of decreasing the modulus of the treated surface was observed using the penetration mode of the dynamic mechanical analysis (DMA). Through further experimentation and consideration using DMA it was found that the ductility of CR-39 polymer was improved while the damping capacity was slightly increased by the treatment. In addition to the surface softening by the treatment, the roughness analysis using the AFM revealed that the surface was smoother for the treated sample than the untreated.

It is well established in strengthening glass products by the ion exchange technique, that the surface hardness of the glass increases if the surface is under compression and decreases if the surface is submitted to tensile stress [34]. Such an effect was not seen in this project, as the nano-hardness (UMIS) measurements showed a decrease in surface hardness of CR-39 lens that is subjected to surface compressive stress. This difference between the surface hardness of glass and the CR-39 lens could be attributed to plasticisation, as Raman experiments showed that some chloroform residue was present in the surface of the CR-39 lens. Also in the surface characterization experiments, the DMA results showed a decrease in both the surface modulus and the Tg. The decrease in surface modulus was also observed using the ultra-micro indentation system (UMIS). It is quite surprising, because the surface modulus should not be affected by generating a surface compressive stress. However, this decrease in surface modulus could also be attributed to the plasticisation effect. Thus, a more ductile layer was generated within the surface of CR-39 lens as a result of the swelling treatment.

It is possible that an alternative explanation for the improved toughness is the presence of a more ductile surface layer without considering surface compressive stress. In addition AFM experiment showed a decrease in surface flaws by the treatment, this is another alternative explanation method for the improved toughness. The current study revealed that the fracture energy was significantly improved both by producing a more ductile layer and by generating a compressive stress into the surface that causes a reduction in surface flaws. In order to understand which mechanism was responsible for the improved toughness of the CR-39 lens as a result of the swelling treatment, we should extract the residual chloroform from the surface completely and measure the fracture resistance again.

7.2 CONCLUSION

In recent years the requirement for tough, fracture resistant materials for optical applications to prevent eye injuries from incidents or impact has become progressively more important. The aim of toughening optical lenses is to produce thinner cross-sectional lenses that are stiffer and harder to fracture.

Previous work had been shown that the CR-39 ophthalmic lens can be toughened by using the concept of interpenetrating polymer networks (IPNs) by the curing of two matchable resins. In the industry the overall optical lens is toughened by placing a thin rubbery layer of primer with a low modulus between the optical polymer and coating layers. These thin layers of primer help slow, or stop a crack from being injected into the bulk material of the ophthalmic lenses. Crazing the optical polymer surface can also help to slow down crack injection and propagation into the bulk of CR-39 ophthalmic lenses. The achievements of this current thesis can be concluded as follows:

- The main goal of this project was to toughen the polymer surface without crazing or introducing any interlayer such as fibre or other particle into the polymeric surface. Crack initiation with a load applied to the lens was investigated, and it was found that a crack initiated from the back surface of the ophthalmic lenses during any incident or impact from the front side of the lens. The main reason for the crack initiating from the backside is that the back surface was found to be under tension stress when any load or impact was applied to the front surface. Stress in the x-direction cause the crack initiation for the spherical lens. It had been found that applying volumetric swelling to the surface of the lens can help reduce tensile stress in the x-

direction significantly. The reduction of stress in the x-direction is proportional to the amount of swelling of the surface.

- It was shown that the CR-39 polymer surface can be toughened by swelling the surface and placing it under compressive stress. The plano CR-39 lens can be considered as a multi-layered residual stressed, composite substrate, after swelling both upper and lower surfaces. The plano CR-39 ophthalmic lens can be toughened by swelling both inner and outer surfaces. The static load test and the dynamic load test have shown a consistent overall improvement in fracture energy of the layered composite structure of the CR-39 ophthalmic lens. Fracture energy was improved by 48% after applying the (SR) coating onto the treated ophthalmic lenses, as a result of the residual compressive stress generated on the inner and outer surfaces of the CR-39 ophthalmic lens. It was found that swelling the upper and the lower surfaces of the ophthalmic lens will convert it into a composite element with two upper and lower compressive stress layers and a neutral tensile stress zone in the middle. Fracture energy has been improved considerably in the absence of the SR coating layer. SR coating is a hard, brittle substrate that allows the crack to initiate and be injected into the bulk material of an ophthalmic lens. The presence of residual surface compression on both upper and lower surfaces not only reduces crack injection but also strengthens the overall ophthalmic lenses.
- The residual stress that was generated from swelling CR-39 ophthalmic lenses was successfully measured by attaching the three point bending device onto a circular polariscope. The residual stress was found to be 14 MPa on both the upper and lower surfaces.

- Polymerisation of acrylic acid into the surface of CR-39 ophthalmic lenses reduced the residual C=C bond in CR-39 polymer from 9% to 7% to a depth of approximately 250 microns. The diffusion and polymerisation of acrylic acid into the surface of CR-39 ophthalmic lenses was fairly homogenous despite the lenses being spherical and convex in shape. Both the diffusion and polymerisation process have to be conducted in a temperature lower than Tg of CR-39 swollen polymer which is approximately 87^{o}C. Through further experimentation and consideration it was observed that the process of applying any kind of coating such as SR coatings has to be done at a temperature lower than Tg of CR-39 otherwise the residual compressive stress layers will be relaxed.
- It has been found from the DMA results that the ratio of $E_{loss}/E_{elastic}$ has increased slightly. This indicates that the damping capacity of the treated CR-39 toughened lenses has increased, which means the treated lens has became more ductile. While the glass transition temperature and modulus of the swollen surface was decreased, overall fracture energy affectively increased. Despite the new swollen surfaces of the lens having a lower modulus of elasticity, the topography of the surface has become smoother. However, this smoother surface helps to slow down the injection of a crack into the bulk material of the lens because is more likely propagate in the interface.
- This study reveals that same technique of applying compressive stress in glass and ceramics can be employed in a polymer to increase the fracture energy of a brittle, highly cross-linked glassy material such as a CR-39 ophthalmic lenses.

7.3 SUGGESTIONS FOR RECOMMENDED FUTURE WORK

Further to the modelling and experimental programs of this project, some future work and experiments are recommended. The suggestions in the following list resulted from the achievements of this current thesis and the possibilities associated with developing good quality products. Suggestions for future work are as follows:

- Further experimental work needs to be performed to find the treatment conditions for determining the optimum fracture energy of CR-39 ophthalmic lenses, particularly when a scratch resistant coating is applied. The optimum fracture energy has to be evaluated in comparison with other polymeric ophthalmic material such as polycarbonate, which is tougher than CR-39.
- To evaluate improvements in fracture energy, it is necessary to perform impact testing of CR-39 ophthalmic lenses toughened by the swelling agent technique and other techniques such as placing a soft layer onto the lens surface or IPNs technique.
- Although the Raman spectroscopy mapping technique has been used to measure the approximate depth of penetration of monomer into the surfaces of CR-39 ophthalmic lens, an alternative depth profiling technique has to be used for a more accurate measurement.
- Perform Raman depth profiling technique for different samples with different depth of penetration of monomer and measure the corresponding fracture energy for each depth using the instrumented impact tester. This procedure

would help to evaluate the depth of penetration of the monomer which produces the optimum fracture energy for CR-39 ophthalmic lenses.

- It is highly recommended that we should extract the chloroform that was diffused in the mixture with acrylic acid into the CR-39 ophthalmic lenses after the diffusion process of the monomer. This extraction process is quite difficult, as the toughened lens should be treated thermally in order to allow the chloroform to evaporate from the treated CR-39 lens. However the high temperature treatment will cause thermal stress relaxation of the toughened lens.
- It would be interesting to try other monomers which have at least two vinyl groups and a long chain distance between two double bonds, such as tri (ethyleneglycol) dimethacrylate, or tetra (ethyleneglycol) dimethacrylate.
- In order to establish the effect of surface flaws on the improved toughness of the CR-39 lens, it would be interesting to generate the same amount of surface flaws to the treated and untreated lenses by using Bayer Abrasion test instrument (located in SOLA Optics) and measure the fracture resistance again.

REFERENCES

1. Kinloch, A.J. and R.J. Young, *Fracture Behaviour of Polymers*. 1983, London, New York,: Applied Science Publisher.
2. Jinks, D., *A variable Radius Roll Test for Measuring the Adhesion of Paint Systems to Deformable Steel Substrates*. 2003, Australia: University of Wollongong.
3. Young, R.J. and P.A. Lovell, *Mechanical properties*, in *Introduction to Polymers*. 1991, Chapman & Hall: London, New York. p. 310-424.
4. McCrum, N.G., C.P. Buckley, and C.B. Bucknall, *Principles of Polymer Engineering*, ed. Edition. 1997: Oxford Science Publications.
5. Glad, M.D. and E.J. Kramer, *Microdeformation and network structure in epoxies.* Journal of Materials Science, 1991. **26**: p. 2273-2286.
6. Vakil, U.M. and G.C. Martin, *Yield and fracture behaviour of cross-linked epoxies.* Journal of Materials Science, 1993. **28**: p. 4442-4450.
7. Frounchi, M., *Fracture Behaviour and Toughening of Poly(Allyl Diglycol Carbonate)*, in *School of Chemical Engineering and Industrial Chemistry*. 1994, University of New South Wales: Sydney , Australia.
8. Dain, S.J., *Pressure testing of ophthalmic safety lenses: the effects on different materials.* American Journal of Optometry and Physiology, 1988. **65**: p. 585-590.
9. Kinney, G.F., *Engineering Properties and Applications of Plastics*. 1975: Wiley. 3-4.
10. Wigglesworth, E.C., *The impact resistance of eye protector lens materials.* American Journal of Optometry and Archives of American Academy of Optometry, 1978. **48**: p. 245-261.
11. Davis, J.K., *Perspectives on impact resistance and polycarbonate lenses.* International Ophthalmology Clinics, 1988. **28**(3): p. 215-218.
12. McAuliffe, P.J., R. Truss, and M. Pittolo, *Modelling the impact testing of prescription lenses.* Journal of Materials Sceince: Materials in Medicine, 1997. **8**: p. 221-226.
13. Roark, R.J. and C.W. Young, *Formulas of Stress and Strain*. 5th edition ed. 1975: New York, McGraw-Hill. p. 476.
14. Scaif, A.L., *A comprehensive look at ophthalmic fracture resistance.* Optometry Weekly, 1976. **67**(52): p. 27-30.
15. Duckworth, W.H. and A.R. Rosenfield, *Basic principles of lens fracture testing.* American Journal of Optometry & Physiological Optics, 1978. **55**(11): p. 751-759.
16. John, C.C., R.B. Greer, R.D. Bruess, G.K. Lee, and A.L. Scaief, *Effects of Coatings on the Fracture Resistance of Ophthalmic Lenses.* Optometry and Vision Science, 1996. **7**(1): p. 8-15.
17. Pittolo, M., R. Truss, M. Frounchi, and R. Chplin, *The failure of optical polymers.* Materials Forum, 1995. **19**: p. 201-208.

18. Frounchi, M., A.T. Westgate, P.R. Chaplin, and P.R. Burford, *Fracture of polymer networks based on diethylene glycol bis (allyl carbonate).* Polymer, 1994. **35**(23): p. 5041-05.
19. Dadbin, S. and R.P. Chaplin, *Morphology and mechanical properties of interpenetrating polymer networks of poly(allyl diglycol carbonate) and rigid polyurethane.* Journal of Polymer Science, 2001. **81**: p. 3361-3370.
20. Dadbin, S., R.P. Burford, and R.P. Chaplin, *Interpenetrating polymer networks of poly(allyl diglycol carbonate) and polyurethane: effect of composition and crosslink density on morphology and mechanical properties.* Polymer, 1994. **37**(5): p. 785-792.
21. Dadbin, S., R.P. Burford, and R.P. Chaplin, *Effect of kinetics on morphology and mechanical properties of poly(allyl diglycol carbonate)-poly(urethane) interpenetrating polymer networks.* Polymer Gels and Networks, 1995. **3**: p. 179-195.
22. Socrate, S., M.C. Boyce, and A. Lazzeri, *A micromechanical model for multiple crazing in high impact polystyrene.* Mechanics of Materials, 2001. **33**: p. 155-175.
23. Wang, Y., J. Lu, and G. Wang, *Toughening and reinforcement of HDPE/CaCO3 blends by interfacial modification-interfacial interaction.* Journal of Applied Polymer Science, 1997. **64**(7): p. 1275-1281.
24. Frounchi, M., *Use of rigid thermoplastics for toughening an optical network polymer.* European Polymer Journal, 2001. **37**: p. 995-1000.
25. Frounchi, M., R.P. Burford, and R.P. Chaplin, *Silica nano-composites of allyl diglycol carbonate resin.* Polymers and Polymer Composites, 1994. **2**(2): p. 77-82.
26. Brandrup, J. and H.E. Immergut, *Polymer Handbook*, ed. r. edition. Vol. 6. 1989: Wiley, New York. P.451.
27. Ide, F., *Plastics Age*. Vol. 34. 1987, New York: Springer. P.152.
28. Matsuda, T., Y. Funea, M. Yoshida, T. Yamamoto, and T. Takaya, *Ophthalmic lens material prepared by unsaturated nitrile-polyfuctional methacrylate-styrenic monomer copolymerization.* Journal of Applied Polymer Science, 1998. **68**: p. 1227-1235.
29. Brandt, N.M., *The anatomy and autopsy of an "impact resistant lens".* American Journal of Optometry & Physiological Optics, 1974. **51**: p. 982-986.
30. Brungs, M.P., *Fracture and failure of glass.* Materials Forum, 1995. **19**: p. 227-239.
31. Uhlmann, D.R. and N.J. Kreidl, *Glass: Science and Technology*. Chemical Strengthening of Glass. 1980, New York, London: Academic Press. 220-222.
32. Berg, K.J., P. Grau, D. Nowak-Wozony, M. Petzold, and M. Suszynska, *On the sensitivity of optical and mechanical characteristic of the Na^+ - Ag^+ exchange process in soda-lime silicate glass.* Materials Chemistry and Physics, 1995. **40**: p. 131-135.
33. Salomonson, J., K. Zeng, and D. Rowcliffe, *Decay of residual stress at indentation cracks during slow crack growth in soda-lime glass.* Acta Materialia, 1996. **44**(2): p. 543-546.
34. Odo, G.Y., L.N. Nougueira, and C.M. Lepienski, *Ionic migration effects on the mechanical properties of glass surfaces.* Journal of Non-Crystalline Solids, 1999. **247**: p. 232-236.

35. Chih-Hung, Y. and H. Min-Hsiung, *Surface strengthening and toughening of Si3N4/TiC layered composite by slip casting.* Journal of Materials Science, 2000. **35**: p. 1037-1041.
36. Wang, Y.H., N.R. Singh, and A.R. Lowden, *Thermal shock behavior of continuous fiber ceramic composite.* Ceramic Engineering and Science Proceeding, 1994. **15**: p. 292-302.
37. Hirano, T. and K. Niihara, *Thermal shock resistance of Si3N4/SiC nanocomosites fabricated from amorphous Si-N-C precursor powders.* Materials Letters, 1996. **26**: p. 285-289.
38. She*, H.J., T. Ohji, and Y.Z. Deng, *Thermal shock behavior of porous silcon carbide ceramics.* Journal of American Ceramics Society, 2002. **85**(8): p. 2125-2127.
39. Easler, E.T., C.R. Bradt, and E.R. Tressler, *Effects of oxidation and oxidation under load on strength distributions of Si3N4.* Journal of American Ceramics Society, 1982. **65**(6): p. 317-320.
40. Jakus, K., J.E. Ritter, and W.P. Rodgers, *Strength of hot-pressed silicon nitride after high temperature exposure.* Journal of American Ceramics Society, 1984. **67**(7): p. 471-475.
41. He, C., L. Wang, and J.G. Wu, *Oxidation of sintered silicon nitride: II mechanical properties.* Journal of Materials Science, 1993. **28**: p. 4829-4834.
42. Vandeperre, J.L., A. Kristofferson, E. Carlstorm, and J.W. Clegg, *Thermal shock of layered ceramic structures with ceramic-deflecting interfaces.* Journal of American Ceramics Society, 2001. **84**(1): p. 104-110.
43. She, J., J. Yang, D.D. Jayaseelan, S. Ueno, N. Kondo, T. Ohji, and S. Kanzaki, *Strength of silicon nitride after thermal shock.* Journal of the American Ceramic Society, 2003. **86**(16): p. 1619-1621.
44. Shyu, J. and W. J., *Surface characteristics of high-strength MgO-CaO-SiO2-P2O5 glass-ceramics.* Journal of Materials Research, 1994. **9**(3): p. 717-722.
45. Bruneni, J.L., *History of the American Ophthalmic Industry*. 1994: John Wiley & Sons Ltd.
46. Agranoff, J., *Modern Plastics Encyclopaedia*. Vol. 56. 1964, New York: McGraw-Hill,. 11.
47. Mark, H.F., N.G. Gaylord, and N.M. Bikales, *Encyclopaedia of Polymer Science and Technology*. Vol. 1. 1964, New York: Wiley-interscience,. 799.
48. Solomon, D.H. and A. Qureshi, *Allyl diglycol carbonate.* Concise encyclopedia of polymer science and engineering, 1996: p. 182-187.
49. Yonemori, S., A. Masui, and M. Noshiro, *Analysis of allyl diglycol carbonate CR-39 polymerization by Raman spectroscopy.* Journal of Applied Polymer Science: Applied Polymer Symposium, 1993. **52**: p. 227-283.
50. O'Sullivan, P.W. and J.H. O'Donnell, *A kinetic Study of Crosslinking Vinyl Polymerization by Laser Raman Spectroscopy.* Polymer Bulletin, 1981. **5**: p. 103-110.
51. Ahmed, S. and J. Stejny, *Polymerization, structure and track recording properties of CR-39.* Nuclear Tracks Radiation Measurements, 1991. **19**(Nov 1-4): p. 11-16.
52. Hill, D.J.T., D.I. Londero, J.H. O'Donnell, and P.J. Pomery, *Polymerization of Diethelyene Glycol Bis(Allyl Carbonate) at 85^{o}C.* European Polymer, 1990. **26**(10): p. 1157-1160.

53. Coolidge, D.J., *An investigation of the mechanical and stress-optical properties of columbia resin, CR-39.* Proceedings of the Society for Experimental Stress Analysis, 1948. **6**(1): p. 74-82.
54. Cloud, G., *Correlation between dispersion of birefringence and transmittance of three polymers.* Journal of the Optical Society of America, 1970. **60**(8): p. 1042-1045.
55. Shirouzu, S., H. Shikuma, N. Senda, M. Yoshida, S. Sakamoto, K. Shigematsu, T. Nakagawa, and S. Tagami, *Stress-optical coefficients in polycarbonates.* Japanese Journal of Applied Physics, 1990. **29**(5): p. 898-901.
56. Ryu, D., T. Inoue, and K. Osaki, *A simple evaluation method of stress-optical coeffcient of polymers.* Nihon Reoroji Gakkaishi (The Society of Rheology, Japan), 1996. **24**(3): p. 129-132.
57. Kukreja, L.M., *Studies on laser-induced irreversible surface softening in thermoset polymer of allyl diglycol carbonate (CR-39).* Journal of Applied Polymer Science, 1991. **42**: p. 115-125.
58. Hill, D.J.T., M.C.S. Perera, and P.J. Pomery, *Dynamic mechanical properties of homopolymers and interpenetrating networks based on diethylene glycol-bis-allyl carbonate.* Polymer, 1998. **39**(21): p. 5075-5083.
59. Yang, F., J.Y. Zhou, V. Kordonski, and S.D. Jacobs, *Indentation size effect of thermoset polymer: Allyl diglycol carbonate (CR-39).* Journal of Materials Science Letters, 1996. **15**: p. 1523-1525.
60. Banerjee, K.R. and P. Feltham, *Deformation and fracture of germanium single crystals.* Journal of Applied Polymer Science, 1974. **9**: p. 1478-1482.
61. Arivuoli, D., F.D. Gnanam, and P. Ramasamy, *Growth and microhardness studies of chalcogenides of arsenic, antimony and bismuth.* Journal of Materials Science Letters, 1988. **7**: p. 711-713.
62. Tabor, D., *Hardness measurement with conical and pyramidal indenters*, in *The Hardness of Metals*. 1951, Clarendon Press: Oxford. p. 95-112.
63. Evans, A.G. and E.A. Charles, *Fracture toughness determinations by indentation.* Journal of American Ceramics Society, 1976. **59**(7): p. 371-374.
64. Wang, H. and X. Hu, *Surface properties of ceramic laminates fabricated by die pressing.* Journal of American Ceramics Society, 1996. **79**(2): p. 553-561.
65. Westbrook, H.J. and H. Conrad, *Determination of Vickers hardness under load-a method considering the viscoelastic behaviour of plastics*, in *The Science of Hardness Testing and its Research Application*. 1971, American Society for Metals: Ohio. p. 291-299.
66. Howes, V.R. and P. Wall, *Relaxation and recovery measurements by the microhardness indentation technique for transparent polymeric materials.* Journal of Applied Polymer Science, 1987. **34**: p. 1125-1133.
67. Glass, B., *Finite Element Mesh Modeling software*. 2000.
68. Hosford, F.W. and M.R. Caddell, *Stress and strain*, in *Metal forming*. 1993, Prentice-Hall, Inc.: New Jersey. p. 1-24.
69. Ewalds, L.H. and H.J.R. Wanhill, *Sustained load fracture*, in *Fracture mechanics*. 1983. p. 286-295.
70. HKS, *ABAQUS Standard V5.8 User Manual*. 1998.
71. Gunasegaram, D.R., I.M. Bidhendi, and N.J. McCaffrey, *Modelling the casting process of plastic ophthalmic lenses.* International Journal of Machine Tools & Manufacture, 2000. **40**: p. 623-639.

72. Andersson, R., G. Toth, L. Gan, and M.V. Swain, *Indentation response and cracking of sub-micron silica films on a polymeric substrate.* Engineering Fracture Mechanics, 1998. **61**: p. 93-105.
73. Schwarzer, N., *Coating design due to analytical modelling of mechanical contact problems on multilayer systems.* Surface and Coating Technology, 2000. **133-134**: p. 397-402.
74. Blake, A., *Design Fundamentals*, in *Practical stress analysis in engineering design*, L.L. Faulkner, Editor. 1990, Marcel Dekker, Inc: New York. p. 399-429.
75. Timoshenko, S. and S. Woinowsky-Krieger, *Symmetrical bending of circular plates*, in *Theory of plates and shells*. 1959, McGraw-Hill: New York. p. 51-78.
76. Young, W.C., *Formulas for flat circular plates of constant thickness*, in *Roark's formulas for stress and strain*. 1989, McGraw-Hill: New York. p. 398-440.
77. HKS*, *ABAQUS Standard V5.7 Theory Manual*. 1997.
78. Sheppard, N., *The Historical Development of Experimental Techniques in Vibrational Spectroscopy*. Handbook of Vibrational Spectroscopy. Vol. 1. 2002, University of East Anglia, Norwich, UK: John Wiley & Sons Ltd. 1-25.
79. Colarusso, P., L.H. Kidder, I.W. Levin, and E.N. Lewis, *Raman and Infrared Microspectroscopy*. Encyclopedia of Spectroscopy and Spectrometry. Vol. 3. 1999, National Institute of Health, Bethesda, MD, USA: John C. Lindon. 1945-1992.
80. Koenig, J.L., *Spectroscopy of polymers*. second ed. 1999: Elsevier.
81. Turrell, G. and J. Corset, *Raman Microscopy Developments and Applications*. 1996, London: Academic Press.
82. Wang, H. and H.R. Brown, *Self Initiated Photopolymerization and Photografting of Acrylic Monomers.* Macromolecular Rapid Communications, 2004. **25**: p. 1095-1099.
83. George, G.S., *Introduction to Infrared and Raman characteristic group frequencies*, in *Infrared and Raman characteristic group frequencies : tables and charts*. 2001: New York. p. 4-47.
84. Wang, H. and H.R. Brown, *Ultraviolet Grafting of Methacrylic Acid and Acrylic Acid on High-Density Polyethelene in Different Solvents and the Wettability of Grafted High-Density Polyethylene.* Journal of Polymer Science, 2004. **42**: p. 253-262.
85. Wang, H. and H.R. Brown, *Ultraviolet Grafting of Methacrylic Acid and Acrylic Acid on High-Density Polyethelene in Different Solvents and the Wettability of Grafted High-Density Polyethylene II.* Journal of Polymer Science, 2004. **42**: p. 263-270.
86. Hetch, *Optics*. 3 ed. Polarization. 1998, New York: Addison Wesley. 318-371.
87. Lounghurst, S.R., *Absorption, Dispersion, and Scattering*, in *Geometrical and Physical Optics*. 1957, Longmans: Great Britain. p. 409-428.
88. Heywood, R.B., *Designing by photoelasticity*. 1952, London: Chapman and Hall Ltd. 1-59.
89. Aben, H., L. Ainola, and J. Anton, *Integrated photoelasticity for nondestructive residual stress measurement in glass.* Optics and Lasers in Engineering, 2000. **33**: p. 49-64.

90. Matthys' Home Page, *Isochromatic Fringes*. 1997, User's manual for the overhead polariscope model 081 (Measurements group, Raleigh, NC 276).
91. Estevez, R., M.G.A. Tijssens, and E. Van der Giessen, *Modeling of the competition between shear yielding and crazing in glassy polymers.* Journal of Mechanics and Physics of Solids, 2000. **48**: p. 2585-2617.
92. Pijnenburg, K.G.W. and E. Van der Giessen, *A novel approach to the analysis of disteributed shear banding in polymer blends.* International Journal for Numerical Methods in Engineering, 2003. **58**: p. 703-721.
93. Black, K., *Testing Hypotheses about Two Populations*, in *Business Statistics For Contemporary Decision Making*. 2004, John Wiley & Sons, Inc. p. 377-384.
94. Bell, T.J., J.S. Field, and M.V. Swain, *Precision hardness & elastic modulus measurements of thin films & cross-sections.* Materials Forum, 1993. **17**: p. 127-138.
95. Kourtesis, G., G.M. Renwick, A.C. Fischer-cripps, and M.V. Swain, *Mechanical property characterization of a number of polymers using uniaxial compression and spherical tipped indentation tests.* Journal of Materials Science, 1997. **32**: p. 4493-4500.
96. Wai, S.W., G.M. Spinks, H.R. Brown, and M. Swain, *Surface roughness: Its implications and inference with regards to ultra microindentation measurements of polymer mechanical properties.* Polymer testing, 2003. **23**: p. 501-507.
97. Sneddon, I.N., *The relation between load and penetration in the axisymmetric Boussinesq problem for a punch of arbitrary profile.* International Journal of Engineering Science, 1965. **3**: p. 47-57.
98. Oliver, W.C. and G.M. Pharr, *An improved technique for determining hardness and elastic modulus using load and displacement sensing indentation experiments.* Journal of Materials Research Society, 1992. **7**(6): p. 1564-1583.
99. Bharat, B., *Nanomechanical Properties of Solid Surfaces and Thin Films*, in *Handbook of Micro/Nano Tribology*. 1999, CRC Press: Boca Raton. p. 433-514.
100. Chan, C.-M., *Atomic Force Microscope (AFM)*, in *Polymer Surface Modification and Characterization*. 1994, Hanser: Munich. p. 6-38.
101. Kevin, M.P., *An Introduction to Dynamic Mechanical Analysis*, in *Dynamic Mechanical Analysis*. 1999, CRC Press: Boca Raton. p. 2-59.
102. Malzbender, J. and G. de With, *Energy dissipation, fracture toughness and the indentation load-displacement curve of coated materials.* Surface Coating and Technonlogy, 2000. **135**: p. 60-68.
103. Lawn, B.R., A.G. Evans, and D.B. Marshall, *Elastic/Plastic indentation damage in ceramics: The median/radial crack system.* Journal of the American Ceramic Society, 1980. **63**: p. 574-581.
104. Hiraga, K., K. Morita, B. Kim, and Y. Sakka, *Fracture Toughness of Yttria-Stabilized Cubic Zirconia (8Y-CSZ) Doped with Pure Silica.* Materials Transactions, 2004. **45**(12): p. 3324-3329.
105. Johnson, K.L., *Normal contact of elastic solids: Hertz theory*, in *Contact Mechanics*. 1985, University of Cambridge: London. p. 84-151.

APPENDIX A: FTIR spectrum for AA polymerisation process

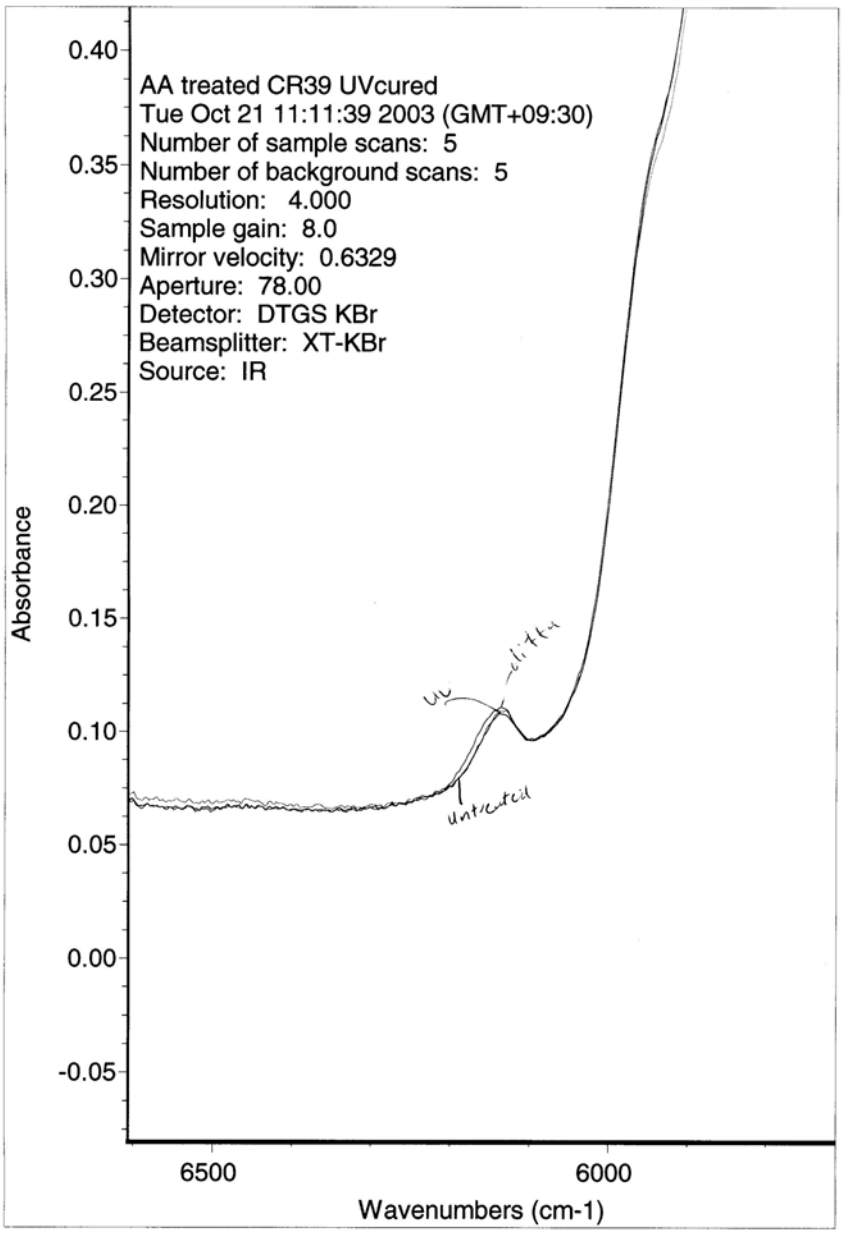

APPENDIX B: Result of drop ball test

DROPBALL - IMPACT RESULTS

File : Impact.xls

EXPT. : Controls Treated DATE :

			A	B	C	D	E	F
NO. OF SAMPLES			7	7				
AVERAGE THICKNESS (mm)								
BALL SIZE	HEIGHT (INS.)	ENERGY (J)						
1/16.36 g	50	0.20						
	55	0.22						
	60	0.24						
	65	0.26						
	70	0.29						
	75	0.31						
	80	0.33						
	85	0.35						
	90	0.37						
2/28.15 g	60	0.42						
	65	0.46						
	70	0.49						
	75	0.53						
3/44.73 g	50	0.56						
	55	0.61						
	60	0.67						
	65	0.72		T4, T7				
	70	0.78		T7				
	75	0.84						
	80	0.89		T5				
	85	0.95						
	90	1.00		T1,				
4/66.64 g	65	1.08						
	70	1.16	7					
	75	1.24	6					
	80	1.33						
	85	1.41	4	T6				
	90							

IMPACT STRENGTH =							
STD. DEVIATION =							
95% Confidence interval =							
Confidence limits are :							